Mathematical Study of Rho GTPases in Motile Cells

by

Alexandra Jilkine

B.S. (Hons.), University of Manitoba, 2003

A THESIS SUBMITTED IN PARTIAL FULFILLMENT OF

THE REQUIREMENTS FOR THE DEGREE OF

Master of Science

in

THE FACULTY OF GRADUATE STUDIES

(Mathematics)

The University of British Columbia

September 2005

© Alexandra Jilkine, 2005

Abstract

Rho family GTPases play an essential role in cell motility, transducing extracellular signal to the actin cytoskeleton. This thesis presents the formulation and analysis of several models concerning three members of the Rho family: Cdc42, Rac, and Rho. Experimental observations of the spatio-temporal dynamics of these proteins give evidence of spatial polarization and mutual exclusion between Cdc42/Rac and Rho, which suggests that the Rho protein system is bistable. Biochemical evidence shows that there is crosstalk between the Rho proteins. However, current biological literature includes multiple (and often contradictory) hypotheses about these mutual interactions. We idealize the indirect pathways between the Rho proteins as direct effects (positive or negative feedback from one protein to another), and investigate the various proposed interactions to determine which of them can give rise to a bistable "toggle switch", alternating between a high level of Cdc42/Rac, low level of Rho steady state and low level of Cdc42/Rac, high level of Rho steady state. We discuss the biological interpretation of our findings.

Next, we investigate a spatial variant of a model with suitable interactions to determine if it can give rise to spatial segregation of Rho proteins. We find that in a suitable parameter regime, a small initial gradient of one of the proteins will become amplified and give rise to long-lasting spatial segregation of Cdc42/Rac and Rho. On a longer timescale, the system eventually reaches a spatially uniform high Cdc42/Rac and low Rho steady state.

Finally, a multi-compartment model for the activation of a single Rho family GTPase that includes a greater level of biological detail is developed. Parameter values for this model are obtained from biochemical literature. This compartment model can be used as a subunit in more realistic models of cell polarization and motility when further details of the biochemistry and interactions of the Rho proteins emerge from experimental data.

Contents

List of Tables

List of Figures

List of Abbreviations

Arp2/3	actin-related protein 2/3
DH	Dbl homology
ECM	extracellular matrix
GDP	guanosine diphospate
GTP	guanosine triphosphate
GEF	guanine nucleotide exchange factor
GAP	GTPase-activating protein
GDI	guanine nucleotide dissociation inhibitor
MLC	myosin light chain
PAK	p21-activated protein kinase
PH	pleckstrin homology
PI	phosphatidylinosytol
PI3K	phosphatidylinosytol 3-kinase
PIP$_2$	phosphatidylinosytol-4,5-biphosphate
PIP$_3$	phosphatidylinosytol-3,4,5-triphosphate
PIP5 kinase	phosphatidylinosytol 4-phosphate 5-kinase
PIX	PAK-interacting exchange factor
ROCK	Rho kinase
SCAR	suppressor of cAMP receptor
WAVE	WASP family verpolin-homologous protein
WASP	Wiskott-Aldrich syndrome protein

Acknowledgements

Chapter 1

Biological Background

1.1 Introduction

Cell migration is an essential process for both multicellular and unicellular organisms. Single celled organisms such as the cellular slime mold *Dictyostelium* migrate in search of food. For multicellular organisms such as ourselves, cell migration is necessary for fetal development, wound repair, and functioning of the immune system. Cancerous cells need to develop the ability to invade surrounding tissue in order to become malignant. Preventing migration of these cells could be important in halting disease.

Cell motility is directed by extracellular factors, often acting as either attractants or repellents. Directed motion in response to an external chemical gradient is known as chemotaxis. These extracellular cues stimulate membrane receptors to elicit complex intracellular changes that allow a cell to move. Cells move forward by coordinating protrusion at the front of the cell and retraction at the rear. The driving force behind cell motility is the polymerization and depolymerization of the actin cytoskeleton, a highly dynamic network of protein filaments found in all eukaryotic cells (Alberts et al., 1994).

Many different molecules are involved in cell migration, including but not limited to, calcium, mitogen activated protein kinase (MAPK), protein kinase C, and phospholipids (Raftopoulou and Hall, 2004; Ridley, 2001b). The small GTPases of the Rho family have emerged as key players among these numerous molecules. They connect membrane receptor signalling with the assembly and disassembly of the actin cytoskeleton. The Rho proteins regulate the rates of actin filament polymerization, capping, and branching. Hence, these proteins play an important regulatory role in all cellular processes driven by actin polymerization, in particular, cell movement. Furthermore, interactions between these proteins link together the processes of membrane protrusion and cell adhesion. Thus, an understanding of these interactions is fundamental to obtaining a better picture of how cells move.

This chapter gives an overview of what is currently known about the Rho GTPases

and their relationship to cell motility. In the following chapters of the thesis, mathematical models that describe temporal and/or spatial distribution of Rho GTPases in motile cells are formulated. We use modelling to address the following questions about the Rho proteins:

1. Can interactions of the proteins proposed in the literature explain the spatial segregation of the proteins in moving cells?

2. Which proposed interactions of the Rho proteins are consistent with the bistable switch behaviour?

3. What biochemical interactions are necessary for switch dynamics?

4. How do the three classes of proteins associated with regulating activity of the small G-proteins regulate the distribution of the protein between active/inactive and membrane-cytosol compartments?

1.2   The Rho Family Proteins

Small GTP-binding proteins are monomeric members of the GTP-binding proteins (G-proteins) superfamily. These proteins consist of a single subunit with molecular mass of 20-30 kDa. Like the larger heterotrimeric G-proteins, they cycle between an active GTP-bound state, and an inactive GDP-bound state, acting as molecular switches in signal transduction pathways. More than a hundred small G-proteins have been identified in eukaryotes and subdivided into five families: the Ras, Rho, Rab, Sar1/Arf and Ran (Takai et al., 2001). Originally identified as Ras-homologous proteins, members of the Rho family came to the attention of biologists when it was discovered that they regulate cytoskeletal reorganization in 1991 (Ridley, 2001a).

We are interested in three of the best studied members of the Rho family: Cdc42, Rac1 and RhoA. These proteins have been shown to regulate cytoskeletal reorganization in numerous mammalian cell types. There is a Rac subfamily (Rac1,Rac2,Rac3, and RhoG) and a Rho subfamily (RhoA, RhoB, and RhoC), comprised of proteins that have similar, though not identical, properties. Current knowledge is predominantly of RhoA and Rac1, which – unlike some of their close relatives – are ubiquitously expressed and assumed to be essential players in cytoskeletal organization in all mammalian cell types. For example, Rac2 is present only in hematopoietic cells, and Rac3 is most highly expressed in the brain (Wennerberg and Der, 2004). Swiss 3T3 fibroblasts, one of the most intensively studied cell lines, contain RhoA, but not RhoB or RhoC (Zerial and Huber, 1995). Hence, we will refer to RhoA and Rac1 proteins as Rho and Rac in the rest of this thesis.

Most of what we know about the Rho proteins' effect on the cytoskeleton comes from the analyses of cell phenotypes exhibited by constitutively active and dominant

negative forms of small G-proteins expressed in, or injected into cells. Constitutively active proteins cannot hydrolyze GTP, remaining in a perpetually active state once activated. Dominant negative forms of a protein have one defective copy of a gene coding for this protein. This is sufficient to have a negative impact on the biological process regulated by the protein. The effect of using constitutively active or dominant negative proteins on motility depends both on the cell lines used and the types of experiments, and is described in the next section.

1.3 Effects of Rho GTPases on Cytoskeleton, Cell Adhesion and Cell Motility

Active Rho is necessary for the formation of stress fibers (actin-myosin filament bundles), formation and maintenance of focal adhesion complexes (integrin containing junctions that connect the stress fibers to the extracellular matrix), and for the contraction of the cell body. It is generally found that constitutively active Rho will actually inhibit cell movement (Ridley, 2001b). It is believed that Rho needs to repeatedly go through the activation cycle to enable turnover of stress fibers and focal adhesions that occurs when a cell moves. A high level of Rho activity means that adhesion to the extracellular matrix is very strong and the cell simply cannot move. However, some cells such as macrophages and neutrophils lack focal adhesions. There Rho only affects cell body contraction, not adhesion (Ridley, 2001b). Another commonly studied organism in cell motility studies, *Dictyostelium*, does not have stress fibers (Firtel and Chung, 2000).

Active Rac is required for the formation of lamellipodia and membrane ruffles [1]. Rac activity is essential for cells to undergo protrusive activity and movement. Constitutively active Rac leads to increased number of pseudopodia and up-regulation of the actin cytoskeleton. Expression of dominant negative Rac prevents pseudopod formation and movement (Ridley, 2001b).

Cdc42 is considered to be the master regulator of polarity in cells from such diverse organisms as humans and yeast (Etienne-Manneville, 2004). Dominant negative Cdc42 greatly reduces the ability of a macrophage to move towards a signal by chemotaxis. These cells move randomly, not following the gradient. This experiment, as well as other evidence, suggest that Cdc42 activity is needed to establish polarity, but is not essential for movement (Nobes and Hall, 1999). Active Cdc42 promotes actin polymerization and is required for extension of filopodia [2]. Rac and Cdc42 also regulate the formation of much

---

[1]**Lamellipodium**– a thin broad membrane protrusion found at the leading edge of migrating cells. Areas of lamellipodium that do not adhere to the substratum project upwards forming **membrane ruffles** (Lodish et al., 2000).

[2]**Filopodia** – thin finger-like projections of membrane used for exploratory purposes (Lodish

smaller, weaker focal complexes associated with lamellipodia and filopodia.

The downstream pathways of the Rho proteins are discussed in Section 1.7 and summarized in Figure 1.3.

1.4   Guanosine Exchange Cycle of the Rho Proteins

In this section the activation-inactivation cycle of the small G-proteins is described. As shown in Figure 1.1, the Rho proteins undergo two coupled cycles: cycling between GDP-bound and GTP-bound conformations, as well as cycling between cytosolic and membrane-bound forms. These two cycles are regulated by three classes of proteins: GEFs (guanine nucleotide exchange factors), GDIs (GDP dissociation inhibitors) and GAPs (GTPase-activating proteins). In Chapter 4 of this thesis, we develop a mathematical model of the activation/inactivation cycle of Rho proteins using experimentally determined parameters for the interaction of Rho proteins with GEFs, GAPs, and GDIs.

GDP-bound proteins are inactive (do not transduce signal). Upon activation, GDP dissociates from the inactive form. GTP binding to the protein then changes conformation of a region that binds a downstream effector (Takai et al., 2001). The small G-proteins intrinsically hydrolyze GTP, thus returning to inactive form after some time. This hydrolysation of GTP is why G-proteins are also called GTPases. I discuss each of the regulators of Rho activation cycle below.

1.4.1   Guanine Nucleotide Exchange Factors (GEFs) and nucleotide exchange

By itself, the dissociation of GDP from the GDP-bound form is an extremely slow reaction, so it is stimulated by various GEFs (also called GEPs or guanine nucleotide exchange proteins in the literature). These, in turn, are regulated by an upstream signal. GEFs accumulate at the leading edge of a motile cell and are believed to function on membranes (Itoh et al., 2002). A GEF releases bound GDP from a Rho protein and forms a binary complex with the protein. The GEF in the complex is then replaced by GTP. See Figure 1.2 for a detailed diagram of the nucleotide exchange process.

Some GEFs are specific for one particular small G-protein. For example, Lbc is specific for Rho, Tiam1 for Rac, and FGD1 for Cdc42 (Mackay and Hall, 1998). Other GEFs, such as Dbl and Vav, are active on all three of Cdc42, Rac, and Rho (Mackay and Hall, 1998). There are about 60 mammalian GEFs which share a DH (Dbl homology) domain that catalyzes the exchange of guanine nucleotides, and is the active site for the GEF activity (Zheng, 2001). More recently, a second Dock family of GEFs, which does

---

et al., 2000).
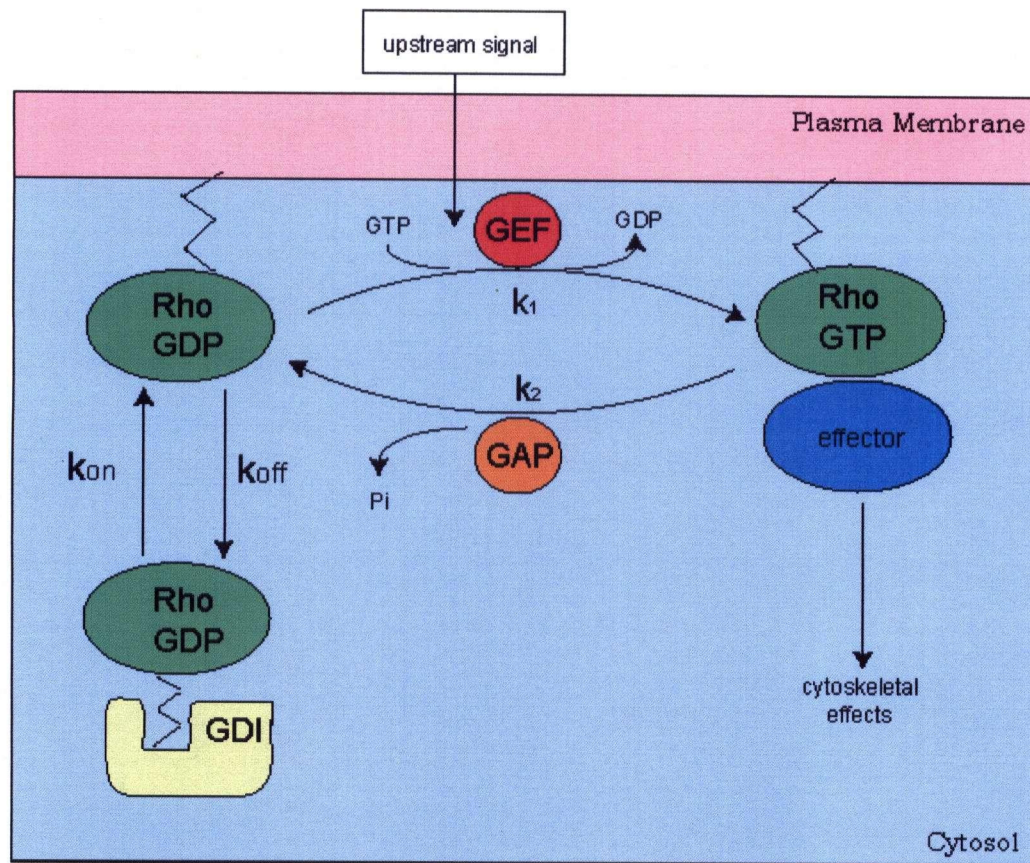
Figure 1.1: Regulation of the activation cycle of the Rho family proteins by GEFs, GAPs, and GDI. On the membrane GDP-bound forms are converted to GTP-bound forms at the rate k_1 with the help of a GEF. Active, GTP-bound forms hydrolyze GTP with the help of a GAP at the rate k_2. Rho GDI preferentially interacts with the GDP-bound forms. Hence, Rho-GDP translocates to the membrane at rate k_{on}, and comes off the membrane at the rate k_{off}. GDI binding leads to inhibition of both GDP dissociation and GTP hydrolysis.

not contain the DH domain, has been discovered (Cote and Vuori, 2002). Dock family GEFs act downstream of integrin receptors (Raftopoulou and Hall, 2004). At the present much more is known about Dbl-homologous GEFs. For a more comprehensive review of DH family GEFs see Zheng (2001) and Schmidt and Hall (2002).

In eukaryotic cells, GEF families outnumber their substrates by a factor of three, so multiple GEFs are capable of activating one GTPase (Schmidt and Hall, 2002). Why there exist so many apparently functionally redundant GEFs is not known, but this over-abundance might be the reason why cellular response to the same stimulus can vary from one cell type to the next. It is possible that, through subcellular localization or additional protein-protein interactions, GEFs can determine which downstream pathways are
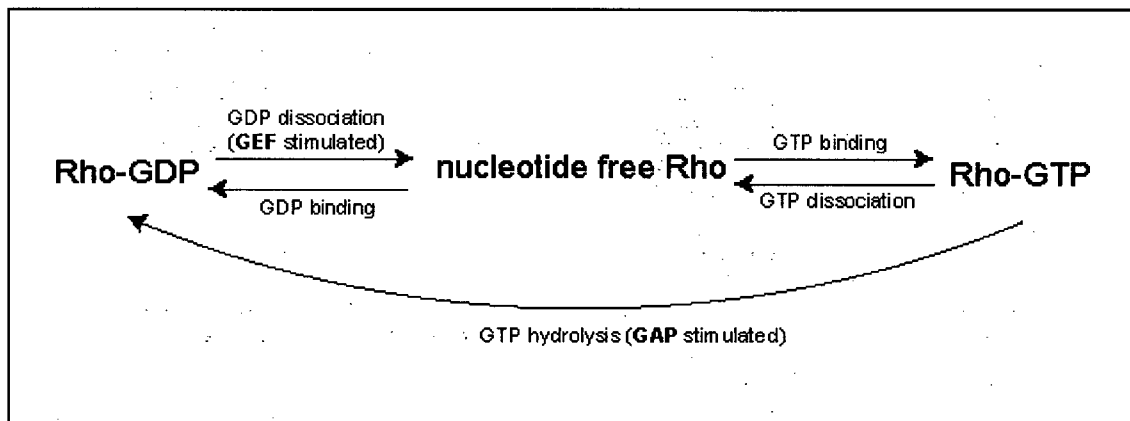
Figure 1.2: A detailed diagram of the nucleotide exchange cycle for a general Rho family protein.

activated by the active protein (Schmidt and Hall, 2002).

Next to a DH domain in a GEF there is a PH (pleckstrin homology) domain, that is common to many molecules involved in cell signalling. Chemoattractants induce the appearance of binding sites for PH domain containing proteins on the leading edge of the cell. These PH binding sites are sharply localized to the stimulated edge of chemotactic cells, even though the change in receptor occupancy between the front and back of the cell is very small (less than 10%) (Parent and Devreotes, 1999). The appearance of these PH domain binding sites is transient for a uniform concentration of chemoattractant, and persistent for a gradient. PH-binding sites appear even if the cell is missing a functional actin cytoskeleton and is incapable of movement (Parent and Devreotes, 1999). The PH domain can also bind to phosphoinositides like PIP_2 and PIP_3. It has been suggested that it is through PH domain interactions that GEFs become activated by extracellular signalling and recruited to membranes (Paduch et al., 2001). In some GEFs, the PH domain negatively regulates the DH domain, and PIP_3 binding relieves this inhibition (Ridley, 2001a). Since PIP_3 is a second messenger that is produced at the leading edge, this can lead to an increase in GEF activity at the leading edge of a cell.

1.4.2 GTPase-activating proteins (GAPs) and GTP hydrolysis

The second class of regulatory proteins, GAPs, stimulate the rate of GTP hydrolysis of the Rho proteins, causing their inactivation. Some GAPs such as p190 act on all three of Cdc42, Rac, and Rho (at least *in vitro*). Others are specific to only one or two of the Rho proteins. There are about eighty different proteins, containing a 140 amino acid long RhoGAP-homology domain, encoded in the human genome. Just as with GEFs, we do not know why there are so many proteins that can potentially downregulate Rho activity.

Many of them have other domains or binding interactions, suggesting other functions. As with GEFs, GAP activity might also be inhibited by another domain of the GAP molecule. This inhibition can be relieved by phosphorylation (Ridley, 2001a). In general, phosphorylation of GEFs and GAPs is a probable mechanism of Rho activity regulation by tyrosine kinase receptors.

1.4.3 Rho GDP Dissociation Inhibitors (GDIs)

The third class of regulatory proteins, GDP Dissociation Inhibitors (GDIs), inhibit the dissociation of the guanine nucleotide, keeping the proteins in one conformation. When bound to GDI, the Rho protein cannot interact with its downstream effectors (Del Pozo et al., 2002). RhoGDI also regulates the association of the Rho family proteins with membranes. GDI has been shown to extract the GDP-bound form of Rho proteins from the membrane to the cytosol, where they are sequestered in an inactive pool (see section 1.5).

In contrast to the numerous GEFs and GAPs, only three RhoGDIs have been identified. RhoGDI-1 (α) binds equally well to RhoA, Rac1, and Cdc42. In contrast, RhoGDI-2 (β) does not bind well to RhoA,Rac1, and Cdc42, binding instead to other less well-known members of the Rho family. RhoGDI-3 (γ) binds with a low affinity to RhoA and Cdc42, and does not bind to Rac1 (Wennerberg and Der, 2004; Olofsson, 1999). Hence, there is essentially only one type of GDI that binds to all the Rho proteins we are interested in. Rho GDI is discussed in more detail in the next section. For a detailed review of GDIs see (Olofsson, 1999).

1.5 Membrane Translocation Cycle of the Rho Proteins

Cdc42, Rac, and Rho are synthesized in the cytosol, and then modified by addition of lipid prenyl group (related to cholesterol) at their C termini. This end then anchors the proteins to the plasma membrane (Robbe et al., 2003; Wennerberg and Der, 2004). Prenylation is often used as a membrane insertion signal (Alberts et al., 1994). The proteins also have an additional tag, referred to as the membrane compartment localizing signal in the literature, which further targets the proteins to specific membrane sites (unknown at this point) (Wennerberg and Der, 2004).

Rho GDI interacts primarily with the GDP-bound form: the efficiency for interaction with the GTP-bound form of the protein is only about 10% of that for the GDP-bound form (Sasaki et al., 1993), although cases of equal strength interaction have also been reported (Nomanbhoy and Cerione, 1996). Both RhoA-GDI1 and Rac1-GDI1 complexes isolated from the cytosol of neutrophils and macrophages were found to contain GDP as the only bound nucleotide at a ratio of one mole of GDP per one mole of complex (Olofs-

son, 1999). However it is possible that under other conditions, GTP-bound proteins may also be in a complex with GDI (Del Pozo et al., 2002).

NMR and X-ray crystallography studies of the Cdc42/GDI complex have shown that GDI binds to two domains of Cdc42, leading to inhibition of GDP dissociation and GTP hydrolysis, and capturing the lipid-modified C-terminus in a hydrophobic pocket within the GDI molecule, allowing the protein to remain in the cytosol (Paduch et al., 2001; Robbe et al., 2003). The proteins have to stay in complex with the GDI in order to remain soluble in the cytosol. The concentration of RhoGDI-1 in the cell is about the same as that of the Rho proteins (Michaelson et al., 2001). In resting cells, the majority of the Rho proteins are cytosolic, and must therefore be bound to GDI. This suggests a high affinity of GDI for Rho proteins, that could be disrupted when a cell is activated.

Unfortunately, the membrane translocation cycle of the Rho proteins is not as well understood as the guanosine exchange cycle. The currently accepted model is that the GDP-bound form of the Rho proteins is present in the cytosol in an inactive 1:1 complex with GDI. GDP needs to dissociate from the inactive form, GTP needs to bind, and GDI needs to be released (though not necessarily in that order) so that the Rho protein can translocate to the membrane to interact with specific effectors (Takai et al., 2001). After performing their function, the proteins are converted to the GDP-bound form by GAPs. They then form a complex with GDI, and return to the cytosol. However, it is not known if all of GDP-bound form returns to the cytosol or if some remains on the membrane. This question is addressed with mathematical modelling in Chapter 4.

The mechanism by which GDI is released from the Rho family proteins is also not yet known. Bokoch et al. (1994) showed that release of Rac from GDI occurred only in the presence of GTP and a membrane component, and not in the presence of membrane and GDP. Two schemes have been suggested for coupling nucleotide exchange to membrane translocation. In the first, guanosine exchange takes place first, and translocation occurs later. In the second, membrane translocation occurs before the GTP-GDP exchange. Robbe et al. demonstrated that the soluble Rac-GDI complex is very poorly activated by the DH-PH domain (active GEF site) (Robbe et al., 2003). Hence Rac has to dissociate from GDI and translocate to the membrane before it can be activated by a GEF.

It is generally believed that the G-protein has to be both in the GTP-configuration and membrane-bound to interact with its effectors and trigger a cellular response, so the cytosolic form of the proteins is assumed to be inactive. When activated, the proteins are translocated to specific membrane sites. However, little is known about the molecular mechanism, that allow the delivery and translocation of Rho proteins to specific sites in cell membranes. It was shown that GDI delivers GTP-bound Rac and Cdc42 to new sites of integrin adhesion at the leading edge of a motile cell (Del Pozo et al., 2002).

It should also be mentioned that mutations that render Rho proteins constitutively

active or dominant negative interfere with binding to GDI, so the proteins will be found bound to plasma and internal membranes (Michaelson et al., 2001).

Some controversies regarding GDI still remain unsolved. The group of Beliveau argues that there is another population of Rho proteins that do not interact with GDI. In their experiments, some of the protein could not be extracted from membrane by GDI (Bilodeau et al., 1999). They also suggest that some of the cytosolic protein is not complexed with GDI, without explaining how that is possible, since post-translational modification (prenylation) should anchor the protein to the membrane. They believe that there is another physiological factor determining whether RhoA interacts with GDI or not. In a later paper they suggest that phosphorylation of the small G-proteins further regulates interaction with GDI and extraction from the membrane (Forget et al., 2002).

Another question that has been raised is whether GDI interacts with the GDP-bound forms of the protein only, or also with the GTP-bound form. Early studies reported that GDI has 10 fold higher affinity for GDP-bound form than for GTP-bound form (Sasaki et al., 1993). But some groups later suggested that GTP-bound forms can also be in complex with GDI in the cytosol (Del Pozo et al., 2002). However, since they are bound to GDI, these GTPases would not be able to interact with downstream effectors. So, although in some circumstances GTP-bound proteins might be present throughout the cell, rather than just on the membrane, it is in regions where membrane translocation is taking place that a small G protein would be able to interact with its effectors. Thus, GDI also controls the spatial distribution of the active Rho proteins.

1.6 Activation of Rho Proteins in Cells

The Rho family proteins become activated in response to various extracellular signals including soluble cytokines, growth factors, and extracellular matrix proteins. Activation occurs via GEFs. For example the Vav family of GEFs are recruited to activated receptors, where they undergo tyrosine phosphorylation, which increases their GEF activity. These GEFs are downstream of EGFR (epidermal growth factor receptor), PDGFR (platelet derived growth factor), as well as Ras. The activation of Rho GTPases is very closely tied to the phosphoinositides. There is a positive feedback loop between PI3K (phosphoinositide 3-kinase) and the Rho proteins (Srinivasan et al., 2003; Weiner et al., 2003; Wang et al., 2002).

The specific mechanism of RhoA activation (as opposed to general principles of activation by GEFs) during cell migration has not been well studied (Raftopoulou and Hall, 2004). More effort has focused on Rac and/or Cdc42 activation.

Rac can get activated by both tyrosine kinase receptors and heterotrimeric G-protein-coupled receptors. This pathway is dependent on PI3K (phosphoinositide 3-

kinase).Two Rac GEFs, Tiam1 and Vav1, are regulated by PI3K products (Ridley, 2001b). The product of PI3K, PIP_3, accumulates at the leading edge of migrating cells via a feedback loop involving Rac (Srinivasan et al., 2003; Weiner et al., 2003). Inhibition of PI3K blocks Rac activation (Ridley, 2001b), and generation of PIP_3 is known to be essential for receptor-mediated activation of Rac (Hall, 1998).

Cdc42 can also be activated by tyrosine kinase receptors in response to growth factors such as epidermal growth factor (EGF) and platelet derived growth factor (PDGF). Like Rac, Cdc42 is activated at the leading edge of motile cells via the PI3K pathway. Unlike Rho and Rac, there has been no reports that PIP 5-kinase is an effector of Cdc42. Cdc42 can also be activated by signals that do not activate Rac. Heterotrimeric G-protein signalling as a response to the chemoattractant C5a activates Cdc42, but not Rac in neutrophils (Etienne-Manneville, 2004).

In addition to soluble factors, the Rho GTPases are also regulated by adhesion to the extracellular matrix (ECM) via transmembrane receptors called integrins. The integrin signalling pathways have not been studied for as long as receptor-mediated activation by soluble factors, but several pathways relating to Rho proteins have been found. Integrin engagement results in a transient decrease in Rho activity, followed by activation (DeMali et al., 2003). The Rac GEF Vav1 is downstream of integrin engagement (DeMali et al., 2003). Also, as stated in an earlier section, integrins can target GDI to sites of adhesion (Del Pozo et al., 2002).

1.7 Downstream Targets of Cdc42/Rac/Rho

Rho GTPases regulate the activity of numerous proteins. These effector [3] proteins clearly link the Rho family to the assembly of filamentous actin. The signal-transduction pathways from the Rho proteins to the cytoskeleton are shown in Figure 1.3 and discussed in more detail below. However, we do not include effectors of Rho proteins in the modelling, and they do not form a major theme in the thesis.

Small G-proteins transduce signals to their downstream effectors only when they are in their active GTP-bound form. Many effectors have autoinhibitory domains, becoming activated when a Rho protein binds and releases this inhibition. This method of activation has been conclusively shown for scaffold proteins such as WASP, Dia, and is believed to hold for other effectors as well (Bishop and Hall, 2000). Rac and Cdc42 have quite a few common downstream effectors, but Rho downstream pathway differs significantly from the Cdc42/Rac pathway, in that it alone affects myosin. Many of the Cdc42/Rac targets, such as WASP, contain a conserved Cdc42/Rac interacting domain (CRIB domain), that binds only the GTP-bound forms (Takai et al., 2001). Hence, markers for

---

[3]Effectors – proteins that bind to Rho GTPases only when the GTPases are in an active state.
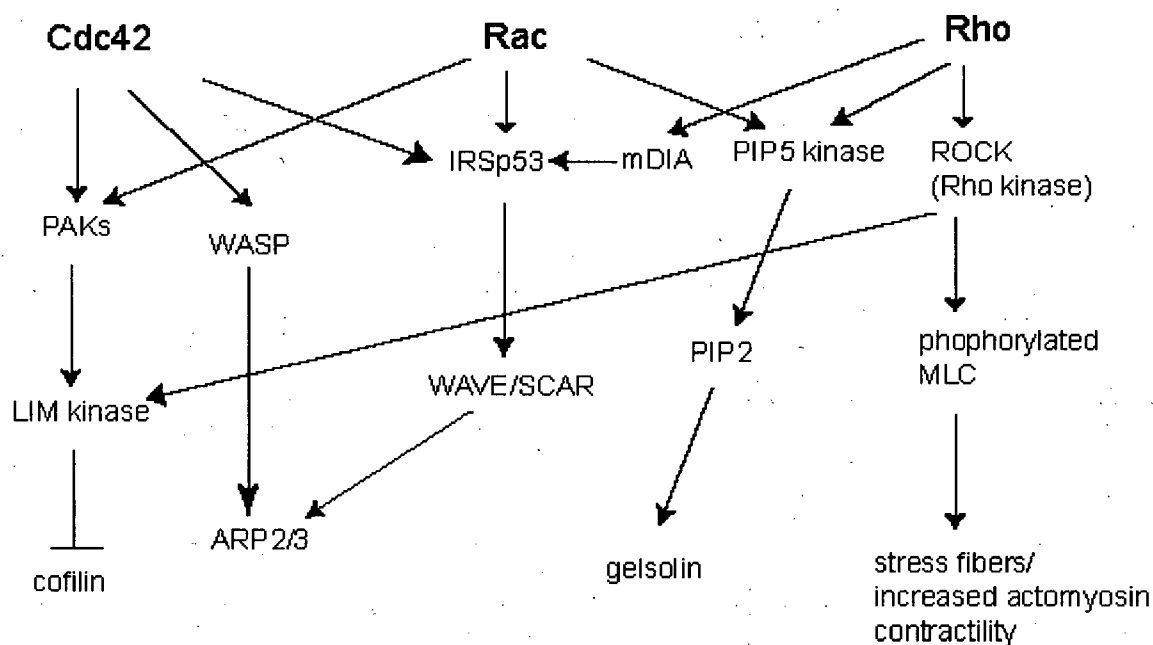
Figure 1.3: Downstream effectors of Cdc42, Rac, and Rho compiled from the following review papers: (Bishop and Hall, 2000; Matozaki et al., 2000; Ridley, 2001a,b). Effectors that have functions unrelated to the cytoskeleton are not shown. See list of abbreviations for full names of effectors. Cofilin, Arp2/3, and gelsolin are actin related proteins. Cofilin cleaves existing filaments, Arp2/3 allows nucleation of filaments, and gelsolin cuts filaments and caps their ends.

measuring or visualizing active Cdc42/Rac proteins often contain the CRIB domain.

1.7.1 Rac Targets

Active Rac stimulates actin polymerization by stimulating the Arp2/3 complex (via the WAVE protein complex). Arp2/3 initiates the formation of new actin filaments on the sides of existing actin filaments, forming a branching actin network. Rac also stimulates actin polymerization by promoting formation of PIP_2. This PIP_2 then binds to capping proteins and removes them from barbed ends of actin filaments at or close to the plasma membrane. Rac also inhibits actin depolymerization by stimulating the activity of LIM-kinase that phosphorylates and inactivates cofilin, a protein that promotes actin depolymerization.

1.7.2 Cdc42 Targets

Cdc42 stimulates actin polymerization by interacting with WASP (Wiscott Aldrich Syndrome protein) and the related N-WASP, leading to activation of the Arp2/3 complex. Note that Rac stimulates activation of Arp2/3 by a different protein complex, WAVE. Both WASP and Arp2/3 are necessary for Cdc42 to trigger actin filament assembly. In a cell free system, Cdc42 was found to stimulate actin polymerization independent of PIP_2 (Mackay and Hall, 1998). However, maximal actin polymerization also requires PIP_2 (Schmitz et al., 2000). Active Cdc42 also directly interacts with part of the cytoplasmic complex that coats membrane regions and promotes budding and formation of vesicles (Helmreich, 2001). So Cdc42 regulates transport between ER and Golgi, explaining why it is often found localized at the Golgi.

1.7.3 Rho Targets

Rho stimulates myosin light chain (MLC) phosphorylation via its downstream target ROCK (Rho kinase) (Ridley, 2001b). The increased level of phosphorylated MLC promotes the interaction of myosin filaments with actin filaments and increases contractility. Rho also activates mDia proteins that together with ROCK induce stress fiber formation. Dia also interacts with profilin, an actin binding protein (Schmitz et al., 2000). ROCK can also phosphorylate LIM-kinase, which, as stated above, will inhibit actin depolymerization through cofilin. Another way Rho can induce actin accumulation is by activation of PIP 5-kinase which will increase PIP_2 levels (Ridley, 2001b).

1.7.4 Conclusions

Rho GTPases have a wide range of cellular targets. Over thirty have been identified as of now (Bishop and Hall, 2000). Most of these targets link the Rho family to cytoskeletal

reorganization. I've described some of the more well-studied effectors such as WASP and ROCK that are known to affect the cytoskeleton, but I did not discuss proteins whose function is unclear, or which serve a specific function in specialized cells. Numerous specialists in the field have suggested that Rho GTPases might interact with different effectors depending on cellular context. However, spatio-temporal differences in GTPase target activity is a big unknown at the present.

1.8   Localization of Rho Proteins in Cells

The location of active Rho family proteins in live mammalian cells has been surveyed by different methods and continues to be an active area of research. It is of particular interest to us, as models of spatial redistribution of Rho GTPases are discussed in Chapter 3

Pull down assays use domains from Rho targets, such as the CRIB domain mentioned in the previous section, that bind only to GTP-bound small G-proteins. Cells are lysed after some time, and the amount of GTP-bound or total protein in the cell at that time is measured. These methods provide no spatial information about protein location, and limited temporal resolution compared to fluorescence methods.

Another visualization method involves producing Rho GTPases that are fused with green fluorescent protein (GFP). The fluorescent protein is transfected into a live eukaryotic cell and visualized by fluorescence microscopy. This method does not distinguish between the active and inactive forms of the Rho protein. The Rho proteins are typically overexpressed in these experiments, and the amount of overexpressed protein exceeds the amount of available GDI that would keep the protein inactive in the cytosol. Thus, the results obtained may not be the same as for endogenous Rho proteins. Another problem with this technique is that GFP-proteins are diffusely dispersed throughout the cell, resulting in a high background noise (Pertz and Hahn, 2004).

Regardless, GFP labelled proteins provided many insights. Michaelson et al. (2001) found that GFP-Rac1 was found predominantly in the plasma membrane. GFP-RhoA was found mainly in the cytosol with only a small amount detected on the plasma membrane (Michaelson et al., 2001). Both Michaelson and other groups found that Cdc42 localizes in the cytosol with enhanced activity on the endoplasmic reticulum (ER) and Golgi complex in addition to being present on the plasma membrane (Ridley, 2001b; Zerial and Huber, 1995). This is probably due to the fact that Cdc42 is involved in regulating ER to Golgi transport and reorienting the Golgi apparatus in direction of cell movement (Hall, 1998).

Expression levels of the GFP-GTPases that were closer to endogenous levels showed more of the fluorescent proteins in the cytosol (due to presumed interaction with GDI). Overexpression of GDI also led to more proteins being present in the cytosol. The membrane compartments to which the proteins localized did not change as a result of these

experiments. Studies of GFP labelled proteins cannot reveal if the membrane-bound small G-proteins were GTP-bound or not. However, transfection of a GEF, Dbl, leads to morphological changes in cells consistent with activated Cdc42/Rac and a redistribution of GFP-labelled Cdc42 and Rac1 to the lamellipodia membrane at the same time is clearly observed.

Newer, more sensitive techniques use fluorescence resonant energy transfer (FRET) to detect Rho family protein activation with a high spatial resolution. FRET detects the interaction of two proteins that have been tagged with a FRET donor/acceptor pair. By using a domain of a Rho protein effector as one of the proteins, FRET can be used to detect when a GTPase undergoes activation and binds to the domain (Pertz and Hahn, 2004). This method was used by Krayanov et al. (2000), who found that, in migrating Swiss 3T3 fibroblasts, active Rac forms a gradient that is highest at the leading edge of the cells (see Figure 1.5). Furthermore, the activation of Rac was restricted to the sites of actin polymerization, independent of total Rac distribution in the cell. Later, the same group visualized active Cdc42 in fibroblasts (Nalbant et al., 2004). Because Nalbant et al. (2004) detected endogenous Cdc42, they could visualize activation of the protein at native concentrations found in the cell. Although their cells are not migrating, a high level of active Cdc42 can be seen at cell edges that are undergoing remodelling (see Figure 1.4). Following kinetics of Cdc42 activation during the extension and retraction of individual protrusions, Nalbant et al. (2004) found a close correlation between extension and retraction and the rise and fall of Cdc42 activation.

Itoh et al. (2002) also used FRET-based probes to measure the activation of Cdc42 and Rac in motile HT1080 cells. Because of the design of their probe, the labelled proteins were unable to interact with GDI and, thus, unable to come off the membrane. Itoh et al. (2002) detected gradients of active Cdc42 and Rac that were highest at the leading edge of the cell. When cells changed direction, these gradients rapidly decreased. They also demonstrated that activity of Cdc42 was highest right at the tip of the leading edge, while Rac activity was highest immediately behind the leading edge.

Unlike Cdc42 and Rac, direct visualization of active Rho in moving cells has not yet been done. It is believed that the distribution of active Rho correlates to the focal adhesion distribution (Bershadsky et al., 2003). Since active Rho is required for retraction of the cell body, it is believed to form an inverse gradient to that of Cdc42 and Rac (Raftopoulou and Hall, 2004).

It should also be mentioned that the relative levels of the Rho proteins in the cell vary with the extracellular matrix composition. Cells are able to respond to changes in matrix composition through crosstalk with integrins (Ridley, 2001b).
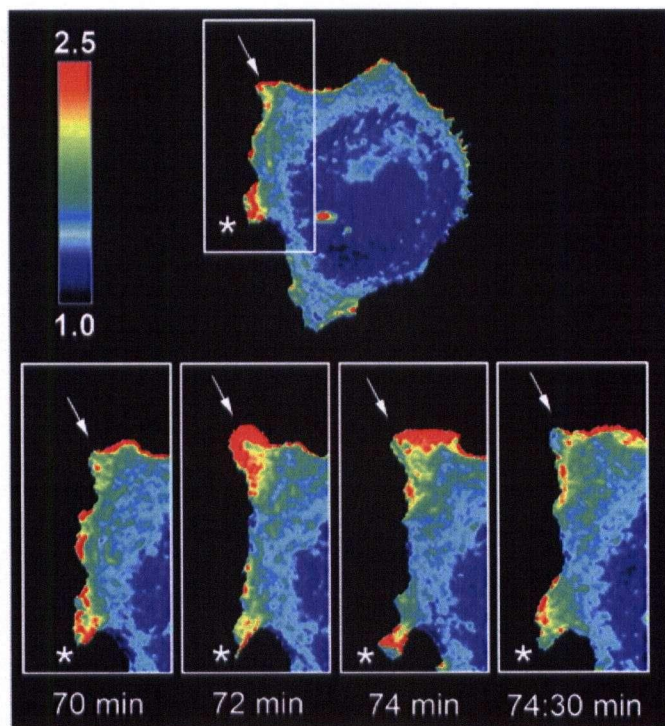
Figure 1.4: Activation of endogenous Cdc42 in a fibroblast during cell spreading. Cdc42 activity is highest (red) near the cell periphery. Cdc42 activity is lowest (blue) in the interior of the cell. Note that cellular protrusions (indicated by arrow and star) have the highest Cdc42 activity. Reprinted with permission from Nalbant et al. (2004). Copyright 2004 AAAS.
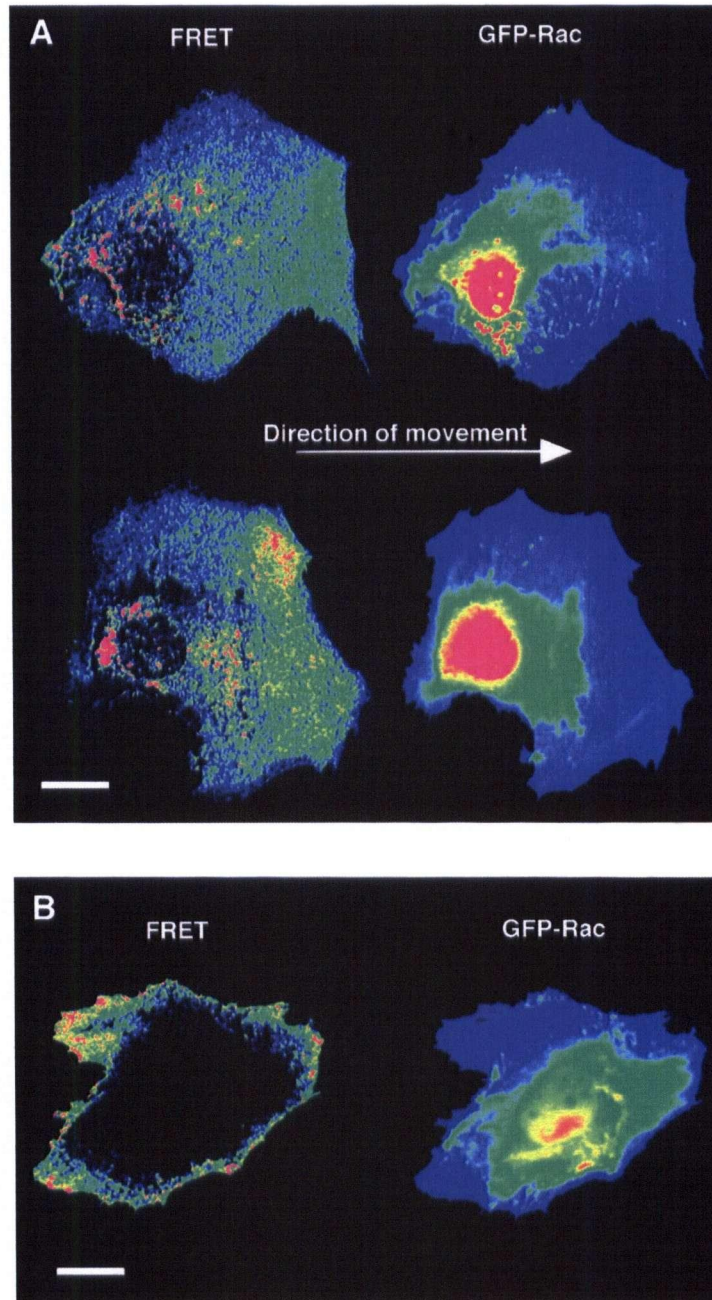
Figure 1.5: **A.** Rac levels in a moving fibroblast. FRET reveals active Rac levels only, while GFP-Rac reveals overall Rac distribution in the cell. The highest concentration of total Rac was seen around the nucleus (red). However, active Rac distribution forms a gradient that is high at the leading edge, where total Rac levels are lowest (blue). **B.** Rac distribution (active form and total) in a nonmotile cell. Here, active Rac is present only at the periphery of the cell, where it had been in contact with other cells in a monolayer. Reprinted with permission from Krayanov et al. (2000). Copyright 2000 AAAS.

1.9 Crosstalk between Cdc42, Rac, and Rho

So far we have outlined the various ways that Cdc42, Rac, and Rho can get activated via receptor mediated signalling, but different Rho family proteins can also activate one another. In Chapter 2 we will mathematically formulate various ways that Cdc42, Rac, and Rho can regulate each other. A polarized cell establishes a front (with high level of active Cdc42 and Rac and a low level of active Rho) and a back (with low level of active Cdc42 and Rac and high level of Rho). Therefore, the crosstalk has to be consistent with these observations. In Chapter 3 we will explore how one suggested Rho interaction pathway determines the spatial distribution of the GTPases.

1.9.1 Classic Rho Cascade

The first report of the crosstalk of Rho family proteins came from the group of Alan Hall (Ridley et al., 1992),who did experiments on Swiss 3T3 fibroblasts. The activation of Cdc42, Rac, and Rho by extracellular factors remains best characterized in those cells. Cdc42, Rac, and Rho can be activated by exposing cells to extracellular growth factors, microinjecting the cells with constitutively active form of the protein, or microinjecting the cell with GEFs. Microinjection of Cdc42 into the cell leads to immediate appearance of filopodia, followed by Rac dependent appearance of lamellipodia and membrane ruffles, then finally by Rho-dependent changes in stress fibers. Microinjection of Rac leads to immediate ruffling and formation of stress-fibers 5-10 minutes later. Microinjection of Rho leads to assembly of stress fibers and focal adhesion within 2 minutes, but no filopodia or ruffles form. Injecting Rac and an enzyme that inactivates Rho leads to ruffle formation, but no stress fibers. This suggests that there is a cascade of small G-protein activation, where active Cdc42 activates Rac, which activates Rho (Ridley et al., 1992; Nobes and Hall, 1995).

It must be pointed out that activation of Cdc42 is not required to activate Rac. However, the activation of Cdc42 is needed in order to restrict Rac activation to the leading edge of the cell (Mackay and Hall, 1998; Nobes and Hall, 1999). Rac is activated by receptor mediated signalling pathways, some of which are the same for both Cdc42 and Rac. However, Rac also responds to signalling from active Cdc42. A recent paper reports that activation of Cdc42 can lead to activation of Rac via allosteric regulation of a Rac-GEF Cool-2 by active Cdc42 (Baird et al., 2005).

1.9.2 Antagonism between Rac and Rho

The activation of Rac by Cdc42 has been observed in numerous other cell lines in addition to the Swiss 3T3. It couples Cdc42-dependent polarization of the cell to Rac-dependent protrusion, and is taken to be ubiquitous. The activation of Rho by Rac is a much more

17

contentious issue. Quiescent Swiss 3T3 fibroblasts have no detectable stress fibers, and when Rac is activated, there is a weak and delayed activation of Rho, producing a few stress fibers. In cells that already have abundant pronounced stress fibers (presumably that means they have higher Rho levels), Rac activation leads to loss of stress fibers (Ridley, 2000; Mackay and Hall, 1998).

After the initial report of Rac activating Rho in Swiss 3T3 fibroblasts, a large number of groups reported antagonism between Rac and Rho. In particular, Sander et al. (1999) reported that signalling by constitutively active Rac inhibited Rho in NIH 3T3 fibroblasts, while Rho activation did not affect the activity of Rac. (Sander et al., 1999) found inactivation of Rho by Rac in epithelial MDCK cells and Cos-7 cells. They proposed that a balance between Rac and Rho activity (Rho acting on Rac through inhibition of Cdc42) determines both the morphology of the cell and its migratory behaviour. Caron (2003) found that activation of Rac resulted in a three to four fold decrease in the levels of active GTP-bound Rho. Zondag et al. (2000) reported that downregulation of Rac activity leads to an increase in Rho activity in NIH 3T3 fibroblasts, supporting reports of Rac inhibiting Rho. Meili and Firtel (2003) concluded that Rac and Rho mutually inhibited each other in neutrophils.

1.9.3 Rac and Rho, Revisited

In many cell lines (particularly in neuronal cells) Rac and Rho seem to be antagonistic to each other and produce opposite morphological behaviour: Rho promotes cell contractility, while Rac promotes cellular protrusion. The contradictory evidence on when Rac activates Rho and when Rac inhibits Rho probably stems from the fact that in early experiments the level of activity of a particular GTPase was not measured, but inferred from appearance of phenotypic traits associated with Rac or Rho activation.

In later experiments, assays were performed on cell lysates that gave the total level of active GTPase in the cell at a specified time, but no spatial information about the distribution of active Rac and Rho in the cell. In addition, cell type, the Rac or Rho activator used, and the relative levels of the small G-proteins also play a role in whether activation or inactivation occurs. Consider the paper by Tsuji et al. (2002). They reported Rho-dependent Rac activation mediated by the Rho effector mDia. However, another Rho effector, ROCK, antagonizes this pathway, so this Rho-dependent Rac activation could only be observed when the ROCK pathway is selectively inhibited. However, only a low level of active Rho is needed for the mDia pathway, while the ROCK pathway requires a high GTP-Rho level. So, presumably, Rho will activate Rac when present in small amounts, but inhibit it in large amounts. To add another level of complexity to the issue, mDia was shown to localize to membrane ruffles in motile cells, while ROCK activity is crucial in the rear. Thus, the two Rho effectors have opposite effects on Rac, and may

operate in different locations in the cell.

1.9.4 Is Rho Crosstalk Occurring at the GTPase level?

It is natural to ask whether the crosstalk described above occurs because one protein is affecting the amount of active form of a different Rho protein, or if protein A is influencing the expression of downstream target(s) of protein B. Hall and coworkers concluded that Rho crosstalk occurs at the GTPase level based on the following indirect evidence. While Cdc42 injected cells give rise to Rac-dependent morphological changes, such as lamellipodia, Rac-null cells that are injected with Cdc42 do not exhibit lamellipodia, which is consistent with Cdc42 or its effectors activating Rac (Nobes and Hall, 1995). Similar reasoning was used to conclude that Rac activates Rho. Later papers provide more conclusive evidence that one GTPase can control the switch mechanism of another. Experimental techniques developed after the classic work of Hall allowed the total level of GTP-bound (active) form of a small G-protein to be measured, and compared with its GTP-level after the active form of another small G-protein has been added. In this way, it could be determined if one protein "activates" or "inactivates" another. Furthermore, the use of mutants unable to undergo cytoskeletal changes showed that reorganization of the cytoskeleton does not play a role in the inactivation of Rho by Rac (Sander et al., 1999).

Of course, crosstalk at the GTPase level does not in any way preclude Cdc42, Rac, and Rho's effectors influencing Rho GTPases' downstream pathways. Many pathways in a cell are "redundant" from a mathematical viewpoint. Combining such "redundant" signalling both upstream and downstream of the GTPases can allow polarization to be more spatially precise and occur on a faster timescale, as well as safeguard against mutations.

1.10 Mathematical Modelling and Rho GTPases

As has been shown in this chapter, Rho GTPases play a very important role in the motility of cells. Subject to intense research since the early nineties, a great deal of information is now known about these proteins. Much more remains to be learned. All the work on the Rho GTPases described above has been experimental. What can be learned from mathematical models? Previous mathematical treatments of chemoattractant gradient sensing and cell polarity focused on the phosphoinositide lipids (Levchenko and Iglesias, 2002; Krishnan and Iglesias, 2004; Subramanian and Narang, 2004) or unspecified second messenger molecules (Postma and Van Haastert, 2001). These theoretical papers contributed to the understanding of cellular response to chemotactic signals. However, to our knowledge, despite experimental observations of the spatial distribution of active forms of Rho family small G-proteins in moving cells (Krayanov et al., 2000; Nalbant et al., 2004),

no one has modelled the spatial segregation of Rho proteins or how it arises in polarized cells. Since the Rho proteins have been shown to have an essential role in cell polarization and affect the dynamics of F-actin formation, we feel that it is of interest to model their dynamics and distribution. Furthermore, a simple "Rho" model that mimics the dynamics of Rho GTPases in motile cells can be used as a module in more complicated models of the cytoskeleton.

Our immediate goal when undertaking this project was to look at various proposed pathways of interaction to determine if they can give rise to the spatial segregation of active Cdc42/Rac and Rho that is believed to exist. Little is actually known about the mechanisms responsible for the crosstalk between the small G-proteins. Based on the evidence in section 1.9.4 we believe that the Rho proteins interact with each other at the GTPase level via GEFs and GAPs. With the exception of an interesting work by Baird et al. (2005) on Rac-GEF Cool-2, which links Cdc42 activation to activation of Rac, the GEFs and GAPs in the Rho crosstalk cascades remain unidentified. Modelling can help shed some light on what is happening.

In Chapter 2 we proceed to formulate several nonlinear ODE models based on the various proposed schemes of Rho crosstalk. We analyze the steady state solutions of these models. In particular, we are interested if these models are capable of bistable behaviour that is consistent with the observed dynamics of the Rho proteins. In Chapter 3 we explore a spatial form of a crosstalk model that satisfies the bistable criterion. In Chapter 4 we return to the activation cycle of a single GTPase, and develop a more detailed model incorporating available biochemical data.

Chapter 2

Modelling the Interactions Between Rho GTPases

2.1 Modelling Approach and Hypothesis

This chapter is concerned with temporal dynamics of the Rho proteins. Our work is based on the following basic assumptions:

- The Rho proteins are not synthesized or degraded during cell polarization, but only undergo conversion between active and inactive forms. In other words, the total level of Cdc42, Rac, and Rho in the cell remains constant over the time scale needed for cells to polarize.

- The pool of inactive (cytosolic) Rac, Rho and Cdc42 is large, and not a limiting factor. Cytosolic forms diffuse approximately 100 times faster than the membrane-bound forms (Postma et al., 2004). We assume that the distribution of the cytosolic forms will be approximately homogeneous in space, even when the active forms are polarized on the membrane. As a result, we only keep track of the active forms of the Rho proteins on the cell membrane.

- Each Rho protein has a basal rate of activation (GTP-loading), and a basal turnover or inactivation rate (GTP-hydrolysis). Activation and inactivation of Rho proteins are indirect processes via the GEFs and GAPs, that were discussed in Chapter 1.

It is known that crosstalk occurs between the Rho small G-proteins (see Chapter 1). We want to investigate the hypothesis that crosstalk at the the GTPase level coupled to lateral diffusion of the proteins enables a cell to form a distinct front and back and become polarized. In this chapter we use mathematical modelling to address the following questions:

1. Which of the proposed interactions of the Rho proteins give rise to toggle switch behaviour, where a system can alternate between two stable steady states?

2. What biochemical interactions are necessary for a three component system to exhibit such dynamics?

Since the detailed biochemistry of the Cdc42/Rac/Rho crosstalk are not known at the moment, this investigation is meant to be an exploration of possible scenarios that might be occurring, rather than a strict formulation of one particular biochemical pathway. Our goal is to be able to answer whether crosstalk interactions, together with diffusion, can lead to spatial inhomogeneity and polarization; and if so, what form these interactions might take.

Since we are only considering the three pivotal Rho proteins (Cdc42, Rac1, and RhoA) in our modelling, we have to represent the indirect crosstalk pathways via other intermediates by simplified direct positive or negative effects, where the concentration of the active form of one protein affects the activation or inactivation rate of another. Since the current literature includes multiple hypotheses for how the small G proteins interact with one another, we test a variety of possible interaction schemes to determine which can give rise to the observed behaviour and which cannot. Modelling can then allow us to reject those schemes that cannot reproduce observed behaviour.

To avoid analyzing all possible interactions that can happen in a three component system, we focus on what is currently known about the interactions of Rac with Cdc42 and Rho. It is believed that Cdc42 activates Rac in a variety of cell types. Recently Baird et al. (2005) reported a mechanism for activation of Rac by Cdc42 via the Rac-GEF Cool-2. Hence we will assume that Cdc42 activates Rac unless noted otherwise.

Note that these models will not deal with additional downstream effects of the Rho proteins, and cannot shed any light on how Rho proteins interact with their effectors. We focus entirely on GTPase level crosstalk between the three Rho proteins only. We do not consider the additional crosstalk between the Rho proteins and Ras, which is known to occur. Crosstalk between Rho proteins and PI3K/PIP$_3$ is also not included at this stage.

2.2 Turing Patterns versus Bistability

If we assume that the Rho proteins move on the plasma membrane only by passive diffusion (no active transport), the spatiotemporal interactions of the active Rho proteins can be modelled by a reaction-diffusion system. Our goal is to investigate under which conditions the reaction-diffusion system can give rise to a spatial pattern similar to one that is observed in polarized cells. Before we begin modelling the spatial distribution of Rho

GTPases, we look at the temporal dynamics necessary for pattern formation in a reaction-diffusion system.

Spatial patterns in reaction diffusion systems are often formed by so-called diffusion driven or Turing instability (Murray, 2001). Diffusion driven instability is obtained when the presence of diffusion causes a stable spatially uniform steady state to become unstable. One of the necessary conditions for the occurrence of diffusion-driven instability is for different components of the system to have different rates of diffusion. The three Rho proteins are all roughly the same size (21 kDa) and diffuse at the same rate. In general, cytosolic proteins diffuse faster than membrane-bound ones, so there is a difference in the diffusion rates of cytosolic forms and membrane-bound forms of Rho GTPases. The diffusion coefficient of the membrane-bound Rho proteins is likely to be similar to that of membrane-bound Ras, around 1 $\mu m^2 s^{-1}$ (Goodwin et al., 2005). Cytosolic forms diffuse approximately 100 times faster than the membrane-bound forms (Postma et al., 2004). However, under our assumption that the cytosolic pool is large and homogeneously distributed, a Turing instability will not occur. Instead, we investigate if spatial patterns can form due to the presence of diffusion in a system with multiple linearly stable steady states.

Some feedback must occur between the proteins for multiple steady states to exist(Ferrell, 2002). Therefore, we begin by examining the crosstalk between the Rho GTPases that has been suggested in the literature to see if it consistent with multiple steady states. We look for an ODE (space independent) model that can have bistable behaviour, switching between a high level of Cdc42/Rac, low level of Rho steady state and low level of Cdc42/Rac, high level of Rho steady state. The simplest such system would have three steady states. Two of these (stable nodes/foci) would correspond to high Cdc42/Rac and low Rho level, and low Cdc42/Rac and high Rho level. The third, a saddle point, would separate the basins of attraction of these two states. Whether the system reaches a high Cdc42/Rac or high Rho steady state will depend on the initial conditions.

Since we are dealing with concentrations of proteins, all steady states need to be strictly non-negative. We assume that each protein is characterized by basic (mass action) production/decay kinetics, and want to determine biologically plausible kinetics for which such dynamics could occur. Once we investigate the well-mixed or local dynamic behaviour consistent with the known dynamics of Rho GTPases, in Chapter 3 we investigate if spatially inhomogeneous steady states can occur by incorporating diffusion of the proteins into the appropriate ODE model(s).

2.3 Interaction Pathways Proposed in the Literature

Based on the discussion above, we proceed to evaluate whether the Rho crosstalk pathways that have been proposed in the biological literature can have a high Cdc42/Rac, low Rho stable steady state and a low Cdc42/Rac, high Rho stable steady state. We do not judge the validity of the experiments on the basis of which these pathways were proposed. Instead, we would like to determine if any of these pathways can result in the type of bistability described in the previous section.

2.3.1 Case I (Nobes and Hall, 1995)

The first evidence of small G-proteins crosstalk was established by the group of Alan Hall during his classic microinjection experiments. Nobes and Hall (1995) propose an activation cascade, where Cdc42 activates Rac, which in turn activates Rho.

$$\text{Cdc42} \longrightarrow \text{Rac} \longrightarrow \text{Rho}$$

This pathway was proposed to explain small GTPase regulated cytoskeletal changes in fibroblasts. It was not hypothesized to lead to spatial redistribution. In fact, very little about the cellular localization of the Rho proteins was known when these experiments were performed.

The proposed cascade does not suffice for bistability. There is no feedback on Cdc42 from any of the other proteins, so Cdc42 will reach an equilibrium value independent of Rac and Rho levels. The Cdc42 steady state value, in turn, will determine the equilibrium level of Rac, and Rac level will determine that of Rho. Some feedback must occur between the proteins for multiple steady states to exist, so we need to look at other possible interactions between the proteins.

2.3.2 Case II (Mackay and Hall, 1998)

After the initial report of Rac activating Rho in Swiss 3T3 fibroblasts from the group of Hall, a large number of other groups reported antagonism between Rac and Rho, as discussed in Chapter 1. Based on this work Mackay and Hall (1998) suggested the following modification to the Rho crosstalk (activation represented by →, inhibition represented by ⊣).

$$\text{Cdc42} \longrightarrow \text{Rac} \rightrightarrows \text{Rho}$$

When a cell has few stress fibers, Rac will activate Rho, but Rac will inhibit Rho if a cell has numerous stress fibers. However, to develop a mathematical model based on this information, we need to know the conditions under which Rac-dependent activation of Rho

becomes Rac-dependent inhibition. Furthermore, as in Case I, lack of feedback to Cdc42 from the other proteins means that Cdc42 will reach an equilibrium value independent of Rac and Rho levels. The Cdc42 level will determine the equilibrium values of Rac and Rho.

2.3.3 Case III (Giniger, 2002)

Giniger (2002) speculated that a cycle of activation might be occurring rather than the activation cascade proposed by Nobes and Hall (1995). The suggested interactions are:
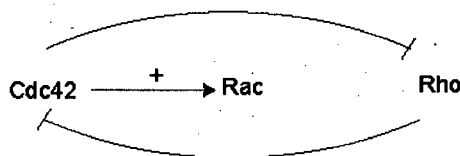
Giniger (2002) suggests that these interactions might explain the cyclic nature of the actin dynamics in neuronal growth cones. Further on, we show that this scheme can have bistable behaviour and lead to a spatial segregation of Cdc42/Rac and Rho in general cell types. Giniger (2002) does not postulate details of the crosstalk terms. In principle, each arrow could denote some effect (positive or negative) on a GEF or GAP that loads or removes GTP from a G-protein. We will explore possible types of effects in our modelling.

2.3.4 Case IV (Evers et al., 2000; Sander et al., 1999)

Evers et al. (2000) and Sander et al. (1999) claim that there is unidirectional inhibition of Rho by Rac at the GTPase level in various cell types. Cdc42 was also found to inhibit Rho, but it was not determined whether this was a Rac dependent effect. No effect on Rac was observed when Rho levels were increased. The effect of Rho levels on Cdc42 was not studied. Although it was not determined if Cdc42-dependent inhibition of Rho occurred independently of Rac, or through Cdc42 regulated activation of Rac, but Evers et al. (2000) andSander et al. (1999) include both effects in their proposed model of Rho GTPase crosstalk.
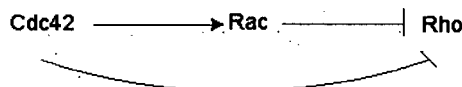
They suggest that the balance between Rac and Rho activity determines the morphology of the cell and whether or not a cell migrates. However, their scheme has the same problems with achieving bistability as Case I and Case II – no feedback from Rac or Rho to Cdc42.

2.3.5 Case V (van Leeuwen et al., 1997)

van Leeuwen et al. (1997) reported that Rac and Rho antagonize one another in neuroblastoma cells. van Leeuwen et al. (1997) didn't directly monitor the GTP state of the proteins, but inferred activation/inactivation through morphological changes in cells, obtaining the following hierarchy:

$$Cdc \xrightarrow{\ +\ } Rac \underset{-}{\overset{-}{\rightleftharpoons}} Rho$$

We will demonstrate later that, although this scheme exhibits bistable behaviour, since Cdc42 is uncoupled from the other proteins, it achieves a steady state that is independent of the distributions of Rac and Rho, which is contrary to experimentally measured gradients of active Cdc42 and Rac in moving cells.

2.3.6 Case VI (Li et al., 2002)

Another study of Rho GTPases in neurons reported that Rac activates Rho, while Rho inhibits Rac (Li et al., 2002). Cdc42 was found to inhibit Rho. If we couple these interactions to the Cdc42-dependent activation of Rac, we obtain the following scheme:

$$Cdc42 \longrightarrow Rac \rightleftharpoons Rho$$
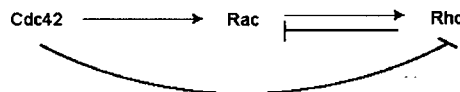
These interaction might result in bistability, but again, the absence of feedback from other small G-proteins to Cdc42 will result in a unique steady state value value of Cdc42 concentration.

2.3.7 Discussion of Schemes Proposed in the Literature

We conclude that, of the six crosstalk pathways surveyed above only one, case III, is consistent with the existence of both a high Cdc42/Rac and a high Rho steady state. We, therefore concentrate on this case in the rest of the chapter. This does not mean that the crosstalk suggested in the other cases does not occur, but that other feedback terms (possibly involving other players such as phospholipids) must also be involved. For example, Evers et al. (2000); Sander et al. (1999) (case IV) found inhibition of Rho by Rac and Cdc42, but didn't examine if Rho inhibits Cdc42. Their proposed model will not permit bistability. However, the scheme shown in Figure 2.1, which is consistent with their experiments allows both a high Cdc42/Rac and high Rho steady states.
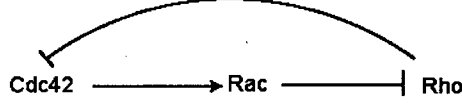
Figure 2.1: An interaction scheme not proposed in the literature that can give rise to bistability.

2.4 Formulation of a Model for Rho Protein Interactions

Let R be the concentration of the active form of a single protein. R can be described by a differential equation of the form:

$$\frac{dR}{dt} = A_R - \delta_R R, \tag{2.1}$$

where A_R is the protein's activation rate and δ_R is the inactivation (turnover) rate. If A_R and δ_R are constant, the system will exponentially approach the unique steady state $R = A_R/\delta_R$. Multiple steady states are possible for some functional forms of A_R and δ_R that depend on R.

Letting C be the number of molecules of active (GTP-bound) Cdc42 on the membrane, R the number of molecules of active Rac on the membrane, and ρ the number of molecules of active Rho on the membrane, we get the following system of the three Rho proteins:

$$\frac{dC}{dt} = A_C - \delta_C C,$$

$$\frac{dR}{dt} = A_R - \delta_R R, \tag{2.2}$$

$$\frac{d\rho}{dt} = A_\rho - \delta_\rho \rho,$$

where the interactions of Cdc42, Rac, and Rho proteins are represented by assumed functional forms of the activation terms (A_C, A_R, A_ρ). We assume that each protein has a constant basal rate of activation (I_C, I_R, I_ρ) as well as a concentration dependent term. The basal decay rates follow first-order kinetics with rate constants $\delta_C, \delta_R, \delta_\rho$ (measured in $\sec^{-1}$).

A verbal model that is consistent with interactions proposed by Giniger (2002) is given by:

$$\frac{dC}{dt} = \text{basal activation - inactivation by Rho - basal inactivation,}$$

$$\frac{dR}{dt} = \text{basal activation + activation by Cdc42 - basal inactivation,}$$

$$\frac{d\rho}{dt} = \text{basal activation + activation by Rac - inactivation by Cdc42 - basal inactivation.}$$

$$(2.3)$$

The notion of "activation" can actually refer to two different processes: an increase of conversion of GDP-bound form to GTP-bound form via GEF activity, or a decrease or slow-down in conversion of GTP-bound form back to GDP-bound form via GAP inhibition. Similarly, downregulation of GTP-bound forms can be caused both by inhibition of GEF activity or by stimulation of GAP activity. Downregulation can also occur due to competition for common GEFs. Theoretically, the Rho proteins can also crosstalk to each other via Rho GDI, that regulates the membrane translocation cycle of all the Rho family proteins. Practically, that does not occur, as GDI is far less specific than the numerous GEFs and GAPs, that can target one particular protein. There have been no reports of GDI selectively targeting one of the Rho proteins in response to signalling.

Our initial modelling for the interactions of small GTPases is based on the following assumptions about activation/inactivation summarized in Figure 2.2:

1. If protein Y activates protein X, then Y speeds up the conversion of the inactive form of X (denoted by X) to active form of X (denoted by X^*) via a GEF.

2. If protein X is inhibited by protein Z, then Z* speeds up the conversion of X^* to X by activating a GAP. The inhibition of X by Z is proportional to the product of the active forms of these proteins, X* and Z*.

We assume that the activation of X by Y is proportional to the concentration Y^* of the active form of the protein Y and is independent of X. This assumption implies that the concentration of inactive proteins is much higher than that of the active proteins, so that over the time course of the activation, the concentration of inactive form does not change significantly and can be considered constant. This assumption agrees with the known biology, as most of the Rho protein is found in an inactive, cytosolic form. Mathematically, this assumption results in a linear activation term kY^* that must be added to the basal activation rate.

If, instead of promoting conversion of X to X^*, Y^* slowed down the conversion of X^* to X via downregulation of an X GAP, the activation would now have to depend on X^*, and, mathematically, the activation term would be a more complicated function of Y^* and X^*. For example, δ_X might be a decreasing function of Y^*.
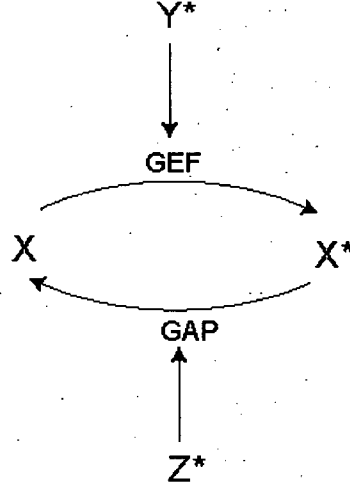
Figure 2.2: Let X and X^* be the inactive and active forms, respectively, of a hypothetical small G-protein. Let Y^* and Z^* be the active form of other small G-proteins. Y^* or Z^* can indirectly affect the conversion of one form to another via a GEF or GAP.

2.5 Model I

Our first model applies the assumptions listed above to (2.3). Model I takes the following form:

$$\frac{dC}{dt} = I_C - \varepsilon C\rho - \delta_C C,$$

$$\frac{dR}{dt} = I_R + \alpha C - \delta_R R, \qquad (2.4)$$

$$\frac{d\rho}{dt} = I_\rho + \beta R - C\rho - \delta_\rho \rho.$$

Here I_C, I_R and I_ρ are the basal activation rates for the small G-proteins, representing GTP binding via GEF activity, and ultimately, regulated by upstream signals. These rates must be positive to have a nonzero level of active Cdc42, Rac, and Rho. I_C, I_R, I_ρ might include a time-dependent pulse, in addition to a constant basal background rate. However stability analysis is done under the assumption that these terms are constant. δ_C, δ_R and δ_ρ are the decay rates of the active forms of the small G-proteins (measured in sec^{-1}). Biologically, the decay rates correspond to GTP-hydrolysis rates (stimulated by GAPs, which might also be affected by the upstream signal). As stated previously, the decay rates are assumed to be proportional to the amount of active forms (first-order kinetics). α and β are the activation of Rac by Cdc42, and the activation of Rho by Rac,

respectively. The inhibition of Rho by Cdc42, and Cdc42 by Rho is a bilinear function of C and ρ.

2.5.1 Analysis of Model I

The goal of this section is to determine by geometric analysis how many steady-states with positive values of C, R, ρ exist for system (2.4). Setting the left side of system (2.4) to zero, and eliminating R from the resulting algebraic system we get the following 2 equations:

$$C = \frac{I_C}{\varepsilon\rho + \delta_C}, \tag{2.5}$$

$$C = \frac{I_\rho + \beta I_R/\delta_R - \delta_\rho\rho}{\rho - \alpha\beta/\delta_R}. \tag{2.6}$$

For the purposes of determining how many steady states there are, it suffices to count the number of solutions to these two equations, i.e. the number of intersections of these curves in the $\rho - C$ plane. These equations also correspond to the C and ρ nullclines, respectively, of the reduced $\rho - C$ plane, obtained by putting R on quasi-steady state.

Graphical analysis demonstrates that only one intersection of these nullclines can occur in the first quadrant of the $\rho - C$ phase plane. The C-nullcline starts at $C = I_C/\delta_C$ for $\rho = 0$ and monotonically decays to 0 as $\rho \to \infty$. The ρ-nullcline has an asymptote at $\rho^* = \alpha\beta/\delta_R$ and a zero at $\rho^+ = [I_\rho + \beta I_R/\delta_R]/\delta_\rho$. Two possible cases can occur: $\rho^+ < \rho^*$ or $\rho^+ > \rho^*$.

The value of ρ^* represents the effective rate at which C activates ρ. ρ^+ is the level of Rho in the absence of Cdc42. The ρ-nullcline has positive (C, ρ) values only for ρ between ρ^+ and ρ^*. If $\rho^+ < \rho^*$, then the ρ-nullcline increases monotonically to ∞ as $\rho \to \rho^*$. Otherwise, the ρ-nullcline is monotonically decreasing between ρ^* and ρ^+. As can be seen in Figure 2.3 in both cases there is a unique positive-valued steady state, which rules out bistable behaviour. Therefore, we need to modify assumptions about activation/inhibition, on which this model was based.

2.5.2 Other Functional Forms of Activation and Inactivation in Model I

For multistability to be possible, a system must exhibit some sort of feedback, such as positive feedback or double negative feedback (Ferrell, 2002). However, that is not a sufficient condition. The set of differential equations governing the system must be nonlinear, and the conditions necessary for the existence of a bistable "switch" are determined by the degree of nonlinearity. (2.4) contains two nonlinear terms: $C\rho$. We saw in the previous section that bistability could not occur in that model. To obtain desired behaviour in our model, further nonlinearity must be introduced into (2.4).
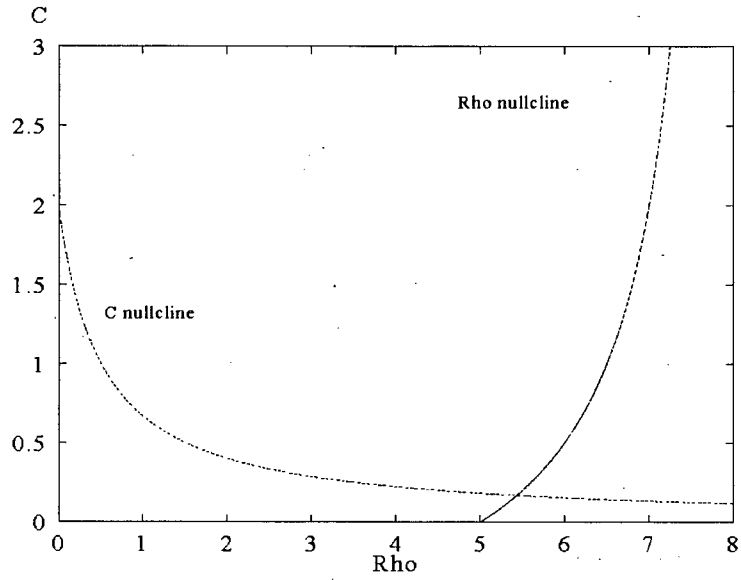
(a)
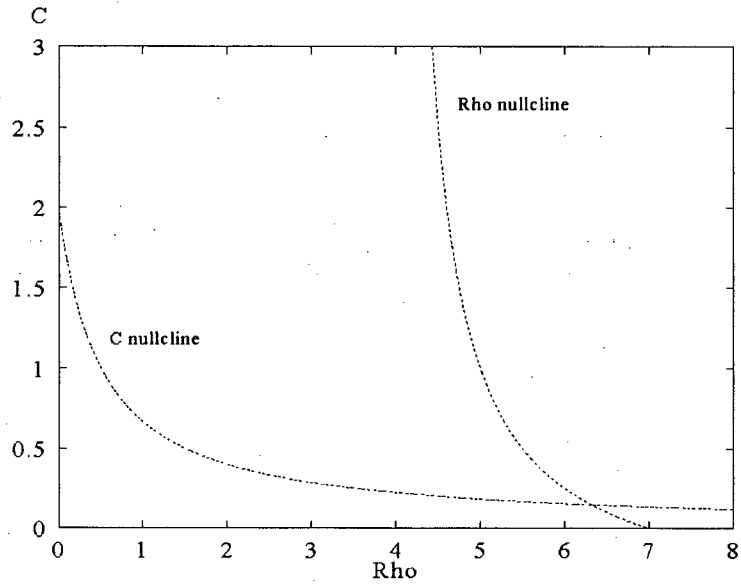
(b)

Figure 2.3: $C - \rho$ phase plane (R is on quasi-steady state) diagrams for Model I. Case (a) occurs when $\rho^+ < \rho^*$. Case (b) occurs when $\rho^+ > \rho^*$, where $\rho^* = \alpha\beta/\delta_R$ and $\rho^+ = [I_\rho + \beta I_R/\delta_R]/\delta_\rho$.

A common nonlinear feature of many models with multiple stable steady states is a sigmoidal shaped profile of activation or inactivation kinetics versus concentration. This sigmoidal shape often occurs due to cooperativity. A simple well-known equation that exhibits bistable behaviour is:

$$\frac{dA}{dt} = s + k_{on}\frac{A^n}{K^n + A^n} - k_{off}A.$$

(2.7)

Here A is the level of an autocatalytic chemical that is also activated by an external source s. For $n > 1$ three steady states are possible (Lewis et al., 1977). We get behaviour qualitatively similar to equation (2.7) if we use a Hill function rather than a constant term I_x for the basal rate of activation of either Cdc42, Rac, or Rho. To include this sort of term in our model, we would have to assume that at least one of Cdc42, Rac, or Rho is activated in an autocatalytic fashion. However, in this case, the bistable behaviour would be a result of autocatalysis rather than interactions of the small G-proteins. Just one of Cdc42, Rac or Rho, taken in isolation would be capable of a high and low steady state. The main hypothesis that we are trying to test in our modelling is that the interactions of the small G-proteins enable a cell to polarize, so we do not consider autocatalytic kinetics of Cdc42, Rac, or Rho in isolation. Instead, we focus on the terms in (2.4) that represent crosstalk between the proteins.
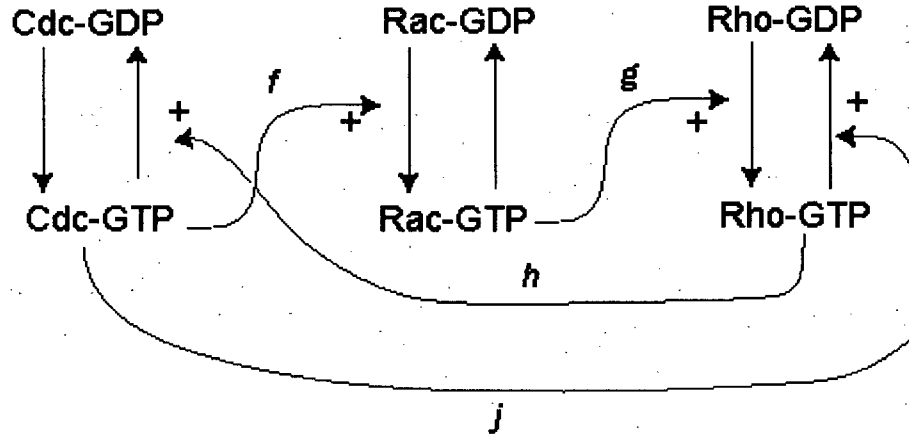
Figure 2.4: Schematic diagram corresponding to Model I. GTP forms are active, GDP forms are inactive. Activation (by a GEF) and inactivation (by a GAP) are represented by vertical arrows and crosstalk is hypothesized to up or downregulate one or the other of these effects

In Giniger's pathway there are four crosstalk terms: activation of Rac by Cdc42, activation of Rho by Rac, inactivation of Cdc42 by Rho, and inactivation of Rho by Cdc42. We assume that activation means speeding up the conversion of the GDP-bound form to a

GTP-bound form, while inactivation mean speeding up the conversion of the GTP-bound form to a GDP-bound form as discussed earlier (see Figure 2.4).

Let f be the activation of Rac by Cdc42, g the activation of Rho by Rac, h inactivation of Cdc42 by Rho, and j the inactivation of Rho by Cdc42. In (2.4) the activation terms, f and g, were linear functions of C and R, while the inactivation terms, h and j, were bilinear functions of C and ρ. The assumptions under which these terms were derived is described in the previous section. We investigated other (biologically plausible) functional forms for f, g, h and j shown in Table 2.1 to see which, if any, can give rise to bistability. The analytical results are given in Appendix A. A summary of investigated functional forms is given in Table 2.2. None of these models have bistable behaviour. We conclude that the interactions shown in Figure 2.4 are incapable of sustaining two stable steady states.

Table 2.1: Functional forms of activation/inactivation rates investigated for models based on the scheme in Figure 2.4.

$f(C)$	$g(R)$	$h(C,\rho)$	$j(C,\rho)$
$f_1 = \alpha C$	$g_1 = \beta R$	$h_1 = \varepsilon C \rho$	$j_1 = C\rho$
$f_2 = \dfrac{\alpha C}{k_1 + C}$	$g_2 = \dfrac{\beta R}{k_2 + R}$	$h_2 = \varepsilon f(C,\rho)$	$j_2 = f(C,\rho)^a$
$f_3 = \dfrac{\alpha C^n}{k_1^n + C^n}$	$g_3 = \dfrac{\beta R^n}{k_2^n + R^n}$		

$^a f(C,\rho)$ is a general positive-valued monotonically increasing function of C and ρ.

Table 2.2: Variations of model I investigated, using the functional forms for activation/inactivation given in Table 2.1. None of these models have bistable behaviour. Details are given in Appendix B.

Functional Forms Used	Model
f_2, f_3, g_1, h_1, j_1	(A.1)
f_1, g_2, g_3, h_1, j_1	(A.2)
$f_2, f_3, g_2, g_3, h_1, j_1$	(A.3)
f_1, g_1, h_2, j_2	(A.4)

2.6 Minimal Requirements for Bistability

Due to the failure of Model I to exhibit bistable behaviour, we proceeded to determine what minimum requirements a three component system must fulfill to obtain the kind of bistable behaviour observed (a high level of Cdc42/Rac, low level of Rho state and

low level of Cdc42/Rac, high level of Rho state) for the interaction scheme suggested by Giniger (2002).

Letting C be the concentration of active (GTP-bound) Cdc42 on the membrane, R the concentration of active Rac on the membrane, and ρ be the concentration of active Rho on the membrane, we get a system of the three Rho proteins described by (2.2):

$$\frac{dC}{dt} = A_C - \delta_C C,$$

$$\frac{dR}{dt} = A_R - \delta_R R,$$

$$\frac{d\rho}{dt} = A_\rho - \delta_\rho \rho.$$

The interactions of Cdc42, Rac, and Rho proteins are represented by assumed forms of the activation terms (A_C, A_R, A_ρ) and inactivation terms $(\delta_C, \delta_R, \delta_\rho)$. Since more than one stable steady state of system (2.2) exists, the activation-decay rates must depend on concentrations of the proteins. In this section we explore through phase plane analysis the requirements on functions A_C, A_R, A_ρ and δ_C, δ_R, δ_ρ. To determine how many steady states system (2.2) has, we reduce the problem to investigating the intersections of two curves in the $\rho - C$ plane, obtained by setting $\frac{dR}{dt} = 0$ and eliminating R. This is formally equivalent to a quasi-steady state analysis. Note that in our modelling we do not assume that Rac reaches equilibrium more rapidly than Cdc42 or Rho, but are just using this approach to learn how many steady states there are.

We proceed in two steps:

1. Determine what type of a two-component $(C - \rho)$ mutually inhibitory system will give rise to the following phase plane:
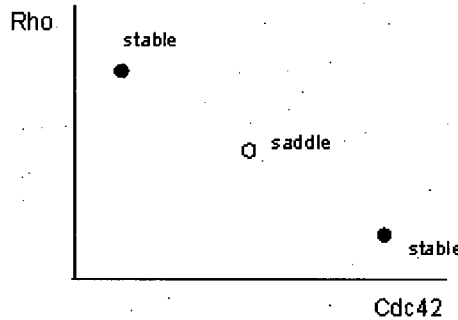
2. Explore how the third component R can modulate this system.

Of course, other strategies could also be used to arrive at a suitable model.

34

2.6.1 Obtaining Bistability in a Reduced Two Component System

Consider the following two-component system:

$$\frac{dC}{dt} = I_C - \delta_C C,$$

$$\frac{d\rho}{dt} = I_\rho - \delta_\rho \rho, \quad (2.8)$$

C and ρ can influence each other in two ways: via the activation terms I_C and I_ρ and via the inactivation terms δ_C and δ_ρ.

First, suppose Cdc42 and Rho influence each other's rate of activation. System (2.8) becomes:

$$\frac{dC}{dt} = f(\rho) - \delta_C C,$$

$$\frac{d\rho}{dt} = g(C) - \delta_\rho \rho. \quad (2.9)$$

Without loss of generality we can rescale the system so that $\delta_C = \delta_\rho = 1$. The nullclines of system (2.9) are just the curves $C = f(\rho)$ and $\rho = g(C)$. We assume that f and g are continuous, positive functions of their arguments for $\rho \geq 0$, $C \geq 0$.

If Cdc42/Rho are assumed to mutually inhibit each other the Rho nullcline needs to satisfy $\frac{d\rho}{dC} = g'(C) \leq 0$. The other curve, $C = f(\rho)$, needs to satisfy $\frac{d\rho}{dC} < 0$, which implies $\frac{dC}{d\rho} = f'(\rho) < 0$. In order for the nullclines to have three intersections one of the curves, say $\rho = g(C)$, needs to be sigmoidal in shape.
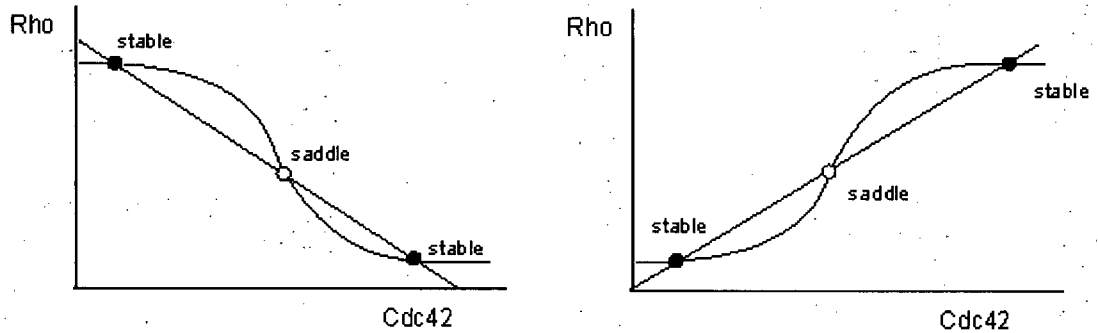
Figure 2.5: Nullcline configurations for a two-component system resulting in bistability. Note that at least one of the nullclines has to be S-shaped in order to get multiple steady states. The configuration on the left has a high Cdc42/ low Rho stable steady state and a low Cdc42/ high Rho stable steady state, so it is compatible with our system. The configuration on the right has a high Cdc42/ high Rho, as well as a low Cdc42/ low Rho stable steady states. It is not compatible with our system.

35
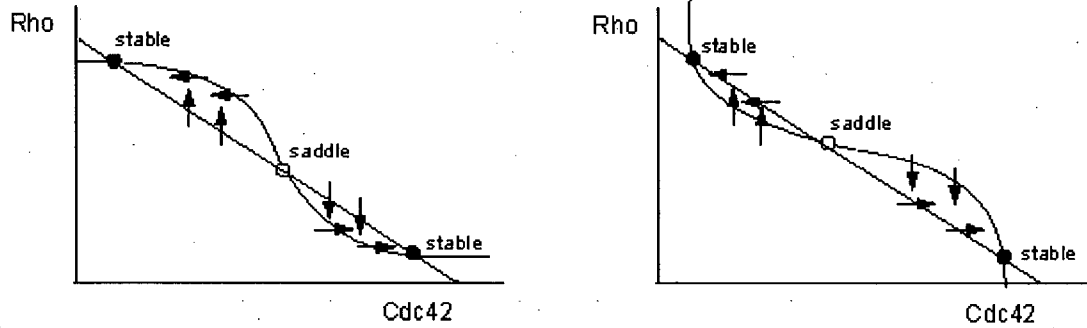
Figure 2.6: Possible nullcline configurations for system (2.8) that have the desired steady state configurations. Note that the second phase plane can be obtained from the first by interchanging the roles of Cdc42 and Rho. Hence we do not need to distinguish between them in our analysis.

A sigmoidal function that satisfies such constraints is

$$\rho = g(C) \approx I_\rho \left[1 - \frac{C^n}{k^n + C^n} \right] = \frac{I_\rho k^n}{k^n + C^n},$$

where n is a Hill coefficient and k a threshold concentration. The Cdc42 nullcline does not need to be sigmoidal, just a decreasing, non-negative function of ρ. A simple choice for $f(\rho)$ is $f(\rho) = \frac{I_C}{k_c + \rho}$.

So the functional form for (2.9) should be:

$$\frac{dC}{dt} = \frac{I_C}{k_c + \rho} - \delta_C C,$$

$$\frac{d\rho}{dt} = \frac{I_\rho k^n}{k^n + C^n} - \delta_\rho \rho. \tag{2.10}$$

Now consider the case where Cdc42 and Rho influence each other's rate of inactivation:

$$\frac{dC}{dt} = I_C - \delta(\rho)C,$$

$$\frac{d\rho}{dt} = I_\rho - \delta(C)\rho. \tag{2.11}$$

The nullclines are given by

$$C = \frac{I_C}{\delta_C(\rho)}, \quad \rho = \frac{I_\rho}{\delta_\rho(C)}.$$

Again, assuming mutual inhibition between Cdc42 and Rho, both nullclines need to be decreasing functions of C. One of the nullclines, say $\rho = \frac{I_\rho}{\delta_\rho(C)}$ needs to be sigmoidal

36

in shape in order for three steady states to exist. Using these constraints we obtain for the Rho nullcline

$$\rho = \frac{I_\rho}{\delta_\rho(C)} = \frac{I_\rho}{k^n + C^n} \Rightarrow \delta_\rho(C) = k^n + C^n.$$

For the Cdc42 nullcline

$$\frac{dC}{d\rho} = -\frac{I_c \delta'_C(\rho)}{\delta^2_C(\rho)} < 0 \Rightarrow \delta'_C(\rho) > 0.$$

For simplicity choose $\delta_C(\rho) = \alpha\rho + \text{constant}$.

So the functional form for (2.11) should be:

$$\frac{dC}{dt} = I_c - \alpha C\rho - \delta_C C,$$

$$\frac{d\rho}{dt} = I_\rho - C^n\rho - \delta_\rho\rho. \tag{2.12}$$

Based on the above reasoning we can conclude that to obtain the desired type of bistability in a two component mutually inhibitory system at least one of the interactions should have some "cooperativity" in order to get an S-shaped nullcline that intersects the other nullcline multiple times.

2.6.2   Adding a Third Component to a Two-Component System

How are the dynamics of the above system affected by a third participant? If active Rac has no effect on Rho, then bistability is solely determined by the Cdc42/Rho system and Rac is a neutral component. If Rac inhibits Rho, we get a variation of a double negative feedback loop, where Cdc42 inhibits Rho both independently and through Rac, and Rho inhibits Cdc42. If Rac activates Rho, then bistability is driven by mutual inhibition between Cdc42 and Rho. Removal of inhibition of Rho by Cdc42 results in a system that is equivalent to a two component negative feedback loop, where Cdc42 activates Rho and Rho inhibits Cdc42. Such a system will result in either a single steady state or an oscillation. A well-known example with these interactions is the Goodwin oscillator (Goodwin, 1965). Alternatively, removal of inhibition of Cdc42 by Rho results in a system that is equivalent to a two component system where Cdc42 both activates and inhibits Rho. In this case only one steady state is possible, as Rho has no influence on Cdc42.

In the most interesting case Rac modulates either one or both of the interactions between Cdc42 and Rho (see Figure 2.7). In system (2.9) functions $f(\rho)$ and $g(C)$ will actually be $f(\rho, R)$ and $g(C, R)$. R will then affect the shape of the nullclines, determining how many times they intersect. Thus, the presence of Rac could be an essential factor for achieving bistability.
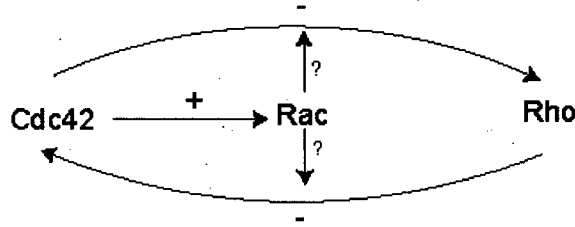
Figure 2.7: Rac can modulate the inhibition between Cdc42 and Rho.

2.7 Model II (Activation-Inhibition Model)

Based on the results of Section 2.6, we consider Model II for the interactions of Cdc42, Rac, and Rho:

$$\frac{dC}{dt} = \frac{I_C}{a_1 + \rho^k} - \delta_C C, \tag{2.13a}$$

$$\frac{dR}{dt} = I_R + \alpha C - \delta_R R, \tag{2.13b}$$

$$\frac{d\rho}{dt} = \frac{I_\rho}{a_2 + C^n} + \frac{\beta R}{a_3 + C^m} - \delta_\rho \rho. \tag{2.13c}$$

Here I_C, I_R, and I_ρ are the basal activation rates in the absence of crosstalk given that all small G-proteins are in the inactive state. a_1 and a_2 describe levels of the proteins that lead to a half-maximal mutual inhibition of Rho and Cdc42; and α and β are the activation of Rac by Cdc42, and the activation of Rho by Rac, respectively. δ_C, δ_R, and δ_ρ are the basal inactivation rates (mediated by GEFs).

What is the biological interpretation of model II? In Model I, we represented the inhibitory effect of one small Rho protein on another by including an inactivation term that was subtracted from the basal activation (GTP-loading) rate. This can be interpreted as speeding up the rate of GTP-hydrolysis (through a Rho GAP). In Model II we suppose Rho proteins inhibit one another through downregulation of the basal activation (GTP-loading) rate. This is a significantly different mechanism of action from that of model I, where inhibition left the activation rate unchanged, but sped up removal of the active form (GTP-hydrolysis). In Model II inhibition means that one protein slows down the GTP-loading rate of another (compare figures 2.4 and 2.8). A reasonable assumption is that GTP-loading is a decreasing function of the concentration of inhibiting protein. One of the simplest functions that describes inhibition of x by y by such a process is $\frac{I_x}{a^k + y^k}$, where I_x is the activation rate of x, and k is the cooperativity of y. We still assume a basal inhibition (GTP-hydrolysis) rate with first order kinetics.

In system (2.13) Cdc42 and Rho are assumed to mutually inhibit each other's rate of basal activation. In addition, the activation of Rho by Rac is also downregulated by the presence of Cdc42 in a similar manner. For low level of active Cdc42, activation of Rho by Rac is nearly linear ($\approx \beta R/a_3$), but dies out to zero as the level of C increases. If we further assume that Cdc42 inhibition of both basal and Rac-induced GTP-loading is the same, then $a_2 = a_3$ and $m = n$. It is possible to obtain bistable behaviour for these dynamics in certain parameter regimes, as can be seen in the reduced (R on QSS) system shown in Figure 2.9. Bistable behaviour for the full three component system is verified in Figure 2.10. Note that at the moment we are using arbitrary parameter values. Certain parameter values, such as decay rates and basal activation rates can be found in the literature. These parameters will be further discussed in Chapters 3 and 4. Other parameters such as α and β are unknown at the moment.
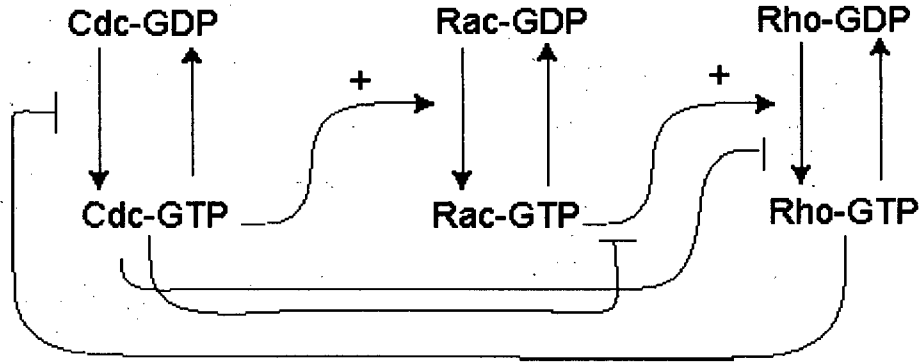
Figure 2.8: Schematic diagram corresponding to Model II (activation-inhibition model)
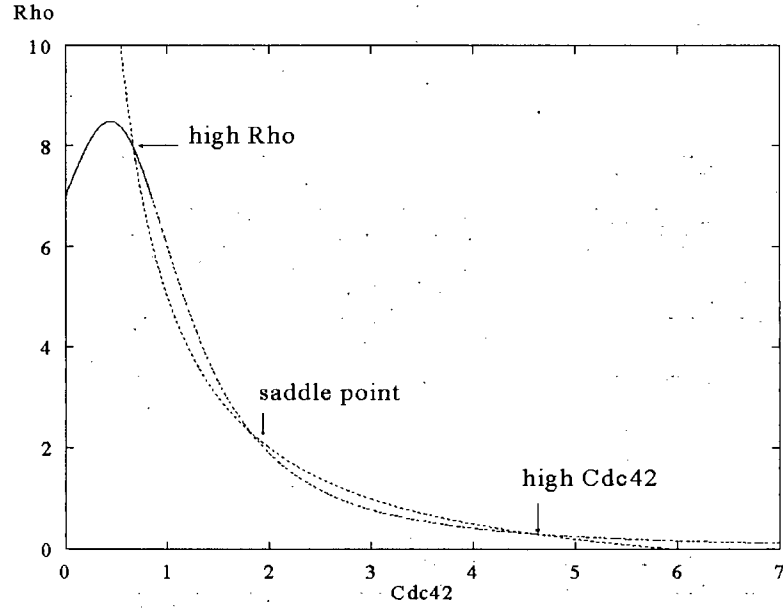
Figure 2.9: The $C - \rho$ phase plane (R is on quasi-steady state as described in the text) for model II (2.13) with two stable steady states separated by a saddle point. Parameter values used: $I_C = 6, I_R = 1, I_\rho = 2, \alpha = 1, \beta = 5, \delta_C = 1, \delta_R = 1, \delta_\rho = 1, k = 1, n = 3, m = 3, a_1 = a_2 = a_3 = 1$.
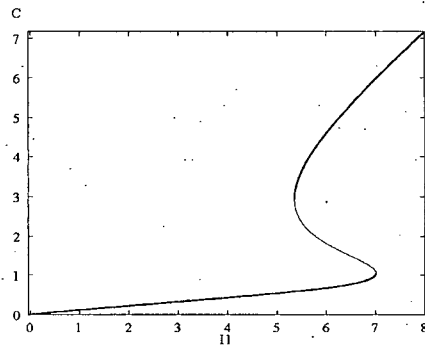
(a)
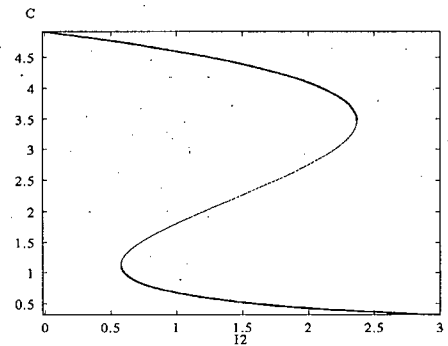
(b)

Figure 2.10: Bifurcation diagrams for Model II using the parameter rate I_C (Cdc42 activation rate) in (a) and I_R (Rac activation rate) in (b). Other parameter values used were: $I_\rho = 2, \alpha = 1, \beta = 5, n = m = 3, \delta_C = \delta_R = \delta_\rho = 1, a_1 = a_2 = a_3 = 1$. Note that for certain parameter regimes, the system is bistable.

40

2.8 Simplified Bistable Versions of the Activation Inhibition Model

Bistable behaviour occurs in model II, but it is not the minimal model with bistability we ask what are the minimal components necessary for bistability. Note that there are two inhibitory terms due to Cdc42 in the Rho equation: $\frac{I_\rho}{a_2 + C^n}$ and $\frac{\beta R}{a_3 + C^m}$ in model (2.13), but only one is needed for mutual inhibition between Cdc42 and Rho.

2.8.1 Model III

Setting $\beta = 0$ (ie, removing the activation of Rho by Rac) leads to a system in which the equations for Cdc42 and Rho are now decoupled from Rac:

$$\frac{dC}{dt} = \frac{I_C}{a_1 + \rho^k} - \delta_C C,$$

$$\frac{d\rho}{dt} = \frac{I_\rho}{a_2 + C^n} - \delta_\rho \rho. \qquad (2.14)$$

This is the classic model for behaviour of a switch, which is known to give bistability if at least one of n or k is greater than 1 (positive cooperativity between the two proteins) (Gardner et al., 2000). Note also that we derived this equation in our analysis of minimum requirements for bistability in a two component system in Section 2.6. See Fig 2.11 for typical nullclines.

Model (2.14) is simpler than model (2.13) because the bistability is achieved wholly through double negative feedback of Cdc42 and Rho, without any effect from Rac. Although, it is capable of bistable behaviour, it is incompatible with the biology, since changing the active Rac levels in a cell affects Rho levels Ridley et al. (1992); Sander et al. (1999).

2.8.2 Model IV

Another simplification of Model II can be obtained by removing the first inhibitory term due to Cdc42 in the equation for ρ.

$$\frac{dC}{dt} = \frac{I_C}{a_1 + \rho^k} - \delta_C C,$$

$$\frac{dR}{dt} = I_R + \alpha C - \delta_R R, \qquad (2.15)$$

$$\frac{d\rho}{dt} = I_\rho + \frac{\beta R}{a_3 + C^m} - \delta_\rho \rho.$$

In model IV, Rho and Cdc42 still mutually inhibit each other's rate of activation. As mentioned in Section 2.6, these interactions are sufficient for bistability. Active Rho
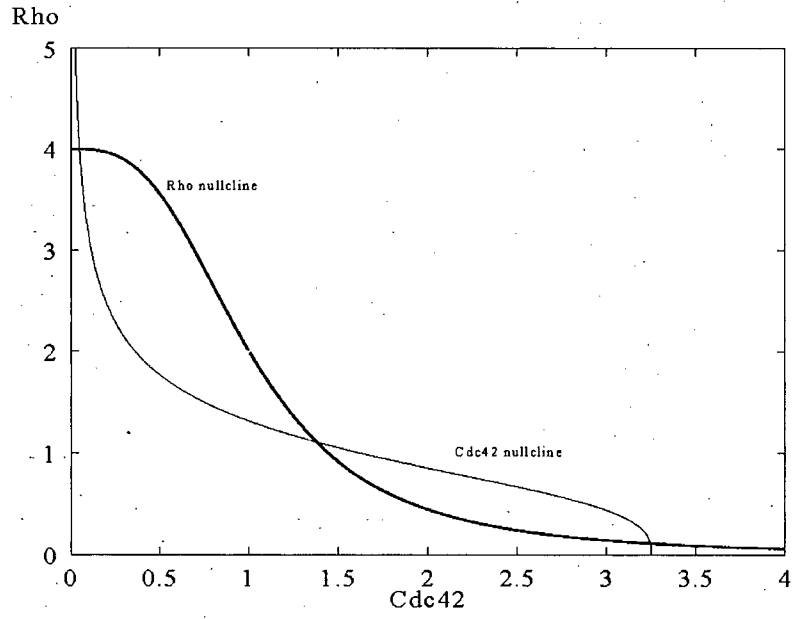
Figure 2.11: $C - \rho$ phase plane for system (2.14). Two stable steady states coexist. Parameters used: $I_C = 6.5, I_\rho = 6, n = k = 3, \delta_C = 2, \delta_\rho = 1.5$.

inhibits the activation (GTP-loading) of Cdc42 (via the $\frac{I_C}{a_1+\rho^k}$ term). However, Cdc42 only inhibits Rac-induced activation, not the basal activation rate I_ρ (see Figure 2.12). Negative feedback of C on ρ is still exerted through the $\frac{\beta R}{a_3+C^m}$ term, allowing bistability (see Figures 2.13 and 2.14). β characterizes the magnitude of the activation of Rho by Rac and determines if bistability can occur. If this value is low then only a high Cdc42 state is possible. If β becomes large enough, the system will always achieve a high Rho state. For intermediate values of β both states are possible (see Fig 2.14).
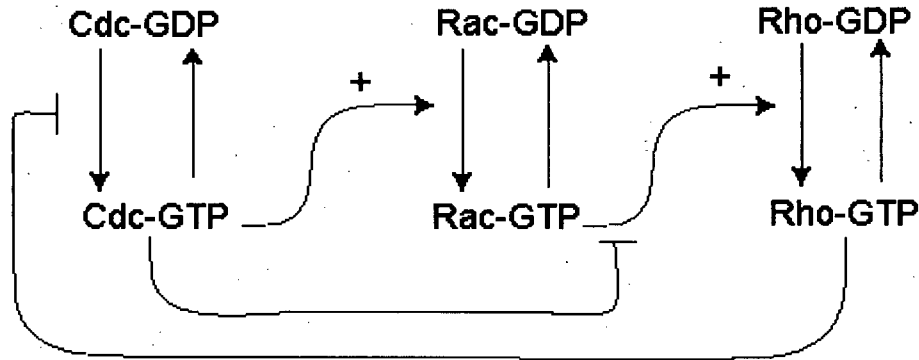
Figure 2.12: Schematic diagram corresponding to model IV.

An experimental way to distinguish between systems (2.13) and (2.15) would be to knock out Rac, and see how increasing Cdc42 levels affects Rho. If no effect is observed, Cdc42 acts on Rho through a Rac-dependent pathway. On the other hand, if Rho levels decrease, we can conclude that Cdc42 inhibits GTP-loading of Rho in a Rac-independent manner. Although model (2.15) is a simpler mathematical model that gives rise to the same qualitative behaviour as model (2.13), it is a worse model from a biological point of view. The result of activation, whether or not it is Rac-induced, is GTP-loading of the inactive form. Neither Rac, nor Cdc42 physically bind to Rho changing its conformation. Hence, there is no reason to suppose that downregulation of a Rho GEF by Cdc42 will selectively inhibit GTP-loading of Rho in some cases and not others.

No other simplifications of Model II will result in a biochemically plausible, bistable system. So we conclude that Model II given by equations (2.13) is a minimal model of Cdc42, Rac, and Rho kinetics that gives bistable behaviour as a result of mutual inhibition of Cdc42 and Rho.
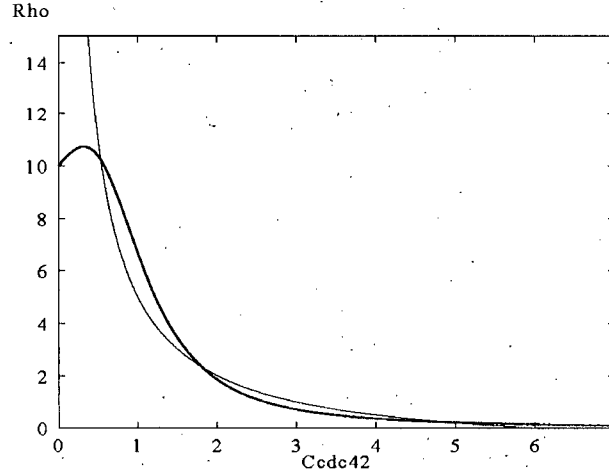
Figure 2.13: Projection of the C and ρ nullsurfaces onto the $C - \rho$ plane, obtained by putting R on quasi-steady state. These curves have the same qualitative shape as the nullsurface projections in model II, allowing bistability. Parameters used: $I_C = 6, I_R = 3, I_\rho = 0, \alpha = 1, \beta = 10, \delta_C = 1, \delta_R = 1, \delta_\rho = 3, k = 1, m = 3$.
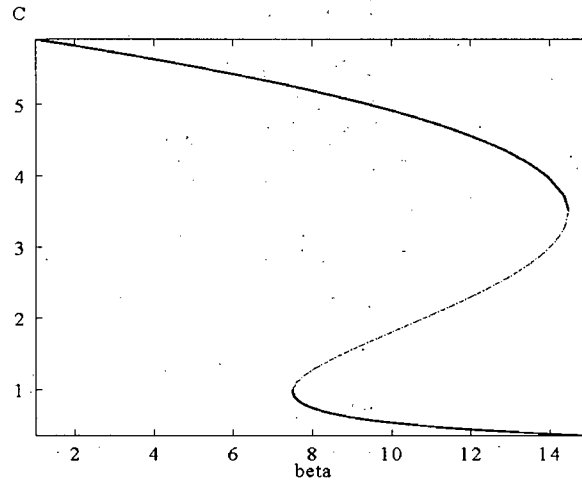
Figure 2.14: Bifurcation diagram for parameter β for the full system (2.15) that verifies bistability seen in the reduced (R on quasi-steady state) system. Parameters used: $I_C = 6, I_R = 3, I_\rho = 0, \alpha = 1, \delta_C = 1, \delta_R = 1, \delta_\rho = 3, k = 1, m = 3$. Note that the basal activation rate for Rho is set to 0, so the only way that Rho is activated is via Rac. If $I_\rho > 0$ lesser value of β is needed to achieve bistability.

2.9 Discussion

In this chapter, we have examined the interaction pathways between the Rho GTPases that have been proposed in the literature. We know from biological data that Rho activity is localized to the back of the polarized cell, and that Rho distribution is inverse to that of Rac and Cdc42. Many biologists believe that this phenomena could be explained by inhibition of Rho by Rac. Since Rac levels are highest at the leading edge, Rho levels will consequently be higher at the back of the cell. However, by itself the inhibition of Rho by Rac does not explain the spatial segregation of Cdc42 and Rho, or why high Rac levels are established at the leading edge in the the first place. If the spatial segregation of the Rho GTPases is due to the interactions of GTPases, **a feedback term to Cdc42 from Rac or Rho is necessary**.

Based on wide agreement in the published literature, we assume that Cdc42 upregulates the activity of Rac. If Rac upregulates Rho, as suggested by experiments of Nobes and Hall (1995), mutual inhibition is necessary between Cdc42 and Rho. This is Giniger's interaction (Case III) described in Section 2.3. If Rac downregulates Rho, as suggested by the experiments of Evers et al. (2000); Sander et al. (1999) there are multiple possibilities that can result in bistability. One possibility is that positive feedback to Cdc42 from Rac establishes a positive feedback loop that results in a high Cdc42/Rac or a low Cdc42/Rac stable steady state. In turn, Cdc42/Rac levels will determine Rho levels. Another possibility is inhibition of Cdc42 by Rho. In this case, mutual inhibition occurs between Cdc42 and Rho via Rac, which could result in bistability.

We explored in detail the interactions of the small G-proteins that were suggested by Giniger (2002). We assumed that the interactions of the small G-proteins are controlled by GEFs and GAPs, so crosstalk of Rho proteins occurs at the GTPase level. We formulated two models that corresponded to two different ways that Cdc42 and Rho can mutually inhibit each other (shown in Figures 2.4 and 2.8). We concluded that inhibition through downregulation of the activation rate (GTP-loading) could result in a suitable bistable system. We also concluded that inhibition via speeding up the removal of the active form (upregulation of GAPs) cannot give rise to such behaviour. Can we conclude on the basis of this modelling that Cdc42/Rho mutual inhibition of the small G-proteins occurs via downregulation of GEFs? The answer is yes, if we assume that the crosstalk is of the form that Giniger (2002) suggested. Experimentally, however, that remains to be determined.

In model II, bistability is driven by mutual antagonism between Cdc42 and Rho. As was shown in the simplified version of the activation inhibition model, Model III, two chemical species inhibiting each other (double negative feedback loop) show similar switch-like behaviour. However, we dismissed various simplifications of Model II on biological grounds, and concluded that Model II given by equations (2.13) is a minimal biochemically

plausible model that gives bistability based on mutual inhibition.

How certain are we that bistability cannot arise due to another cause? We did not include any autocatalytic terms in our models, since we felt that in that case the resulting bistable behaviour would be a result of autocatalytic properties of a single protein, not due to the interactions between the three. We also did not come across any evidence of a positive feedback loop occurring between the Rho proteins in the literature. However, a positive feedback loop between Rac and the phosphoinositide PIP_3 has been reported (Srinivasan et al., 2003; Weiner et al., 2003). We did not explore the effect of those dynamics at this stage. Inclusion of PIP_3 will be part of future work.

Our conclusion is that without autocatalysis or a positive feedback loop, double inhibition is necessary. For a system without any positive feedback, an even number of negative feedback terms is needed in order to achieve multistability (Ferrell, 2002). Models with a single or triple negative feedback term have an autoregulatory mechanism, and either have a single stable steady state or exhibit oscillations (Ferrell, 2002). So our hypothesis that spatial segregation of the Rho proteins in motile cells is achieved through crosstalk of Cdc42, Rac, and Rho requires that two of the Rho proteins be inhibited due to the crosstalk.

Chapter 3

Spatial Extension of the Activation-Inhibition Model

As stated in Chapter 2, the spatial distribution of the active Rho proteins can be modelled by a reaction-diffusion system. The reaction, in this case, is the crosstalk of Rho GTPases. In this chapter we investigate whether the reaction-diffusion system can give rise to a spatial pattern similar to one that is observed in polarized cells. As discussed in Chapter 2, we do not believe that the pattern formation in the Rho system is due to a Turing instability, as all the active Rho proteins diffuse at the same rate. Instead, we test whether addition of diffusion to a system with multiple stable steady states can cause spatial inhomogeneities.

Recall that we are only keeping track of the active forms of the Rho GTPases that are found on the plasma membrane, treating the cytosolic pool as a limitless reservoir. We consider simple lateral diffusion as the only means for movement along the membrane. The proteins can, of course, dissociate from the membrane and re-associate later at a different location. These association/dissociation rates are dependent on the concentrations of the proteins.

3.1 Spatial Form of the Activation Inhibition Model

3.1.1 Equations

Including diffusion in equations (2.13) leads to the reaction-diffusion system:

$$\frac{\partial C}{\partial t} = D\nabla^2 C + \frac{I_C}{a_1 + \rho^k} - \delta_C C,$$

$$\frac{\partial R}{\partial t} = D\nabla^2 R + I_R + \alpha C - \delta_R R, \tag{3.1}$$

$$\frac{\partial \rho}{\partial t} = D\nabla^2 \rho + \frac{I_\rho}{a_2 + C^n} + \frac{\beta R}{a_3 + C^m} - \delta_\rho \rho.$$

Here C, R, ρ are concentrations of Cdc42, Rac, and Rho, respectively, in μM. Time is measured in seconds and distance in μm. Model (3.1) is nonlinear system of PDEs. Therefore, it is difficult to obtain any analytic results. Hence we will use numerical solutions to explore the properties of the spatial activation-inhibition model.

3.1.2 Boundary Conditions
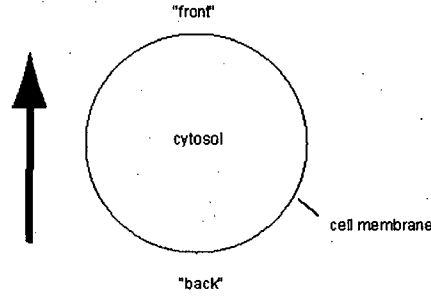
Figure 3.1: Schematic representation of a moving cell.

We have to specify the appropriate domain for system (3.1). We would like to solve system (3.1) in one spatial dimension, but we have to be clear how to interpret the results for a three-dimensional cell. To interpret the geometry, we consider two different approaches. The first, shown in Figure 3.2 (a), is a thin slice of the plasma membrane from the top of the cell. In that case, the domain for our spatial problem is a line, $0 \le x \le L$, where L is a cell diameter. The boundary conditions are at the front and back of the cell. Since the proteins cannot diffuse out of the cell, it is appropriate to have no flux boundary conditions at $x = 0, L$. An alternative, shown in Figure 3.2 (b), is to treat the cell as a disk-like object, and the cell membrane as the perimeter of that disk. In that case, the domain is an interval in 1 D ($0 \le x \le \pi L$) with periodic boundary conditions. We consider both approaches.
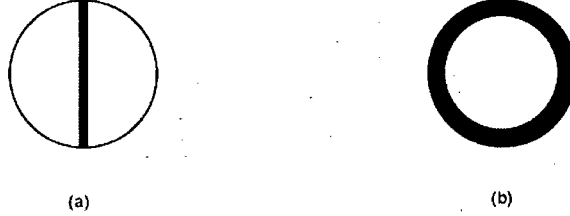
Figure 3.2: Two ways of interpreting the model in one spatial dimension: (a) as a slice from the top of the cell and (b) as the boundary of a disk.

3.1.3 Parameter Estimates for the Spatial Model

Most parameters in the Activation-Inhibition Model (3.1) are unknown. However, certain ballpark estimates can be made for the rates of diffusion, decay, and basal activation of the proteins.

Table 3.1: Concentrations of Rho GTPases in Cos1 cells (fibroblasts) as determined by immunoblotting. Calculated from values in Michaelson et al. (2001)

Protein	Concentration (μM)
Rho	3
Rac	7
Cdc42	2.5

- The typical size of a eukaryotic cell is $10\,\mu m$, so we take the domain to be $0 \leq x \leq 10\,\mu m$ for no flux boundary conditions, and $0 \leq x \leq \pi \cdot 10\,\mu m$ for periodic boundary conditions.

- The diffusion rate of Rho GTPases has not been measured, probably because the proteins cycle on and off the membrane. However, the diffusion coefficient of heterotrimeric G-proteins in the membrane has been reported to be $0.1\ \mu m^2 s^{-1}$ (Postma et al., 2004). In addition, the diffusion of membrane-bound Ras, a small GTPase with the same molecular weight, is around $1\ \mu m^2 s^{-1}$ (Goodwin et al., 2005). Therefore, diffusion coefficient of membrane-bound Rho GTPases is of the order 0.1-1 $\mu m^2 s^{-1}$.

- The average membrane lifetime of a Rac molecule is 2 sec (Sako et al., 2000), giving a decay rate of 0.5 sec^{-1}. GAP-stimulated GTP hydrolysis of Rho has been measured to be 1.5 sec^{-1} (Zhang and Zheng, 1998). Therefore, we take the decay rates $\delta_C = \delta_R = \delta_\rho = 1$ sec^{-1}.

- In the absence of interactions, the steady state level is given by

$$C = \frac{I_C}{a_1 \delta_C}, \; R = \frac{I_R}{a_2 \delta_R}, \; \rho = \frac{I_\rho}{\delta_\rho}.$$

Based on data in Table 3.1, we can see that concentrations of Rho GTPases are in the micromolar range. Thus, knowing the decay rates and the fraction of protein that is membrane-bound, we can estimate the basal activation rates. Using the decay rate estimates above, and taking $a_1 = a_2 = 1$ for simplicity, we obtain I_C, I_R, I_ρ are in the range of μM sec^{-1}) if the measured protein is assumed to be in active form.

3.2 Results

Numerical simulations of a one-dimensional membrane strip with no flux boundary conditions (shown in Figure 3.2(a)) were carried out using the method of lines in XPP simulation package [1]. We used a spatial step size of $\Delta x = 0.1 \mu m$. Runge-Kutta method of order 4 was used for solving the resulting ODEs with a time step of $\Delta t = 0.005\,s$. A diffusion coefficient of 0.01 $\mu m^2/s$ for initial simulations unless specified otherwise. Later, it was found that a diffusion coefficient of 0.1-1 $\mu m^2/s$ of membrane-bound small G-proteins is more realistic. The effect of varying the diffusion coefficient is described in Section 3.5. Other parameter values were chosen in the bistable range of the corresponding ODE system (2.13). Exact parameter values and the simulation code is given in Appendix B.

3.2.1 Effect of Initial Conditions

Because system (3.1) is in a bistable regime, which steady state is reached depends on the initial conditions. With a spatially uniform initial condition of $C(x) = 4, R(x) = 8, \rho(x) = 2$ (arbitrary units of concentration), the system will approach the (spatially homogeneous) high Cdc42 steady state. Changing one of the initial conditions to $R(x) = 9$ makes the system approach the high Rho steady state, due to the positive effect of Rac on Rho.

Next, consider an asymmetric initial Rac distribution, where the left half of domain is initialized to 8, and the right half of domain is initialized to 9. The results of this simulation are shown in Fig 3.4 (a) and Fig 3.3. This asymmetry is amplified, and the spatial segregation of the small G-proteins seen in the figure persists for hundreds of seconds. This distribution, however, is not a steady state, but a travelling wave slowly moving towards a spatially homogeneous steady state (see Fig 3.4 (b)). As expected, the final steady state is the same as for the ODE system (2.13).

---

[1] The XPP package was developed by Bard Ermentrout of the University of Pittsburgh. It is available from http://www.math.pitt.edu/~bard/xpp/xpp.html
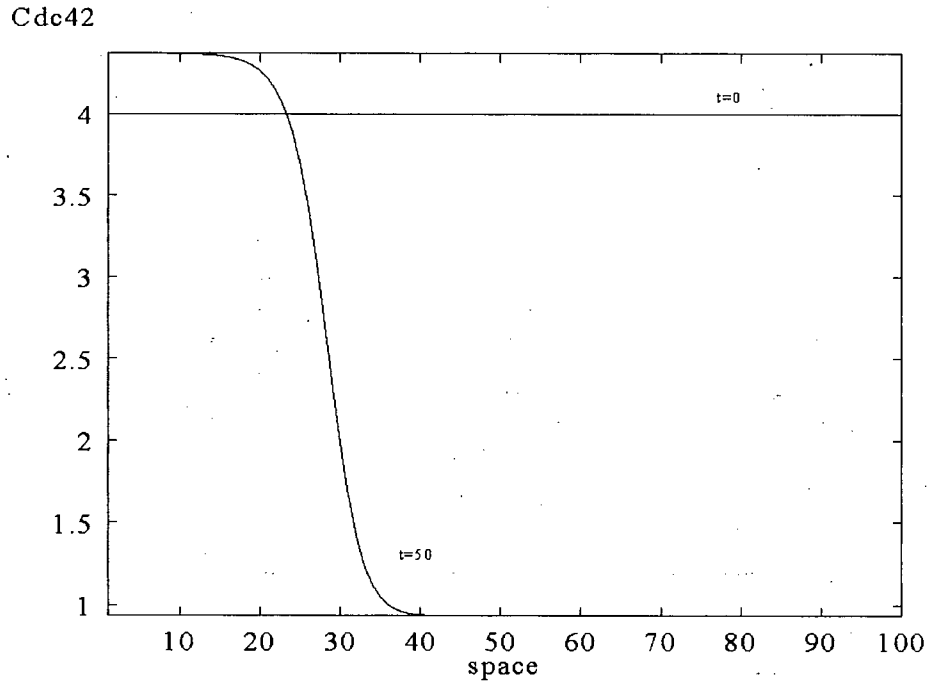
Figure 3.3: Cdc42 spatial profile at different times for system (3.1) with Neumann BCs. As described in the text, the initial Cdc42 level is 4 and Rho level is 2 μM. For Rac, left half of the domain was initialized to 8, and the right half to 9, as described in the text. The diffusion coefficient is 0.01 $\mu m^2/s$. Other parameter values were chosen in the bistable range of the corresponding ODE system (2.13). See Appendix B for exact parameter values.
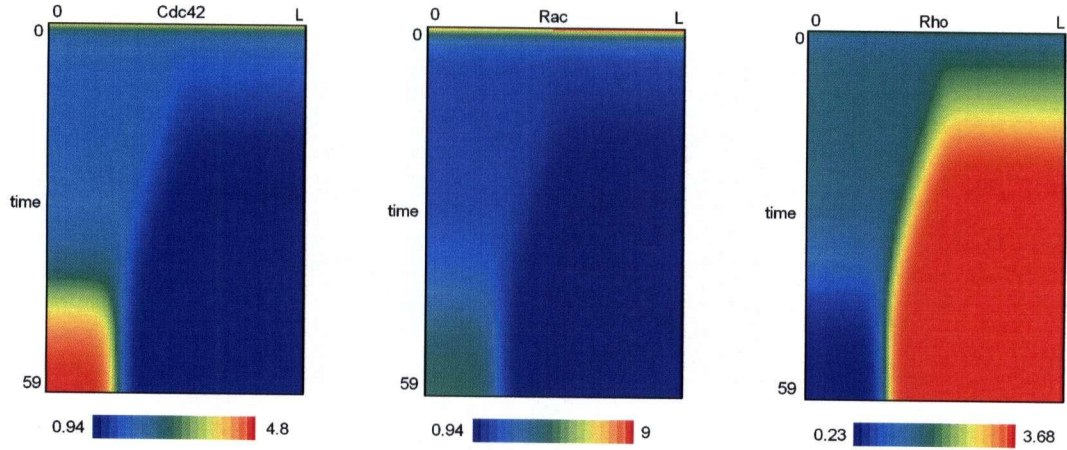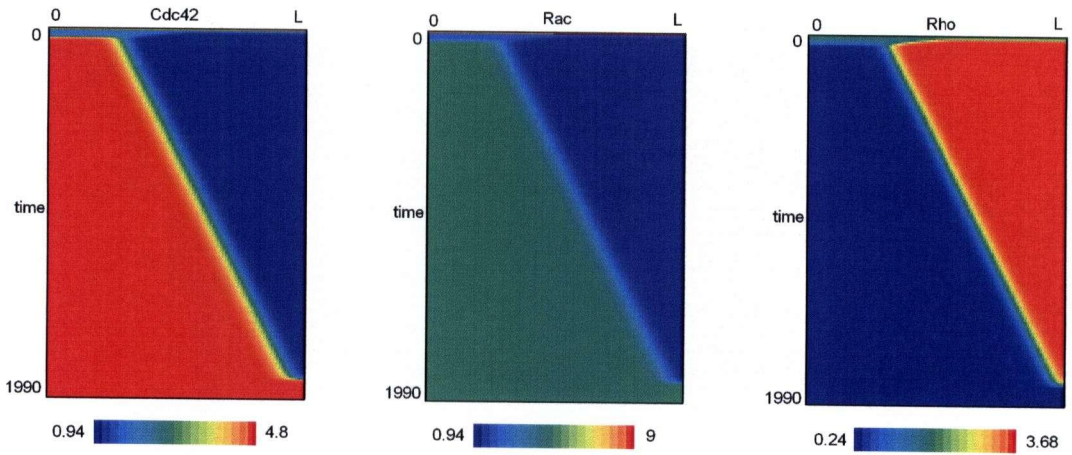
Figure 3.4: Spatiotemporal solutions to model (3.1) with Neumann BCs. The same initial conditions and parameters as in Figure 3.3. Time is on the y-axis, space is on the x-axis. (a) An initial asymmetry in the Rac distribution leads to spatial segregation. (b) Increasing the length of the run to $t = 1990\,s$ we see that the system eventually approaches a high Cdc42/low Rho steady state.

In the bistable regime, long persistent spatial segregation can appear due to amplification of a gradient (Figure 3.8) or random noise (Figure 3.6) in the initial distribution of one of the small G-proteins. In other regimes, the noise will quickly be damped out (Figure 3.7). In general, long-lasting spatial heterogeneity will develop if the perturbation in the system is large enough that the concentration of one of the Rho proteins falls in different basins of attractions at different portions of the domain.

Numerically, it appears that if long-lasting spatial segregation is achieved, the system always tends to a high Cdc42 state. If the system approaches the high Rho steady state, the time scale is faster by several orders of magnitude. No stable spatially inhomogeneous steady state exists.
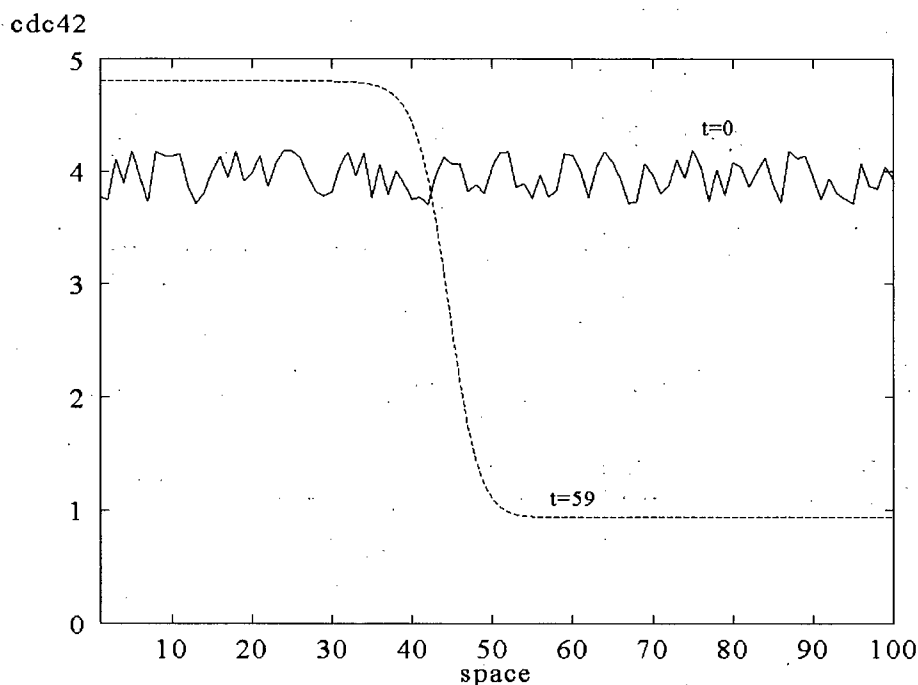
Figure 3.5: In a bistable regime, a noisy initial condition in the distribution of one of the proteins leads to spatial segregation. The concentration of Cdc42 (μM) along the cell is shown at time 0 and 59 (seconds). See also Figure 3.6 for an additional example of polarization arising due to noise.
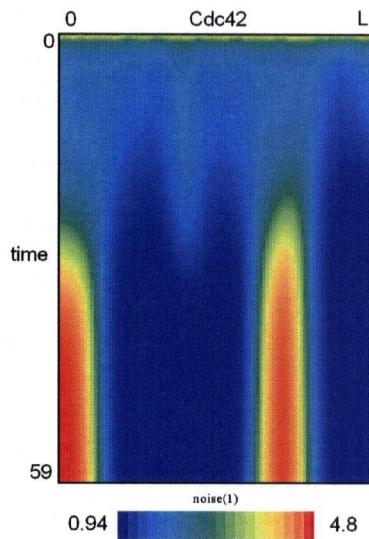
Figure 3.6: The initial distribution of Cdc42 is constant with an additional noise term. The noise is uniformly distributed in the interval (0,1). The noise leads to "spontaneous polarization" of Cdc42. Note that it is possible to have more than one area of high Cdc42 activity form. However, the final state of the system is still a spatially homogeneous steady state.
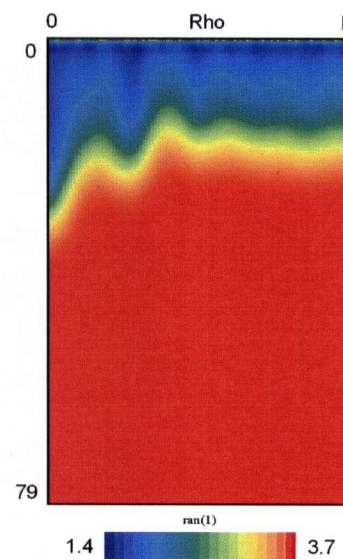
Figure 3.7: If system (3.1) is in a monostable regime, the presence of noise in the initial conditions is damped out. The magnitude of noise is the same as in Figure 3.6.
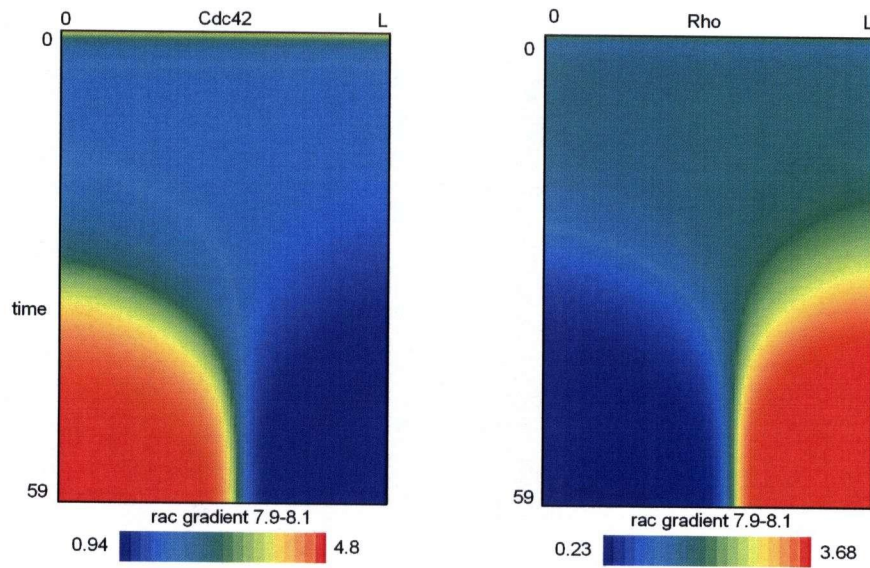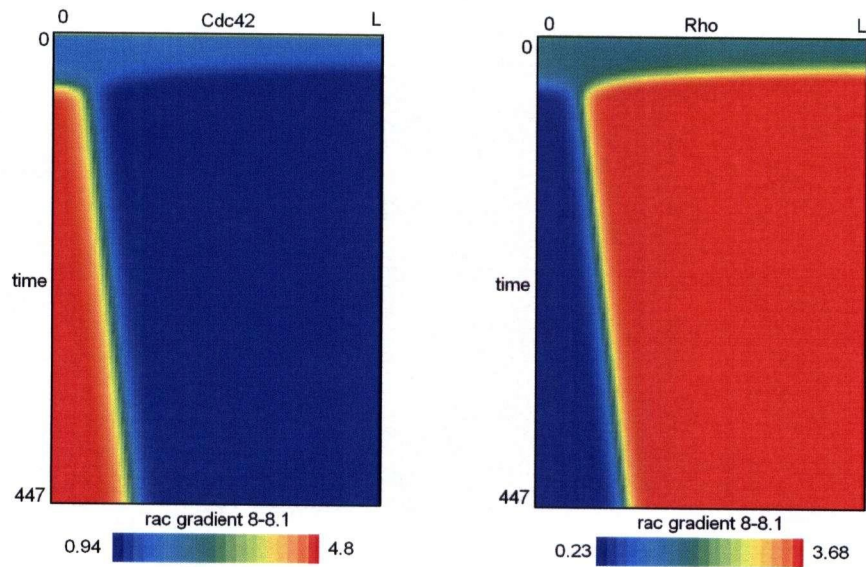
Figure 3.8: Spatiotemporal solutions to model (3.1) with Neumann BCs (a) A small initial gradient in level of active Rac is amplified. (b) Over longer time scale we can see a travelling wave solution emerge.

3.3   Numerical Experiments

The morphological effects of the Rho proteins on the cytoskeleton were first discovered due to a series of microinjection experiments, where active forms of the proteins or GEFS that activate the Rho proteins were injected into cells. Hall (1998) Later microinjection experiments led to the discovery of crosstalk between the proteins.Ridley et al. (1992); Nobes and Hall (1995) These experiments motivate our numerical experiments. We simulate the injection of active protein into the cell by adding a time and space dependent pulse to the equation for the relevant protein. Such stimulation could cause the system to jump from one steady state to another. We simulated the injection of each of the three Rho proteins.

3.3.1   Spatially Homogeneous Pulses

Spatially homogeneous injection of active Cdc42 above a certain threshold will cause the system to approach a high Cdc42/low Rho steady state, while an injection of active Rac or Rho will force a high Rho steady state. If the pulse is below the threshold, the system will recover, and there will be no change in stability of the steady state. We simulated an injection across the entire spatial domain (we also experimented with only "injecting" part of the domain) The injection is characterized by two parameters: pulse duration and amplitude. Since there is a threshold that needs to be reached by the end of the pulse, a pulse of shorter duration needs a higher amplitude to produce a response (see Figures 3.9 and 3.10). The amplitude and duration that were required to exchange the stability of the system depended on the initial conditions.

3.3.2   Spatially Inhomogeneous Pulses

The above results were obtained for pulses across the entire spatial domain. Not surprisingly, this resulted in spatially homogeneous changes in steady states. Spatial heterogeneity can only appear if the stimulus is applied non-uniformly (see Figure 3.11). The width of the pulse influences the outcome. If the pulse is too "skinny", the system will always recover, and no exchange of stability will take place. Thicker pulses require a smaller duration and amplitude to change the stability of the steady states. But, as before, the final state of the system is a spatially homogeneous steady state.

3.3.3   Biological Interpretation

In the biological experiments, either constitutively active proteins or their GEFs were injected into the cell. The localization of the active forms of the proteins to appropriate locations in the cell is outside the control of the experimenter. Our model only includes
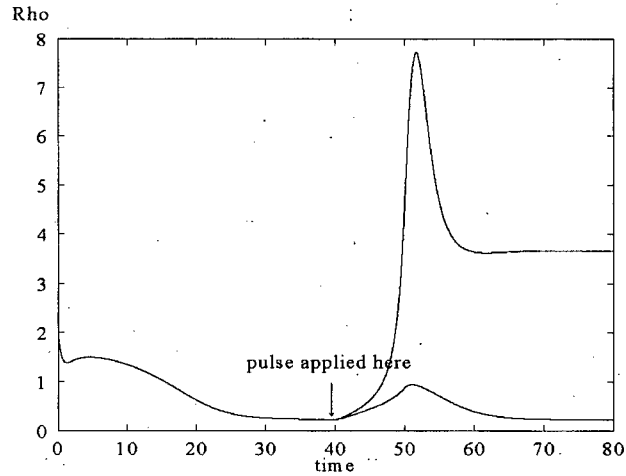
Figure 3.9: Concentration of Rho as a function of time at one spatial mesh point. A pulse of active Rac is injected into system (3.1) at time 40 for 10 seconds (amplitude of the pulse is 3 for the top curve and 2 for the bottom curve).
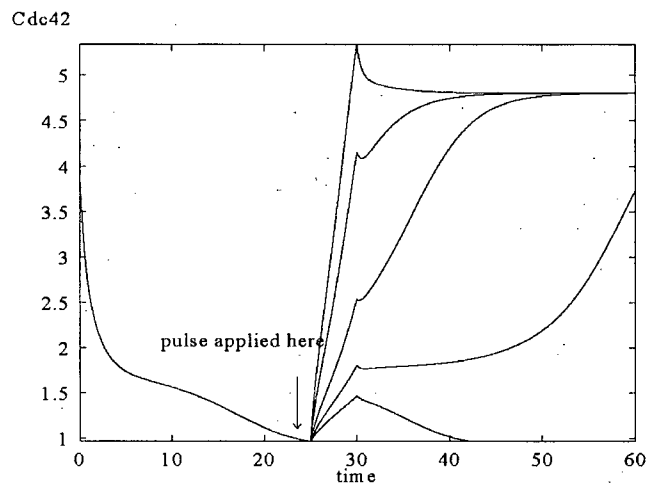
Figure 3.10: Level of Cdc42 as a function of time at one spatial mesh point. A pulse of active Cdc42 is injected into the system at time 25 for 5 seconds. Since, the duration of the pulse is shorter than in the previous figure, a larger amplitude is needed to force the system to change steady states

57
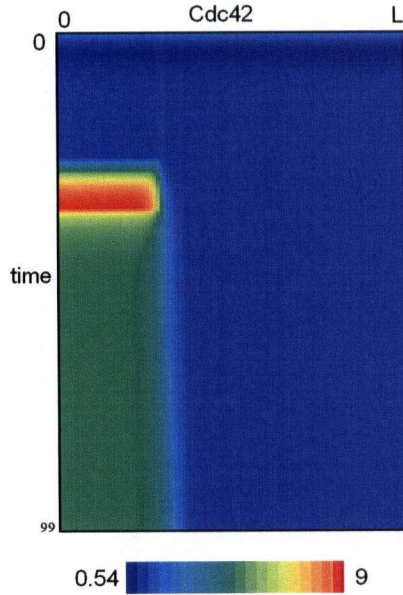
Figure 3.11: Spatial distribution of Cdc42 through time. A pulse of amplitude 5 is injected at time 25 for 10 seconds for $0 \leq x \leq 3\,\mu m$ (30 spatial mesh points). On the spatial domain where the stimulus was delivered, Cdc42 jumps to a high level steady state and remains there after the stimulus is removed.
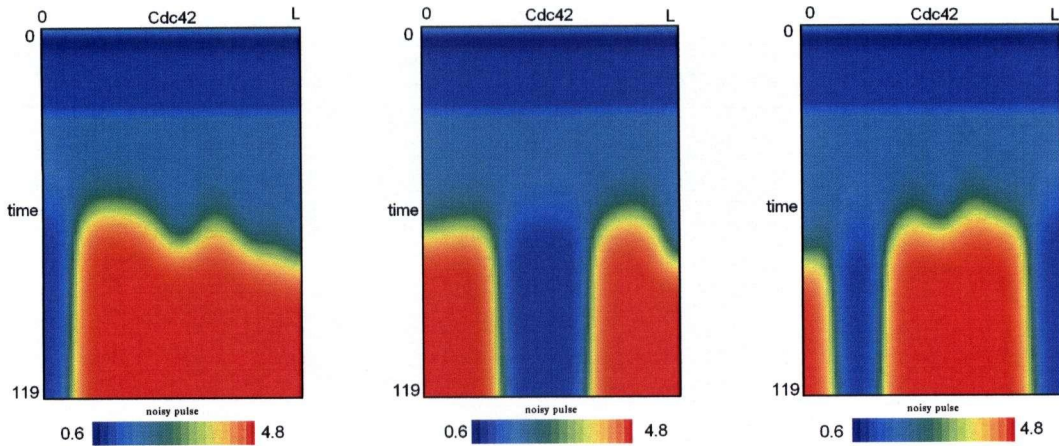
Figure 3.12: If a uniform pulse is applied across the entire spatial domain, no spatial homogeneities can ever develop. However, some noise in the amplitude allows spatial patterns, similar to those obtained in simulations with non-uniform ICs, to develop. We show three different runs, where the amplitude of the pulse was chosen from a normal distribution with a mean of 0.3 and a variance of 0.8. Initial conditions were $C = 2, R = 9, \rho = 2$.

58

the membrane-bound forms of the three proteins. Since the pulse is an additional time-dependent activation term added to the dynamics, in effect, what we are simulating with these numerical experiments is the translocation of the new active proteins to the plasma membrane. In cells, microinjection of active proteins brings on a cellular response similar to that induced by an extracellular stimulus, such as a growth factor. This response is typically development of filopodia and lamellipodia, and stress fiber development. Although, the microinjected cell does not begin moving, the morphology of the actin cytoskeleton changes and polarization must occur, which we interpret as spatial segregation of Cdc42/Rac and Rho. Applying a spatially uniform pulse to the entire domain does not result in spatial segregation. However, making the pulse amplitude "noisy" can create spatial heterogeneity (see Figure 3.12) Presumably there also exist small spatial fluctuations in the rate that the microinjected proteins come on the membrane.

3.4 Activation-Inhibition Model with Periodic Boundary Conditions

The simulations were redone on the domain $0 \leq x \leq \pi d$ with periodic boundary conditions, where the typical diameter of the cell is $10 \, \mu m$. The behaviour of the model was found to be similar to that with no flux boundary conditions (see Figure 3.14). If the parameters are in the range where bistability is possible, and the initial conditions for Cdc42, Rac, and Rho are close to the unstable saddle point, then quite low levels of noise in the initial conditions give rise to spontaneous polarization. The perimeter of a circular cell randomly establishes a "front" with high levels of Cdc42 and a "back" with high levels of Rho.

A modification has to be made for modelling a gradient of one of the small G-proteins for these types of boundary conditions. A front of chemoattractant which activates one of the small G-proteins, say Cdc42, results in an initial sinusoidal profile of active Cdc42 around the periphery of the cell, with a maximum at the side of the cell facing the front, and a minimum at the side of the cell farthest from the front. (see Figure 3.13). Since it is non-uniform, this initial condition becomes amplified, resulting in polarization. If the sinusoidal initial gradient is coupled to noise, polarization of the cell periphery no longer occurs at random, and a "front" will now form on the side of the cell with the highest level of chemoattractant.

chemoattractant front

.cell

Initial level of Cdc42

Figure 3.13: When a cell is exposed to a front of chemoattractant, the periphery of the cell will be exposed to the chemoattractant unevenly. Hence, the initial distribution of the protein activated by the chemoattractant will be sinusoidal.

Figure 3.14 *(on the next page)*: Evolution of Cdc42 on the cell membrane through time. The x-axis is the position on the perimeter of the cell shown in Figure 3.1 (b). The spatial grid used is 100 points. The y-axis is time. For parameters used see Appendix B. In (a) and (b) the initial distribution of small G-proteins on the membrane is constant (Cdc42=3.7, Rac=7.8, Rho=1.7) with an added noise term. The distribution of the noise is UNIF(0,0.5). (c) Initial profile of Cdc42 is $4 + 0.2\sin(\pi x/100)$ where x is the spatial grid. The initial profiles of Rac and Rho are constant (8.2 and 2, respectively) The small spatial profile gets amplified with time. (d) Without the initial sinusoidal profile the system will go to a steady state of low Cdc42/high Rho.
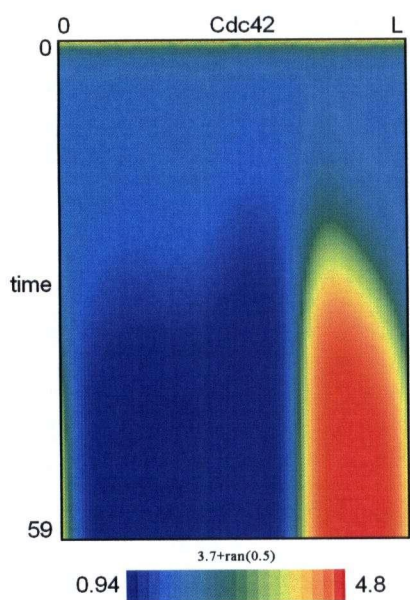
(a)
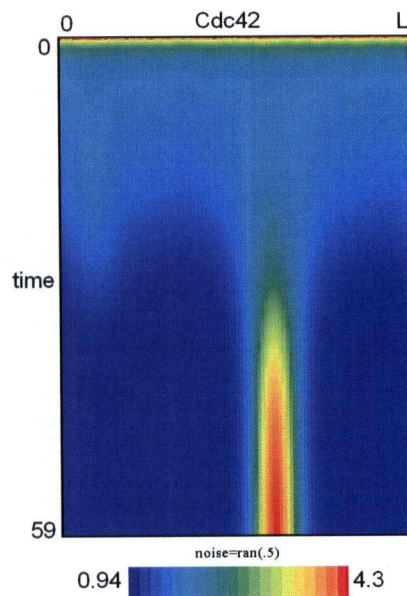
(b)
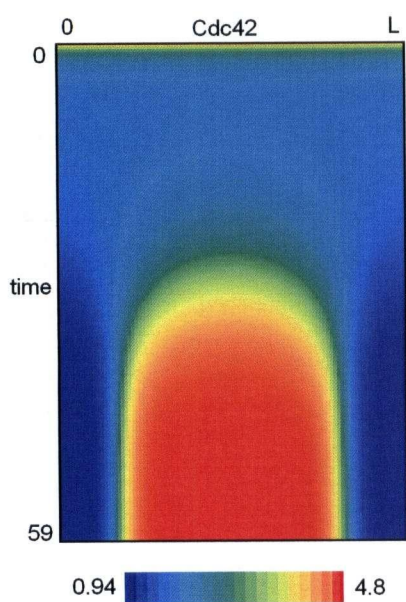
(c)
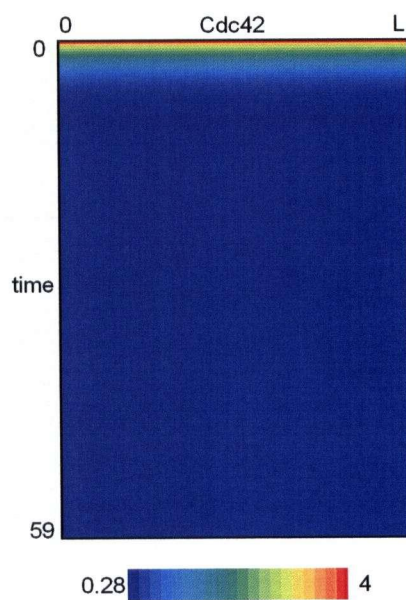
(d)

3.5 Effect of Diffusion Coefficient on the Timescale of Heterogeneity

The initial simulations were done with a diffusion coefficient of 0.01 $\mu m^2/s$. Later, it was found from the literature that a diffusion coefficient of 0.1-1 $\mu m^2/s$ of membrane-bound small G-proteins is more realistic. In Figure 3.5, the timescale of Cdc42/Rho polarization is compared for different diffusion coefficients. It can be seen that the speed of the travelling wave is several times faster for the higher diffusion coefficient. In general, the same results hold for spatial heterogeneity induced by noise. The spatially uniform steady state is usually reached in about four hundred seconds, compared to about two thousand seconds for the smaller diffusion coefficient. Since cells are capable of persistent motion, we conclude that in its current state system (3.1) cannot account for spatial polarization seen at the physiological level. It would be interesting to analytically calculate the wave speed either for the full three variable system, or a reduced two dimensional system in order to see more clearly effect of diffusion and spatial domain on the wave speed.
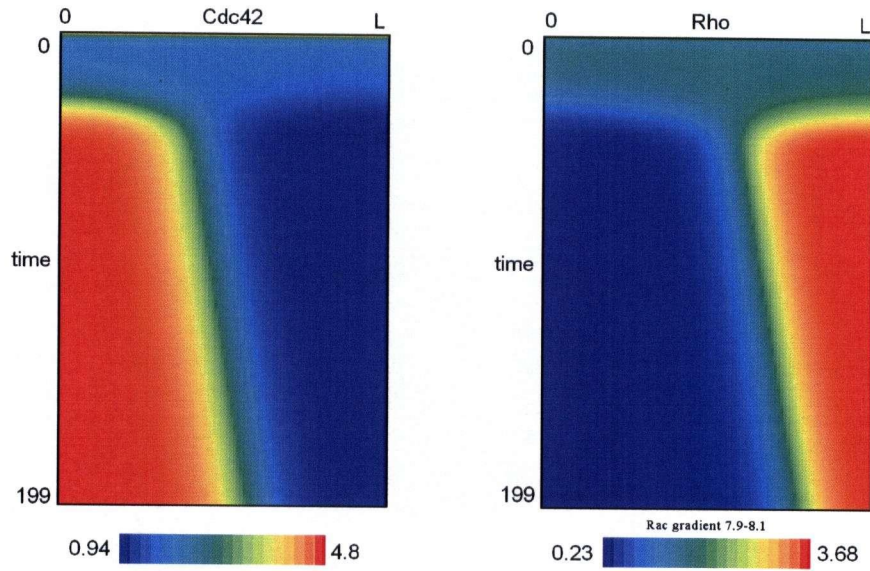
(a)
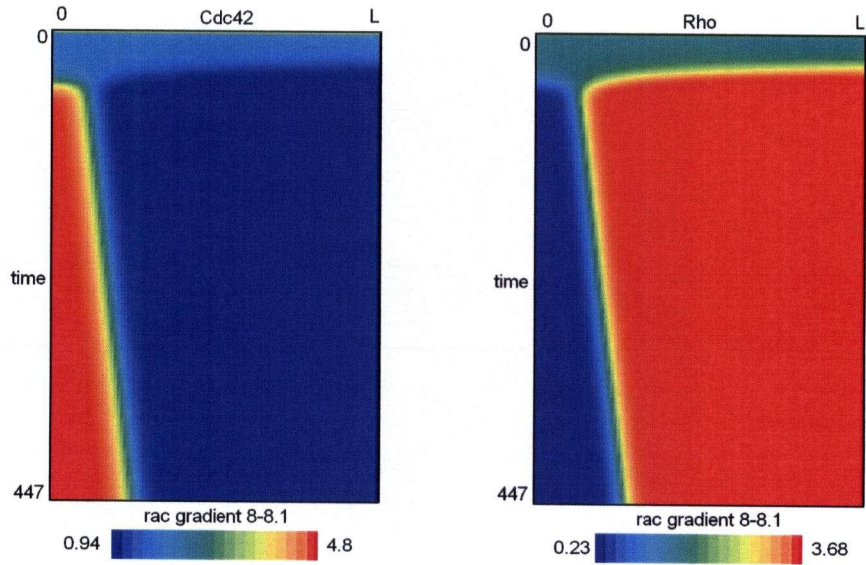
(b)

Figure 3.15: Spatiotemporal solutions to model (3.1) with Neumann BCs. Comparing the timescale of polarization in system (3.1) for different diffusion coefficients. (a) Diffusion coefficient of 0.1 $\mu m^2/s$ is used. (b) Diffusion coefficient of 0.01 $\mu m^2/s$ is used. Note the different timescale on the y-axis.

3.6 Discussion of Spatial Form of the Activation-Inhibition Model

In this chapter we showed that the spatial form of the activation-inhibition model is capable of exhibiting long-lasting spatial segregation of Cdc42/Rac and Rho in the parameter range where the model is bistable. If we view the spatial segregation of active Cdc42/Rac and Rho as indicative of cell polarization, then this model suffers two limitations. First, under no flux boundary conditions the system sometimes develops multiple "hot spots" of Cdc42 activity. If we consider a formation of a "spot" of high Cdc42 activity as the front of the cell, this is a problem, as a cell, obviously can have only one front and back. This issue of multiple "hot spots" of activity does not seem to come up in simulations with periodic boundary conditions, and is clearly related to the size of the diffusion coefficient relative to the size of the domain. These "hot spots" do eventually merge, as the system goes to a spatially uniform steady state. However, as mentioned earlier, long-persisting heterogeneity seems to result in a high Cdc42/Rac and low Rho steady state. From a biological viewpoint, it is more reasonable to believe dynamics that tend to a non-homogeneous steady state (meaning a cell will remain polarized) or return to baseline, meaning the cell has adapted to the signal. Including the faster diffusing inactive forms and keeping track of the total Rho protein concentration in the Synthesis Inhibition Model stops the travelling wave and allows persistent polarity (Stan Marée, personal communication).

Another problem, common to all models that exhibit bistability, has to do with loss of sensitivity and "locking". All bistable systems exhibit hysteresis. The initial conditions of the problem will determine which steady state the system will approach. If the initial conditions are close to the unstable saddle point, then just a small perturbation determines which steady state the system will approach. Once that direction is established, however, the system does not switch back and forth between states. Instead, the system now requires a large "push" in order to change states. The reason for this can be seen by looking at the bifurcation diagrams for the model (Figure 2.10). Once the solution jumps from one stable solution branch to another, it will remain there once the stimulus that triggered the jump is gone. But a moving cell remains sensitive, and can change directions in response to changes in the environment. Cells can detect chemical gradients as small as 2%. It is not viable for a cell to stop responding to future gradients if it has detected a gradient already. Because our model deals only with small G-proteins, which are an intermediate component in signal transduction to the cytoskeleton, the model implicitly assumes that the extracellular chemoattractant gradient translates into a gradient of GEF activity along the membrane. Hence, the questions of extracellular gradient amplification and cellular adaptation to increasing or decreasing chemoattractant levels are not addressed in this thesis.

64

Chapter 4

Compartmentalization of Rho GTPases and Parameter Estimation

Our previous modelling treated the cytosolic pool of the small G-proteins as a vast reservoir, where the concentrations of the inactive cytosolic forms of the Rho proteins remained constant over space and time. As a result, we only needed to keep track of membrane-bound active forms of the proteins. We now remove this assumption, and keep track of both membrane-bound and cytosolic forms of the Rho proteins.

The models in this chapter deal with transitions between cytosol and membrane that is undergone by each Rho family protein. They are multi-compartment models with overall conservation of protein. The flux between the different compartments depends on GEF, GAP, and GDI levels, which, in turn, are influenced by the extracellular signals. Although these models do not include interactions between Cdc42, Rac, and Rho, they allow us to test which biological parameters will be most important in determining the relative distribution of the protein between various active and inactive forms. Furthermore, many parameter estimates for these models can be obtained from experimental papers. Using various parameter values we can calculate the flux rates and predict the distribution between different compartments for a single Rho protein. Since the distribution between compartments in unstimulated versus stimulated cells is known, we can estimate how realistic our model is, as well as determine which parameters the model is most sensitive to.

This compartmental model can later be combined with the interactions of the GTPases discussed earlier, to assemble a more predictive model of Rho protein crosstalk.

4.1 Features of a General Membrane Translocation Model

4.1.1 Biological Details

As discussed in detail in Chapter 1, the Rho proteins undergo two coupled cycles shown in Figure 4.1. The proteins cycle between GDP-bound and GTP-bound conformations, and between cytosolic and membrane-bound forms. These two cycles are regulated by three classes of proteins: guanine nucleotide exchange factors (GEFs), GDP dissociation inhibitors (GDIs), and GTPase-activating proteins (GAPs) (Takai et al., 2001).

All Rho proteins are post-translationally modified with lipids at their C termini. The covalent attachment of a prenyl group (related to cholesterol) anchors a water-soluble protein to a membrane after it is synthesized in the cytosol (Alberts et al., 1994). It has been demonstrated that GDI extracts the GDP-bound form from the membrane to the cytosol, where it is held in an inactive pool. The currently accepted theory is that the Rho proteins have to be bound to GDI in order to remain in the cytosol. In resting (non-motile) cells, the majority of Rho proteins are cytosolic, and therefore, inactive.

Two schemes have been suggested for coupling GTP loading and membrane translocation. In the first, guanosine exchange takes place first in the cytosol, and translocation occurs later, possibly due to decreased affinity of GDI for the GTP-loaded form. In the second scheme, membrane translocation occurs prior to GTP-GDP exchange. Robbe et al. (2003) demonstrated that the soluble Rac-GDI complex is very poorly activated by the active GEF site(DH-PH domain). Hence, Rac tends to dissociate from GDI and translocate to the membrane before it is activated by a GEF. So we assume that GDI dissociation/membrane translocation occurs prior to nucleotide exchange in our modelling.

Table 4.1: Compartmentalization Model Variables

Variable	Meaning
R or R_{GDI}	cytosolic Rho protein (in complex with GDI)
R_{GDP}	membrane-bound GDP-bound protein (in complex with a binding site)
R_{GTP}	membrane-bound GTP-bound protein (in complex with a binding site)
B	free membrane binding sites
GDI_{free}	free GDI in cytosol

4.1.2 Issues to Address

A satisfactory model accounting for observed cellular behaviour should have an equilibrium with most of the protein in the cytosolic state for an unstimulated cell. Upon activation (increase in GEF and GAP rates), a fraction of the cytosolic protein (it is unclear exactly how much from the data) should translocate to the membrane, and become activated

66
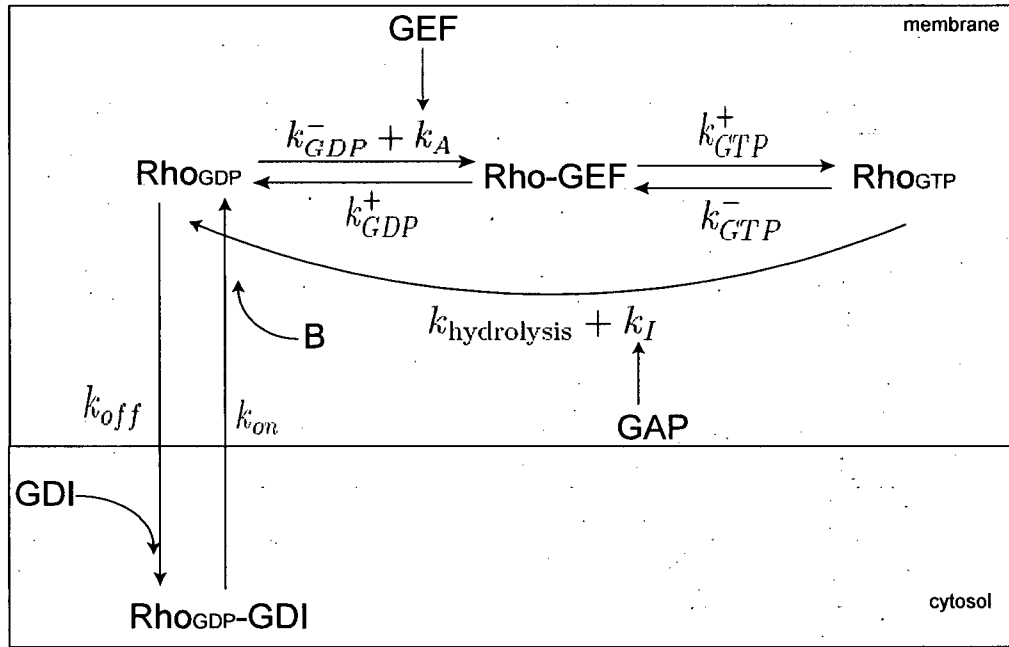
Figure 4.1: Full model of the activation and membrane translocation cycles of a Rho GTPase. In this model, Rho-GDP alone is capable of coming off and on the membrane. To move into the cytosol, Rho-GDP needs to bind to a GDI molecule. All membrane-bound proteins are assumed to be attached to a membrane binding site, B. Little is known about the molecular mechanisms that allow the delivery and extraction of Rho proteins at specific sites in cell membranes. Nucleotide exchange can only take place on the membrane. Dissociation of GDP from the GDP-bound form is an extremely slow reaction. For Rho GTPases to be effective molecular switches, GDP dissociation is stimulated by various GEFs. GEFs form a binary complex with the nucleotide-free protein, stabilizing the transient nucleotide-free protein configuration (Zheng, 2001). GEFs dissociate when GTP binds to this transient complex. Although the GDP/GTP exchange reaction is reversible, in reality it almost never occurs. Instead, GTP is hydrolyzed to GDP. This process is stimulated by various GAPs. Only GTP-bound forms of the protein are active and can bind to Rho effectors.

(Michaelson et al., 2001). A maximum level of active Rho should be reached within a minute of stimulation (Kurokawa et al., 2004). We would like to achieve this behaviour in our compartmental model.

A complete model for the compartmentalization of a Rho family protein should include both cytosolic and membrane-bound forms of the protein, as well as GDI, which limits how much protein is present in the cytosol, and Rho membrane binding sites, which determines how much protein is present on the membrane. The notation for the model variables is given in Table 4.1. We analyze two simplifications of this full model: one with membrane-binding sites but without explicit modelling of GDI binding, and one with GDI binding, but without membrane sites. We simulate exposure to extracellular signal by increasing the GEF and GAP rates. As a result, the protein should redistribute from cytosolic to membrane-bound, GTP-loaded form. To test the validity of our model, we observe the timescale needed to reach a new steady state from cytosolic initial conditions once an extracellular signal is received, as well as the distribution of protein between compartments at the steady state. We then compare both of these models to the observed Rho compartmentalization in cells.

The main purpose of this chapter is to better understand how the activation of Rho GTPases is controlled by three classes of regulators, GEFs, GAPs, and GDI. We use a combination of parameter values obtained from literature sources and numerical simulation to determine what the *in vivo* GEF/GAP rates should be for both stimulated and unstimulated cells. We also examine how affinity of Rho proteins to membrane binding sites and cytosolic GDI affects the balance between membrane and cytosol compartments.

4.2 Estimating Nucleotide Exchange Rate Parameters

We model the nucleotide exchange cycle, shown in the top half of Figure 4.1, as a two compartment model with apparent rates of conversion from one compartment to another:

$$\text{Rho}_{\text{GDP}} \underset{k_2}{\overset{k_1}{\rightleftharpoons}} \text{Rho}_{\text{GTP}}.$$
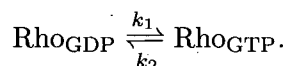
Parameter values for the nucleotide exchange are summarized in Table 4.7, were based on literature values stated in (Menard et al., 1992; Newcombe et al., 1999; Zerial and Huber, 1995; Zhang and Zheng, 1998) and (Zheng, 2001). All measurements were done *in vitro*. (Zerial and Huber, 1995) is an encyclopedic summary of small G-protein protein characteristics, is, in turn, based on a review of literature dating back to 1995.

We need to estimate the apparent compartment flow rates k_1 and k_2 from experimentally determined parameter values in Table 4.2. The rates of nucleotide dissociation (k^-_{GDP} and k^-_{GTP}) are comparable. It can be seen from Table 4.2 that $k^-_{GDP} \approx k^-_{GTP}$ and are on the order of $10^{-3} - 10^{-4}\,s^{-1}$. In the presence of GDI, the nucleotide exchange rate

Parameter	Meaning	Value	Comments	Citation
k_{GDP}^-/k_{GTP}^-	rate of GDP/GTP dissociation	$1.7 \times 10^{-4}\,\mathrm{s}^{-1}$	in RhoA	[1]
		$5.8 \times 10^{-4}\,\mathrm{s}^{-1}$	in Cdc42	[1]
		$1.5 \times 10^{-3}\,\mathrm{s}^{-1}$	in Rac	[2]
k_{GDP}^+/k_{GTP}^+	rate of GDP/GTP association	unknown	$k_{GTP}^+ \gg k_{GDP}^+$	[3]
$k_{\mathrm{hydrolysis}}$	innate GTP-hydrolysis rate	$8.3 - 16.7 \times 10^{-4}\,\mathrm{s}^{-1}$	in Cdc42	[1]
		$7.7 \times 10^{-4}\,\mathrm{s}^{-1}$	in RhoA	[1]
		$3.6 \times 10^{-4}\,\mathrm{s}^{-1}$	in RhoA	[4]
		$4.8 \times 10^{-3}\,\mathrm{s}^{-1}$	in Rac1	[5]
k_I	GAP-stimulated hydrolysis rate	$3.3 \times 10^{-2}\,\mathrm{s}^{-1}$	unspecified GAP in Cdc42	[1]
		$1.61\,\mathrm{s}^{-1}$	p190 GAP in RhoA	[4]
k_A	GEF-stimulated GDP dissociation rate	$5.8 \times 10^{-3}\,\mathrm{s}^{-1}$	Dbl in Cdc42	[1]

Table 4.2: Experimentally Determined Nucleotide Exchange Rates. Cited references: [1] (Zerial and Huber, 1995), [2] (Newcombe et al., 1999), [3] (Zheng, 2001), [4] (Zhang and Zheng, 1998), [5] (Menard et al., 1992).

falls to less than $6 \times 10^{-6} \, s^{-1}$, (Newcombe et al., 1999), consistent with the fact that GDI interferes with nucleotide exchange. So nucleotide exchange is assumed negligible when GDI is bound to the protein in the model.

Numerical values for GTP and GDP association rates are difficult to determine given the unstable nature of the nucleotide free G-protein. However, GDP dissociation is believed to be the rate-limiting step in replacing GDP by GTP. Because cells have a 10-fold GTP to GDP ratio, a nucleotide free Rho protein is much more likely to bind to GTP (Zheng, 2001). Therefore, we approximate the rate at which a GDP-bound protein changes to a GTP-bound protein by the GDP dissociation rate, as we assume that GDP-dissociation rate is the limiting step ($k_{GDP}^{-} \ll k_{GTP}^{+}$).

In addition to the reversible reactions of nucleotide dissociation/association, there is also an irreversible reaction of GTP-hydrolysis. A GTP-bound protein is much more likely to undergo GTP hydrolysis than dissociation of GTP followed by GDP binding. Therefore, we approximate the rate at which a GTP-bound protein changes to a GDP-bound protein by the GTP hydrolysis rate, $k_{hydrolysis}$.

We also need estimates for the rates of GEF-stimulated GDP-dissociation (k_A) and GAP-stimulated GTP hydrolysis (k_I), since they will determine the nucleotide exchange rates *in vivo*. These rates are known to less accuracy than the other parameters, and probably vary by several orders of magnitude depending on cell type and stimulus. At present, there is no information in the literature about the concentrations of Rho GEFs/GAPs in activated cells. Numerous proteins can act as GEFs or GAPs to the Rho proteins, so it seems reasonable to assume that that the activation/inactivation of Rho proteins is not limited by the amounts of GEFs/GAPs. We therefore treat k_A, k_I as constants.

Based on the experimental data, we simplify the full nucleotide exchange cycle of a small G-protein, shown in figure 4.1 to:

$$\text{Rho}_{\text{GDP}} \underset{k_2}{\overset{k_1}{\rightleftharpoons}} \text{Rho}_{\text{GTP}},$$
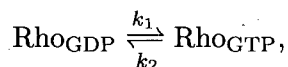
where $k_1 = k_{GDP}^{-} + k_A$ and $k_2 = k_{\text{hydrolysis}} + k_I$.

4.3   Membrane Binding Sites for Rho Proteins

In this section, the interactions of Rho proteins with membrane binding sites are discussed and a corresponding model is formulated. A bimolecular reaction between a cytosolic protein and a binding site is assumed to take place in order for protein to translocate to the membrane.

4.3.1 Biological Justification

Evidence suggests that Rho proteins bind to specific membrane binding sites. Bokoch et al. (1994) first reported that in neutrophil membranes release of Rac from GDI and membrane translocation only occurs in the presence of GTP and an unknown membrane component. Boukharov and Cohen (1998) reported high affinity between GTP-bound RhoA and an unidentified integral membrane component in erythrocytes. Del Pozo et al. (2004) reported that Rac1 binds to components of low density cholesterol-rich domains (lipid rafts) in the plasma membrane. However, no quantitative information is known about the numbers of these cholesterol-rich domains, and even their existence is still controversial.

The only quantitative estimate of these unidentified Rho protein binding sites comes from the paper by Boukharov and Cohen (1998). Based on the estimate of Boukharov and Cohen (1998), we consider a model with a limited number of Rho binding sites on the membrane. For proteins to translocate to the membrane, a bimolecular reaction between a cytosolic protein and a free binding site must take place. We use the data in Boukharov and Cohen (1998) for the number of Rho binding sites and affinity of the Rho protein to the binding site. We do not keep track of GDI in this model, as Boukharov and Cohen (1998) did not provide any data on GDI in their paper. Effectively, we assume that GDI has a passive role in the translocation process; i.e. it is bound to cytosolic proteins, but does not actively extract the membrane-associated form.
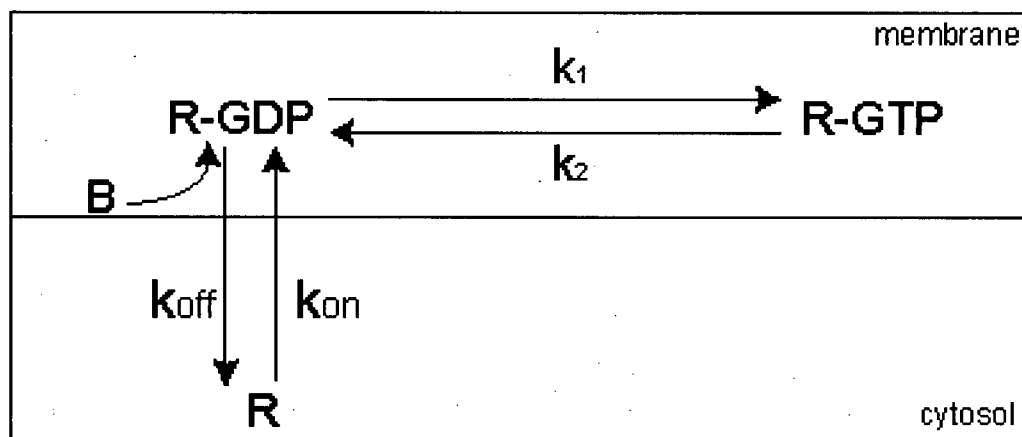
Figure 4.2: A schematic diagram of the Binding Site Model of Rho translocation. The cytosolic form of the protein, R, is assumed to be in a complex with GDI, but GDI is not modelled explicitly. The full nucleotide exchange cycle shown in Figure 4.1 has been reduced to a simple two compartment module, with simple flow rates from one compartment to another The membrane-bound forms, R-GTP and R-GDP, are in complex with a binding site, B.

4.3.2 The Binding Site Model Formulation

Consider one of Cdc42, Rac, or Rho in isolation from other Rho proteins. Let R be the number of molecules of the (inactive) cytosolic form of the Rho protein, and R_{GTP} the number of molecules of the active membrane-bound form (GTP-bound). We will assume that all cytosolic forms are GDP-bound. Let B be the number of molecules of free Rho binding sites on the membrane, and R_{GDP} the number of molecules of membrane-bound inactive form (GDP-bound). We formulate the model in number of reactant molecules per cell, rather than concentrations to avoid complications due to different volumes of the membrane and cytosol compartments.

We model the activation of the protein as a two-step process: membrane translocation of the cytosolic form, followed by nucleotide exchange. The biochemical model is given by:

$$R + B \underset{k_{off}^B}{\overset{k_{on}^B}{\rightleftharpoons}} R_{GDP} \qquad \text{(binding to membrane sites)} \qquad (4.1)$$

$$R_{GDP} \underset{k_2}{\overset{k_1}{\rightleftharpoons}} R_{GTP} \qquad \text{(nucleotide exchange)} \qquad (4.2)$$
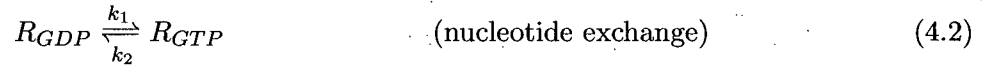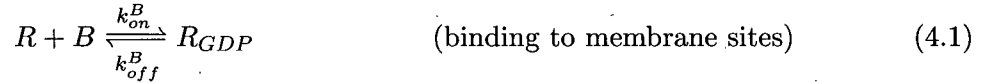
where $k_1 = k_{GDP}^- + k_A$ and $k_2 = k_{\text{hydrolysis}} + k_I$, as derived in the previous section. The equations corresponding to the biochemical model are:

$$\frac{dR}{dt} = k_{off}^B R_{GDP} - k_{on}^B RB$$

$$\frac{dR_{GDP}}{dt} = k_{on}^B RB - k_{off}^B R_{GDP} - k_1 R_{GDP} + k_2 R_{GTP} \qquad (4.3)$$

$$\frac{dR_{GTP}}{dt} = k_1 R_{GDP} - k_2 R_{GTP}.$$

Conservation of Total Protein

The total number of binding sites ($\mathbf{B_t}$) and the total amount of Rho protein ($\mathbf{R_t}$) in the cell are conserved. Hence, we can eliminate some variables from the model, using

$$B = \mathbf{B_t} - R_{GDP} - R_{GTP}, \qquad (4.4\text{a})$$

$$R = \mathbf{R_t} - R_{GDP} - R_{GTP}. \qquad (4.4\text{b})$$

Reduction and Dimensionless Formulation

Substituting in equations (4.4) we obtain the following system:

$$\frac{dR_{GDP}}{dt} = k_{on}^B(\mathbf{R_t} - R_{GDP} - R_{GTP})(\mathbf{B_t} - R_{GDP} - R_{GTP})$$

$$- k_{off}^B R_{GDP} - k_1 R_{GDP} + k_2 R_{GTP}, \tag{4.5}$$

$$\frac{dR_{GTP}}{dt} = k_1 R_{GDP} - k_2 R_{GTP}.$$

Let

$$R_{GDP}^* = \frac{R_{GDP}}{\mathbf{R_t}} \text{ and } R_{GTP}^* = \frac{R_{GTP}}{\mathbf{R_t}}$$

be the fractions of total protein in GTP-bound and GDP-bound membrane-associated form. Similarly, $R^* = \dfrac{R}{\mathbf{R_t}}$ is the fraction of total protein in cytosolic form. Then (4.5) reduces to:

$$\frac{dR_{GDP}^*}{dt} = k_{on}^B(1 - R_{GDP}^* - R_{GTP}^*))(\alpha - R_{GDP}^* - R_{GTP}^*)$$

$$- k_{off}^B R_{GDP}^* - k_1 R_{GDP}^* + k_2 R_{GTP}^*, \tag{4.6}$$

$$\frac{dR_{GTP}^*}{dt} = k_1 R_{GDP}^* - k_2 R_{GTP}^*,$$

where $\alpha = \mathbf{B_t}/\mathbf{R_t}$ is the ratio of total binding sites to total amount of Rho protein, $k_1 = k_{GDP}^- + k_A$ and $k_2 = k_{\text{hydrolysis}} + k_I$. The units for k_1, k_2 and k_{off}^B are sec^{-1}, and k_{on}^B is measured in $\text{cell sec}^{-1} \text{molecules}^{-1}$. It is easy to show that system (4.5) has a unique biologically relevant steady state. The formula for the steady state is derived in Appendix C.

Table 4.3: Dimensionless Variables for Model (4.6)

VARIABLE	MEANING
R_{GDP}^*	fraction of protein in GDP-bound (inactive) form on the membrane
R_{GTP}^*	fraction of protein in GTP-bound (active) form on the membrane
R^*	fraction of protein in cytosolic (inactive) form
α	ratio of total binding sites to total protein

Table 4.4: Experimental Data for Binding Site Model. Cited references: [1] Sako et al. (2000), [2] Nomanbhoy et al. (1999), [3] Boukharov and Cohen (1998). Total membrane binding sites and protein were measured for erythrocyte cells.

PARAMETER	MEANING	VALUE	SOURCE
k_{off}^B	membrane dissociation rate	$0.5s^{-1}$ for Rac	[1]
		$0.133s^{-1}$ for Cdc42	[2]
$K_d = k_{off}^B/k_{on}^B$	membrane affinity	$1\text{-}5\,\text{nM}^{-1}\text{s}^{-1}$ for RhoA	[3]
k_{on}^B	membrane binding rate	$.1\text{-}.5\,\text{nM}^{-1}\text{s}^{-1}$ for RhoA	[1] and [3]
k_{on}^B	membrane binding rate	$.026\text{-}.133\,\text{nM}^{-1}\text{s}^{-1}$ for RhoA	[2] and [3]
$\mathbf{B_t}$	total membrane binding sites	$(1-2)\cdot 10^3$ binding sites per cell	[3]
$\mathbf{R_t}$	total Rho protein	$(1.3 \pm 0.3)\cdot 10^3$ molecules	[3]

4.3.3 Parameter Estimates for the Binding Site Model

Biologically plausible parameter estimates are needed to compare the behaviour of equations (4.6) to observed behaviour. As there is not enough data about each individual protein, we take a composite of available data, seen in Table 4.4, and assemble a model for an arbitrary member of the Rho family. As new data emerges, the model can be refined and adapted to a specific GTPase and cell type.

Values for $k_1 = k_{GDP}^- + k_A$ and $k_2 = k_{\text{hydrolysis}} + k_I$ can be determined from Table 4.2. We have two independently, obtained experimental values for k_{off}^B in Table 4.4. The k_{off}^B value in Sako et al. (2000) was obtained by measuring the average membrane lifetime of individual molecules of YFP-labelled Rac. The k_{off}^B value in Nomanbhoy et al. (1999) was obtained by measuring the release rate of Cdc42 from membrane in the presence of saturating concentration of GDI.

We need to convert the estimate for k_{on}^B to the units of cell sec^{-1} molecules^{-1}. The volume of a human erythrocyte is approximately $90\,\mu m = 9\cdot 10^{-14}$ L. (Mammal Erythrocyte Sizes: http://www.genomesize.com/cellize/mammals.htm). Further, using the conversion factor

$$1\,\text{nM} = 6.02\cdot 10^{14}\text{ molecules/L}.$$

we obtain

$$1\,\text{nM} = 6.02\cdot 10^{14}\text{ molecules/L} \times 9\cdot 10^{-14}\text{ L/cell} = 54\text{ molecules/cell}.$$

Hence,

$$k_{on}^B = 2\cdot 10^{-3} - 1\cdot 10^{-2}\text{cell sec}^{-1}\text{ molecules}^{-1}\text{ or } 0.5\cdot 10^{-3} - 2.5\cdot 10^{-3}\text{cell sec}^{-1}\text{ molecules}^{-1}.$$

From Table 4.4 the total amount of protein $R_t \approx 1000$ molecules/cell and the ratio of total binding sites to total protein $\alpha \approx 1$.

4.3.4 Numerical Observations

System (4.6) was simulated in XPPAUT using the parameter values described above. In a resting cell, the majority of the protein is in cytosolic form, with only 2-3 % present on the membrane, (Boukharov and Cohen, 1998). So in the simulation all Rho protein was assumed to be in cytosolic form ($R^*_{GDP} = R^*_{GTP} = 0$) for the initial conditions.

We used a value of k_{off} as determined by Sako et al. (2000) by measuring the average membrane lifetime of individual YFP-labelled molecules. Nomanbhoy et al. (1999) obtains the same order of magnitude for k_{off} using a different method. However, we have no sources other than Boukharov and Cohen (1998) for estimating the affinity of membranes to Rho proteins. The k_{on} rate used in the simulations was a lower bound obtained from K_d determined by Boukharov and Cohen (1998) and this k_{off} value. The level of GEF and GAP activity, total protein, and ratio of binding sites to protein was varied throughout the simulations.

Time Course to Equilibrium

We are interested in how long it takes the Rho protein to translocate to the membrane from the cytosol (initial conditions are $R^*_{GDP} = R^*_{GTP} = 0$) once an extracellular signal is received. Simulations were performed both with and without GEF and GAP rates (k_A and k_I) added to the basal GTP loading/hydrolysis rates (k^-_{GDP} and $k_{hydrolysis}$). Without the k_A and k_I terms, system (4.6) is fairly stiff. This can be seen by comparing the magnitude of the two eigenvalues of the system (-1.9 and $9.5 \cdot 10^{-4}$). It takes over 100 minutes for the system to reach the analytically determined equilibrium. Including the k_A and k_I terms (using values in Table 4.2) changed the eigenvalues to approximately -1.9 and -0.03, and the system approached equilibrium much faster. In this case it takes about 3 minutes to reach equilibrium.

Table 4.5: Time course to equilibrium in Binding Site Model depends on GEF and GAP rates (k_A and k_I). Parameters k_A and k_I appear in system (4.5) as $k_1 = k^-_{GDP} + k_A$ and $k_2 = k_{hydrolysis} + k_I$.

k_A (sec^{-1})	k_I (sec^{-1})	Time to reach equilibrium (sec)
0	0	> 6000
0.005	0.03	200
0.05	0.03	100
0.5	0.3	10
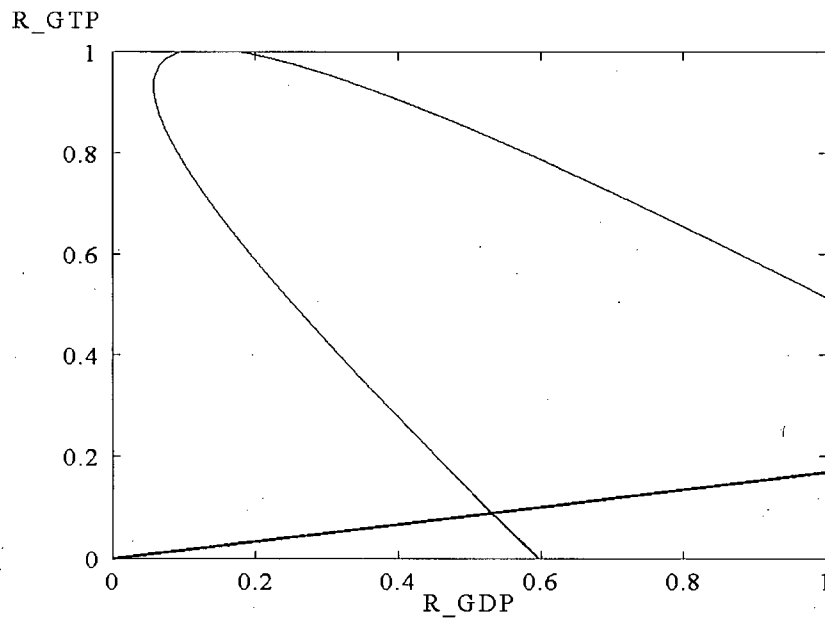
Figure 4.3: Phase-plane diagram for the Binding Site Model, showing the nullclines and the biologically relevant steady state. Parameter values used are given in Tables 4.2 and 4.4. The steady state distribution of the Rho protein forms are $R^*_{GDP} = 53\%$, $R^*_{GTP} = 9\%$, $R^* = 38\%$.

GEF Effect k_A (sec^{-1})	GAP effect k_I (sec^{-1})	Total protein R_t	Binding Sites to Protein Ratio α	Fraction Protein GDP-bound, R_{GDP}^*	Fraction Protein GTP-bound, R_{GTP}^*	Fraction Protein Cytosolic, R^*
0	0	1000	0.5	0.298	0.074	0.628
0	0	1000	1	0.505	0.126	0.369
0	0	1000	2	0.674	0.169	0.157
0	0	2000	0.5	0.337	0.084	0.579
0	0	2000	1	0.577	0.144	0.279
0	0	2000	2	0.728	0.182	0.09
0.005	0.03	1000	0.5	0.313	0.053	0.634
0.005	0.03	1000	1	0.531	0.09	0.379
0.005	0.03	1000	2	0.714	0.121	0.166
0.005	0.03	2000	0.5	0.357	0.06	0.583
0.005	0.03	2000	1	0.61	0.103	0.287
0.005	0.03	2000	2	0.774	0.131	0.095
0.5	0.3	1000	0.5	0.16	0.265	0.575
0.5	0.3	1000	1	0.273	0.455	0.272
0.5	0.3	1000	2	0.343	0.571	0.089
0.5	0.3	2000	0.5	0.171	0.286	0.543
0.5	0.3	2000	1	0.3	0.499	0.201
0.5	0.3	2000	2	0.358	0.596	0.046

Table 4.6: Distribution of Protein at Equilibrium for Model (4.6). R_{GDP}^*, R_{GTP}^*, and R^* are calculated for various k_A, k_I, R_t and α values using the steady state solution derived in Appendix C.

Relative Distributions of the Proteins

Using parameter estimates from Tables 4.2 and 4.4, model (4.5) does not give realistic compartment distributions. At steady state most of the small GTPase is bound to the membrane in inactive (GDP-bound) form R^*_{GDP}. To test if this phenomenon was caused by the fact that the amount of total protein and membrane binding sites is approximately equal, we varied the ratio of total binding sites to protein (dimensionless parameter α). As can be seen from Table 4.6, changing the ratio of binding sites to total protein, α, from 0.5 (twice as much binding sites as protein) to 2 (twice as much protein as binding sites) has a large effect on R^*_{GDP} values. Predictably, a larger α leads to more protein binding to the membrane. However, changing α does not greatly affect R^*_{GTP} values.

Instead, as can be seen from Table 4.6, k_A and k_I have an important effect on the distribution of the membrane-bound forms between R^*_{GDP} and R^*_{GTP}, but do not significantly change the proportion of protein that is cytosolic. For example, increasing k_A 100 times and k_I 10 times increases R^*_{GTP} 50 times, halves R^*_{GDP}, but only changes the cytosolic fraction by a factor of 1.4. Examining the parameter values in Table 4.2 we find that $k_A < k_I$. Hence, including k_A and k_I actually decreases the amount of active Rho protein on the membrane from 12.6% of the total Rho protein to 9 % for $\mathbf{R_t} = \mathbf{B_t} = 1000$ molecules/cell, as the rate of conversion from GTP to GDP is larger than replacement of GDP by GTP. However, if $k_A > k_I$ then, as expected, inclusion of GEF and GAP rates will result in an increase of GTP-bound forms. It should be noted, however, that this effect occurs due to depletion of the intermediate membrane-bound, GDP-loaded form, rather than a significant translocation of cytosolic form to the membrane that is observed biologically.

4.3.5 Discussion of the Binding Site Model

Even though model (4.6) is a simple ODE model, involving only one of the small G-proteins, simulations with the literature-determined parameter values give some insights into the dynamics of the activation process. Simulation with the experimentally obtained values for k_{GTP} and k_{GDP} confirms that a basal level of GEF and GAP activity is needed in nonmotile cells. The GTP hydrolysis and GDP dissociation rates determined *in vitro* are so low that the timescale of conversion of R^*_{GDP} to R^*_{GTP} is extremely slow (thousands of seconds).

Including the GEF and GAP rates obtained from the literature shows that the GEF and GAP rates *in vivo* must be higher than the estimates in the literature obtained from *in vitro* experiments, since these parameters, not the k_{on} and k_{off} rates, limit how quickly the cell responds to signal. This conclusion, of course, depends on the assumption made in the model that only GDP-bound forms are present in the cytosol. If GTP-bound forms

could also bind to GDI and come off the membrane then these proteins become activated by binding to the membrane at the rate k_{on}, and do not go through an intermediate membrane-bound GDP-bound inactive state. However, in that case, activation of the Rho protein would not depend on GEFs or GAPs, contradicting biological data.

The way that the limited binding sites model is formulated, the extracellular signal (acting via GAPs and GEFs) only affects the kinetics between R^*_{GDP} and R^*_{GTP}. As can be seen in Table 4.6 in the absence of GEF and GAP effects ($k_A = k_I = 0$) only 37% of the protein is in cytosolic form. This is in contradiction to the observation that most Rho protein is cytosolic in unstimulated cells (Michaelson et al., 2001).

To address the discrepancies between observed cell behaviour and the behaviour of system (4.6), consider the assumptions that went into the limited binding sites model. We used the standard biochemical assumption that a bimolecular reaction has to occur between a cytosolic protein and free binding site and that membrane binding is limited due to the number of binding sites. Model (4.6) did not include the fact that GDI extracts proteins from the membrane and sequesters them in the cytosol. The results obtained from the membrane binding sites model suggest that the effects of Rho GDI in Rho protein activation by external signal cannot be ignored. We will look at a model including Rho GDI dynamics in the next section.

4.4 GDI Dynamics and Rho Proteins

In this section, we discuss the interactions of Rho proteins with membrane binding sites and formulate a model that includes the dynamics of GDI interactions. Like the Binding Site Model discussed earlier, this model is a simplified version of the complete model of Rho protein translocation shown in Figure 4.1.

A GDP-bound Rho protein and a free GDI molecule have to bind in order for the protein to come off the membrane. Since the protein has to be GDI-bound to remain in the cytosol, the process of membrane binding can be viewed as one of GDI dissociation.

Unlike the Binding Site Model, this GDI Model includes the affinity of GDI for the membrane-bound protein, and subsequent sequestering of the protein in the cytosol. It does not include the affinity of the membrane for Rho or specific membrane binding sites that were included in model (4.5). A schematic diagram corresponding to the GDI dynamics model can be seen in Figure 4.4.

4.4.1 The GDI Model Formulation

Let R_{GDI} be the number of molecules of cytosolic Rho protein and GDI be the number of molecules of free GDI. As before, let R_{GDP} the number of molecules of membrane-bound,
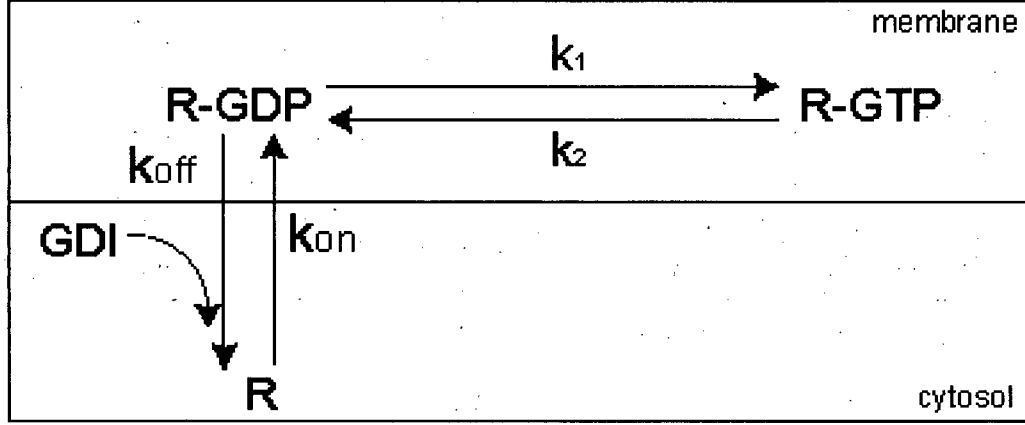
Figure 4.4: A schematic diagram corresponding to the GDI Model of Rho translocation. The membrane-bound forms, R-GTP and R-GDP, are converted to each other at rates k_1 and k_2, respectively. In addition GDI can bind to the GDP-bound form and extract it from the membrane at rate k_{off}.

GDP-bound protein, R_{GTP} the number of molecules of membrane-bound, GTP-bound protein.

The biochemical model is given by:

$$R_{GDI} \underset{k_{off}^{GDI}}{\overset{k_{on}^{GDI}}{\rightleftharpoons}} R_{GDP} + GDI \quad \text{(membrane translocation due to GDI dissociation)} \quad (4.7)$$

$$R_{GDP} \underset{k_2}{\overset{k_1}{\rightleftharpoons}} R_{GTP} \quad \text{(nucleotide exchange on membrane)} \quad (4.8)$$
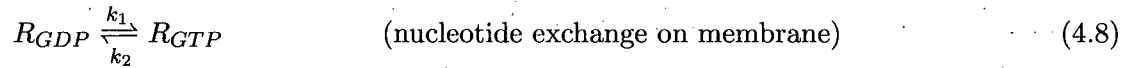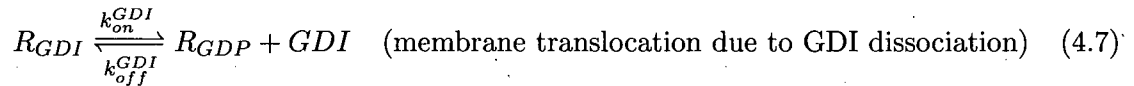
The units for k_1, k_2 and k_{on}^{GDI} are $\sec^{-1}$, and k_{off}^{GDI} is measured in cell $\sec^{-1}$ molecules^{-1}. Note that the units for k_{on}^{GDI} and k_{off}^{GDI} are reversed compared to the k_{on}^B and k_{off}^B rates in model (4.5). In the latter, we viewed membrane association as a bimolecular reaction between the cytosolic protein and a membrane binding site, while here we view membrane dissociation as a bimolecular reaction between a membrane-bound protein and GDI. It is important to realize that both views are idealizations of the complicated process of membrane translocation, which includes GDI dissociation, a conformational change in the protein, and binding to the membrane. All the other parameters are the same as for the Binding Site Model, and are described in Table 4.2. In particular, $k_1 = k_{GDP}^- + k_A$ and $k_2 = k_{\text{hydrolysis}} + k_I$, as before.

4.4.2 Derivation of Equations for the GDI Model

The equations corresponding to the biochemical model are:

$$\frac{dR_{GDI}}{dt} = k_{off}^{GDI} R_{GDP} GDI - k_{on}^{GDI} R_{GDI},$$

$$\frac{dR_{GDP}}{dt} = k_{on}^{GDI} R_{GDI} - k_{off}^{GDI} R_{GDP} GDI - k_1 R_{GDP} + k_2 R_{GTP}, \qquad (4.9)$$

$$\frac{dR_{GTP}}{dt} = k_1 R_{GDP} - k_2 R_{GTP}.$$

Total GDI in the cell is conserved and total Rho protein is also conserved, so

$$GDI = \mathbf{GDI_t} - R_{GDI}$$

$$R_{GDP} = \mathbf{R_t} - R_{GDI} - R_{GTP}.$$

Eliminating, R_{GDP} from the equations, we obtain:

$$\frac{dR_{GDI}}{dt} = k_{off}^{GDI}(\mathbf{R_t} - R_{GDI} - R_{GTP})(\mathbf{GDI_t} - R_{GDI}) - k_{on}^{GDI} R_{GDI},$$

$$\qquad (4.10)$$

$$\frac{dR_{GTP}}{dt} = k_1(\mathbf{R_t} - R_{GDI} - R_{GTP}) - k_2 R_{GTP}.$$

4.4.3 Dimensionless form of System (4.10)

As before, we want to change the number of molecules of various forms of Rho protein to fractions of the total amount of Rho in the cell. Let

$$R_{GDI}^* = \frac{R_{GDI}}{\mathbf{R_t}} \text{ and } R_{GTP}^* = \frac{R_{GTP}}{\mathbf{R_t}}.$$

Then (4.10) becomes

$$\frac{dR_{GDI}^*}{dt} = \widehat{k_{off}}(1 - R_{GDI}^* - R_{GTP}^*)(1 - \beta R_{GDI}^*) - k_{on}^{GDI} R_{GDI}^*,$$

$$\qquad (4.11)$$

$$\frac{dR_{GTP}^*}{dt} = k_1(1 - R_{GDI}^* - R_{GTP}^*) - k_2 R_{GTP}^*,$$

where $\beta = \dfrac{\mathbf{R_t}}{\mathbf{GDI_t}}$ is the ratio of total Rho to total GDI molecules, and $\widehat{k_{off}} = k_{off}\mathbf{GDI_t}$ is the maximum rate of membrane extraction of R_{GDP} (occurring when the total GDI in the cell $\mathbf{GDI_t}$ is available for binding). $\widehat{k_{off}}$ has the units of sec^{-1}.

Table 4.7: Experimentally determined parameters for the interaction of Rho proteins with GDI.

PARAMETER	VALUE	PROTEIN	REFERENCE
k_{on}^{GDI}	$1.4 \cdot 10^{-3}\, s^{-1}$	Rac1	(Newcombe et al., 1999)
$K = k_{on}/k_{off}$	0.4 nM[a]	Rac1	(Newcombe et al., 1999)
$K = k_{on}/k_{off}$	30 nM[b]	Cdc42	(Nomanbhoy and Cerione, 1996)
$\widetilde{k_{off}}$	0.133 sec^{-1}	Rac1	(Nomanbhoy et al., 1999)

[a]Results of Newcombe et al. (1999) show that GTP-bound forms are unable to bind well to GDI (at least two orders of magnitude weaker than GDP-bound forms.)

[b]Nomanbhoy and Cerione (1996) obtained a similar K value (28 nM) for GDP-bound Cdc42, suggesting that GDI can bind to both GDP and GTP forms of Cdc42.
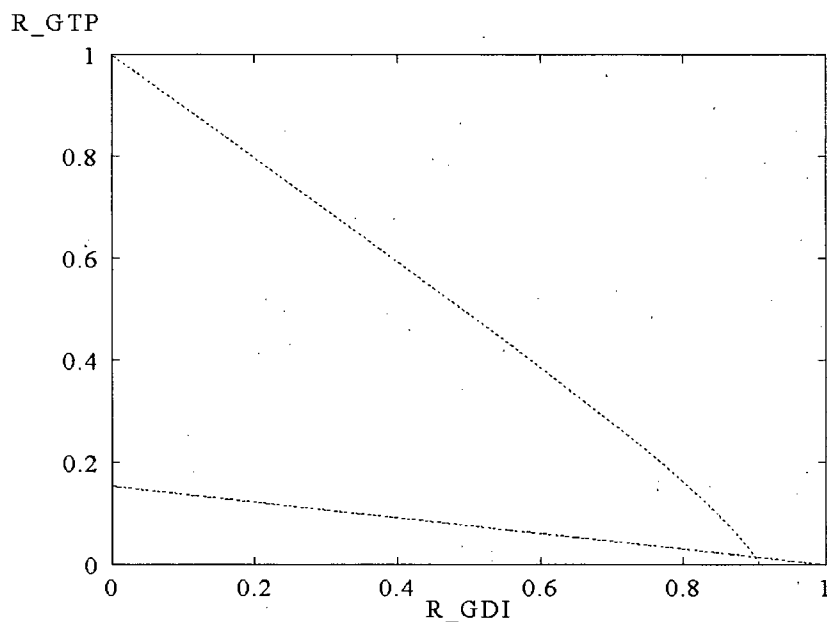
Figure 4.5: Phase-plane diagram for the GDI Model, showing the nullclines and the biologically relevant steady state. Parameter values used are given in Tables 4.2 and 4.7.

4.4.4 Rho GDI Parameter Values

Parameter values for the GDI model, summarized in Table 4.7, were based on literature values stated in (Newcombe et al., 1999; Nomanbhoy and Cerione, 1996; Nomanbhoy et al., 1999). All measurements were done *in vitro* using fluorescently labelled GDI.

Michaelson et al. (2001) measured the relative ratio of Rho GTPases and GDI in three cell lines (see Table 4.8). He also measured the amount of protein in 10^6 cells allowing us to calculate the number of molecules of each protein in each cell type(see Table 4.9). Michaelson et al. (2001) also noted that the molar sum of Cdc42, Rac and RhoA is approximately equal to the molar amount of GDI in each of three cell lines, and that the amount of Rac in each cell types exceeded the amount of Cdc42 or Rho.

Table 4.8: Ratio of Rho GDI to Rho GTPases in three cell lines. Measured by Michaelson et al. (2001)

CELL LINE	GDI/RhoA	GDI/Rac	GDI/Cdc42	GDI/(RhoA+Rac+Cdc42)
MDCK (epithelial)	5.6	2.3	7.4	1.1
COS1 (fibroblasts)	7.4	2.0	11.6	1.1
ECV (epithelial)	3.4	1.8	5.3	0.8

Table 4.9: Cellular content (in numbers of molecules) of Rho GTPases and Rho GDI in three cell lines as determined by immunoblotting. Calculated from values in Michaelson et al. (2001)

CELL LINE	GDI	RhoA	Rac	Cdc42
MDCK (epithelial)	$74 \cdot 10^5$	$16 \cdot 10^5$	$36 \cdot 10^5$	$15 \cdot 10^5$
COS1 (fibroblasts)	$4 \cdot 10^5$	$9.7 \cdot 10^5$	$24 \cdot 10^5$	$7.5 \cdot 10^5$
ECV (epithelial)	$40 \cdot 10^5$	$14 \cdot 10^5$	$24 \cdot 10^5$	$14 \cdot 10^5$

4.4.5 Numerical Simulations

For numerical simulations of system (4.11), we used the value for k_{on}^{GDI} and $\widetilde{k_{off}}$ given in Table 4.7. The nucleotide exchange parameters used were the same as those used in the numerical simulations of (4.6). The effect of total protein to GDI ratio, β, as well as GEF and GAP effects is described below.

The data of Table 4.8 suggest that the ratio of Rho GDI to the sum of the three GTPases is close to one in the three cell types shown. System (4.11) keeps track of a single Rho protein, but β values ranging from 0.5 to 2 were used in the simulations. The distribution of protein between cytosol and membrane is quite sensitive to β, as shown by Figure 4.6. In general, all the available GDI is used up in binding, and the remaining

GEF Effect k_A (sec^{-1})	GAP effect k_I (sec^{-1})	Total Protein to GDI Ratio β	Fraction Protein GDI-bound R^*_{GDI}	Fraction Protein GTP-bound R^*_{GTP}	Fraction Protein GDP-bound R^*_{GDP}
0	0	0.5	0.912	0.071	0.018
0	0	1	0.795	0.164	0.041
0	0	2	0.476	0.419	0.105
0.005	0.03	0.5	0.97	0.004	0.026
0.005	0.03	1	0.894	0.017	0.089
0.005	0.03	2	0.494	0.082	0.425
0	0	2	0.476	0.419	0.105
0.05	0.03	0.5	0.949	0.032	0.019
0.05	0.03	1	0.846	0.097	0.058
0.05	0.03	2	0.487	0.322	0.191
0.5	0.3	0.5	0.949	0.032	0.019
0.5	0.3	1	0.846	0.096	0.058
0.5	0.3	2	0.487	0.321	0.192

Table 4.10: Distribution of Protein at Equilibrium for the GDI Model. R^*_{GDI}, R^*_{GTP}, and R^*_{GDP} are calculated for various k_A, k_I, and β values, using the expression for steady state of system (4.10) derived in Appendix C.

protein stays on the membrane. Hence, we expect that if all three proteins are included in a model of membrane translocation, there will be competition for GDI between the Rho proteins. Small differences in GDI affinity between the three proteins can make a large difference in one Rho protein remaining active and another protein mostly moving to the cytosol.
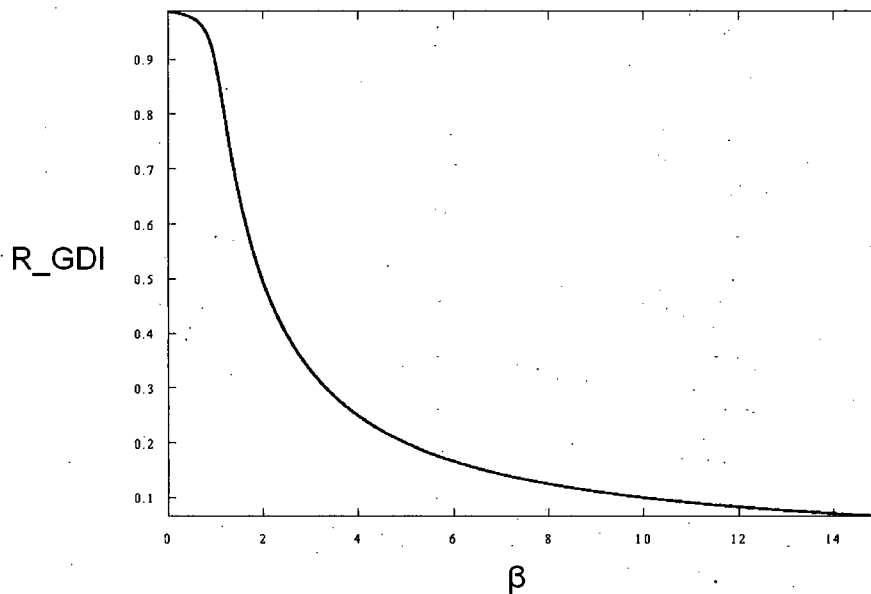
Figure 4.6: A bifurcation diagram for the proportion of protein that is cytosolic (R_{GDI}) versus β in the GDI Model. β is the ratio of total protein to GDI.It can be seen that R_{GDI} drops sharply around $\beta = 2$. This suggests that the ratio of protein to GDI should be carefully controlled in the cell, as varying it slightly changes the equilibrium distribution significantly.

The effect of GEFs and GAPs on redistribution of the Rho protein between the different forms can be seen in Figure 4.7. An increase in GEF activity for a fixed GAP (k_I) value increases the fraction of protein that is GTP-bound. However, as can be seen in Table 4.10, increasing GEF and GAP values simultaneously does not result in significant protein redistribution.

Finally, the GDI model, like the Binding Site Model suggest that GEF and GAP effects are needed in order to reach steady state on a reasonable time scale. However, it was not possible to make the transient time scale very fast in simulations of the GDI model by increasing GEF and GAP as we did in the Binding Site Model. The fastest time that system (4.11) could reach equilibrium is about 400 sec. The time to reach steady
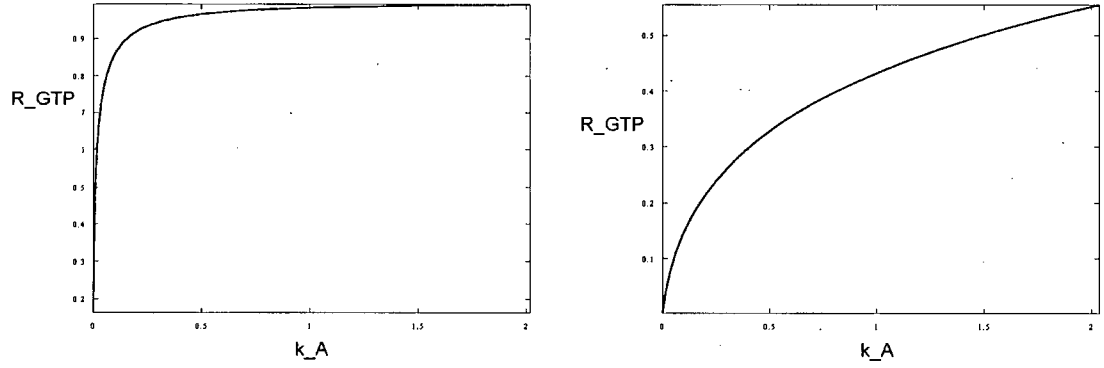
Figure 4.7: The effect of increasing GEF activity on steady state value for active protein R^*_{GTP} in the GDI Model. Increasing k_A increases R^*_{GTP}, but the effect depends on GAP activity k_I. On the left $k_I = 0$, on the right $k_I = 0.03$.

state was limited by the fixed k_{on} and $\widehat{k_{off}}$ values used in the simulations.

4.5 Discussion

Using parameter values obtained from the literature, the steady state of the Binding Site Model has a much higher proportion of the Rho protein in cytosolic form as compared to the GDI Model. This was expected, as the GDI Model assumes that GDI has a certain affinity to GDP-bound forms, extracting them from the membrane, while the Binding Site Model assumes an affinity between the Rho proteins and the membrane binding sites instead. In reality, both processes take place. Based on the predictions of the two models we conclude that affinity to GDI is an important factor that cannot be ignored when modelling the compartmentalization of Rho proteins. Due to uncertain data about the number of Rho binding sites and their biochemical properties, we feel that at this stage binding sites should not be included in a model of Rho protein compartmentalization. In reality most of the Rho protein is cytosolic, which agrees well with the GDI model.

Although the GDI Model agrees with observed protein distributions better than the Binding Site Model, there are experimentally described phenomena that neither model adequately describes. For example, it has been observed that incubation of cell lysates with GTP leads to translocation of Rho protein from cytosol to the membrane, while preincubation with GDP has the opposite effect (Fleming et al., 1996). This effect is explained by the higher affinity of GDI to GDP-bound forms. However, in our modelling we assume that GDI-binding prevents nucleotide exchange since the nucleotide exchange rate for bound GDI is at least 100 times slower. Therefore, in our model preincubation with GDP or GTP only affects the nucleotide state of the membrane-bound forms. If we convert all the membrane-bound fraction to R^*_{GTP} or R^*_{GDP}, there is no net change in the fraction of cytosolic protein. So in both models there is no translocation to or from the cytosol at steady state due to nucleotide loading. To account for this phenomenon one way to modify the model is to include the negligible nucleotide exchange that occurs when GDI is bound. However, that would require us to subdivide the cytosolic pool into two separate populations, and keep track of each one.

An important fact to note is that in neither model is membrane translocation directly stimulated by extracellular signal. k_{off} and k_{on} are treated as constants. Our modelling indicates that the distribution of the proteins between various compartments is highly sensitive to GDI and membrane affinity, and we expect some mechanism for modifying that affinity in response to extracellular signal is present. Biological literature has focused on identifying the GEFs responsible for the activation of Rho GTPases. There is some indication, however, that membrane translocation parameters, k_{off} and k_{on}, are also being regulated. Del Pozo et al. (2002) reports that integrin receptors regulate dissociation of GDI. Occupied receptors increase membrane affinity for Rac, leading to GDI dissociation and Rac targets being activated in the vicinity of activated integrins (Grande-Garcia et al., 2005).

Chapter 5

Conclusion

5.1 Summary of Our Work

The goal of this research project was to create a mathematical model that can reproduce the spatial redistribution of Rho GTPases in response to extracellular clues. We found reports in the biological literature that antagonism between Cdc42/Rac and Rho leads to distinct cytoskeleton morphology at the front and back of the cell. This suggested to us that the Rho protein system is bistable, achieving either a high level of Cdc42/Rac and low level of Rho steady state, or a low level of Cdc42/Rac and high level of Rho steady state, depending on the initial conditions. We examined the schemes for the interactions of the Rho proteins proposed in the literature, and found that without additional feedback most of them cannot account for bistable behaviour. The double negative feedback loop in the interactions proposed by Giniger (2002) could supply the necessary mechanism for the switching mechanism.

Our initial attempts to build a biochemically plausible model based on Giniger's connectivity diagram that gives rise to bistability were not successful. Influenced by the mechanism of a bistable toggle switch described in Gardner et al. (2000), we created a model, where Cdc42 inhibited the activation of Rho, and vice versa. Numerical simulation of the spatial variant of this Activation-Inhibition Model revealed that addition of diffusion can give rise to long-lasting spatial segregation of Cdc42/Rac and Rho. This phenomenon can occur due to amplification of an already existing gradient and due to random noise in the initial conditions. On a longer timescale, the system eventually reaches a spatially uniform high Cdc42/Rac and low Rho steady state.

The Activation-Inhibition model of Rho dynamics had many simplifying assumptions (not explicitly including the effects of Rho regulators: GEFs, GAPs and GDIs). In addition, we developed a more biologically detailed model of the activation cycle of a Rho GTPase, using biochemical parameters obtained from experimental literature. Two variants were explored: one explicitly modelling the affinity of GTPases to the membrane,

88

and another including the effects of the regulator Rho GDI. The GDI model was found to better agree with experimental observations. The GDI model showed that the fraction of protein that is membrane-bound and active, is very sensitive to the ratio of Rho GTPases to Rho GDI, suggesting that a way for the cell to control Rho GDI concentration can lead to a rapid transfer of cytosolic protein to the membrane and vice versa.

5.2 Future Work

The work in this thesis can be extended in several ways:

- Developing a more complete model for the spatial segregation of Rho GTPases that includes both membrane-bound and cytosolic forms.

- Use the GDI model as a starting point for a more biologically realistic model for Rho protein polarization that includes Rho GDI.

- Using the Activation-Inhibition Model as a "polarization" module in models of cell motility, where Rho signalling to the cytoskeleton is included.

We discuss these directions below.

5.2.1 Extending the Model

In Chapters 2 and 3 we treated the cytosolic pool of the small G-proteins as a limitless reservoir of available substrate for the active forms. The concentrations of the inactive cytosolic forms of the Rho proteins were assumed to remain constant over space and time. As a result, we derived a reaction-diffusion system of the form:

$$\frac{\partial \mathbf{u}}{\partial t} = \mathbf{f}(\mathbf{u}) + D\nabla^2 \mathbf{u},$$

where $\mathbf{f}(\mathbf{u})$ are the interaction kinetics of the Rho proteins, and D is the diffusion coefficient matrix. Because the diffusion coefficient is the same for all components of the reaction-diffusion system, pattern formation due to Turing instability cannot occur. However, we have to consider the fact that the cytosolic forms of the Rho proteins, as well as Rho GDI have diffusion coefficients that are approximately hundred times faster than those of the active membrane-bound forms. Hence, some form of Turing mechanism might be at work in the Rho system. Computer simulations by Stan Marée of Utrecht University have revealed that inclusion of Rho GDI in the Activation Inhibition Model does not give permanent spatial polarization with realistic diffusion coefficients. However, inclusion of the inactive cytosolic forms achieves persistent polarity due to depletion effects (Stan Marée, personal communication). Another approach would be to combine a model of Rho

interactions, similar to the Activation Inhibition Model with a detailed biochemical model for the activation of a single Rho protein that was discussed in Chapter 4.

5.2.2 Application to Models of Cell Motility

The Rho proteins are known to influence the rates of actin polymerization, capping and side branching. Therefore a model for the the spatiotemporal distribution of Rho GTPases can be coupled to models of cellular processes driven by actin polymerization. As an example, consider an effector of Cdc42 and Rac, Arp2/3, that nucleates new actin filaments at the leading edge. By assuming a Cdc42-dependent nucleation rate in a model for branching of actin filaments, we obtain a nucleation zone at the leading edge. Similarly, we obtain a Rho promoted zone of actin-myosin contraction at the rear of the cell. Figure 1.3 demonstrates other ways how actin dynamics are influenced by Rho proteins. The major obstacle to this modelling is not knowing the rate constants or concentrations at which these effects take place.

Bibliography

B. Alberts, D. Bray, J. Lewis, M. Raff, K. Roberts, and J. Watson. *Molecular Biology of the Cell.* Garland Publishing, Inc., third edition, 1994.

D. Baird, Q. Feng, and R. Cerione. The Cool-2/α-Pix protein mediates a Cdc42-Rac signaling cascade. *Current Biology*, 15:1–10, 2005.

A. Bershadsky, N. Balaban, and B. Geiger. Adhesion-dependent cell mechanosensitivity. *Annual Review of Cell and Developmental Biology*, 19:677–695, 2003.

D. Bilodeau, S. Lamy, R. Desrosiers, D. Gingras, and R. Beliveau. Regulation of Rho protein binding to membranes by RhoGDI: Inhibition of releasing activity by physiological ionic conditions. *Biochem. Cell Biol.*, 77:59–69, 1999.

A. Bishop and A. Hall. Rho GTPases and their effector proteins. *Biochemical Journal*, 348:241–255, 2000.

G. Bokoch, B. Bohl, and T. Chuang. Guanine nucleotide exchange regulates membrane translocation of Rac/Rho GTP-binding proteins. *Journal of Biological Chemistry*, 269: 31674–31679, 1994.

A. Boukharov and C. Cohen. Guanine nucleotide-dependent translocation of RhoA from cytosol to high affinity membrane binding sites in human erythrocytes. *Biochemical Journal*, 330:1391–1398, 1998.

E. Caron. Rac signalling: a radical view. *Nature Cell Biology*, 5:185–187, 2003.

J. Cote and K. Vuori. Identification of an evolutionarily conserved superfamily of DOCK180-related proteins with guanine nucleotide exchange activity. *Journal of Cell Science*, 115:4901–4913, 2002.

M. Del Pozo, N. Alderson, W. Kiosses, H. Chiang, R. Anderson, and M. Schwartz. Integrins regulate Rac targeting by internalization of membrane domains. *Science*, 203: 839–842, 2004.

M. Del Pozo, W. Kiosses, N. Alderson, N. Meller, K. Hahn, and M. Schwartz. Integrins regulate GTP-Rac localized effector interactions through dissociation of Rho-GDI. *Nature Cell Biology*, 4:232–239, 2002.

K. DeMali, K. Wennerberg, and K. Burridge. Integrin signaling to the actin cytoskeleton. *Current Opinion in Biology*, 15:572–582, 2003.

S. Etienne-Manneville. Cdc42-the centre of polarity. *Journal of Cell Science*, 117:1291–1300, 2004.

E. Evers, G. Zondag, A. Malliri, L. Price, J. ten Klooster, R. van der Kimmel, and J. Collard. Rho family proteins in cell adhesion and cell migration. *European Journal of Cancer*, 36:1269–1274, 2000.

J. Ferrell, Jr. Self-perpetuating states in signal transduction: positive feedback, double-negative feedback and bistability. *Current Opinion in Chemical Biology*, 6:140–148, 2002.

R. Firtel and C. Chung. The molecular genetics of chemotaxis: sensing and responding to chemoattractant gradients. *BioEssays*, 22:603–615, 2000.

I. Fleming, C. Elliott, and J. Exton. Differential translocation of rho family GTPases by lysophosphatidic acid, endothelin-1, and platelet-derived growth factor. *Journal of Biological Chemistry*, 271:33067–73, 1996.

M. Forget, R. Desrosiers, D. Gingras, and R. Beliveau. Phosphorylation states of Cdc42 and RhoA regulate their interactions with Rho GDP dissociation inhibitor and their extraction from biological membranes. *Biochemical Journal*, 361:243–254, 2002.

T. Gardner, C. Cantor, and C. J.J. Construction of a genetic toggle switch in *Escheria Coli*. *Nature*, 403:339–342, 2000.

E. Giniger. How do Rho family GTPases direct axon growth and guidance? A proposal relating signalling pathways to growth cone mechanics. *Differentiation*, 70:385–396, 2002.

B. Goodwin. Oscillatory behavior in enzymatic control processes. *Advances in Enzyme Regulation*, 3:425–438, 1965.

J. Goodwin, K. Drake, C. Remmert, and A. Kenworthy. Ras diffusion is sensitive to plasma membrane viscosity. *Biophysical Journal*, 89:1398–410, 2005.

A. Grande-Garcia, A. Echarri, and M. Del Pozo. Integrin regulation of membrane domain trafficking and Rac targeting. *Biochemcial Society Transactions*, 33:609–613, 2005.

A. Hall. Rho GTPases and the actin cytoskeleton. *Science*, 279:509–514, 1998.

E. Helmreich. *The biochemistry of cell signalling.* Oxford University Press., 2001.

R. Itoh, K. Kurokawa, Y. Ohba, H. Yoshizaki, N. Mochizuki, and M. Matsuda. Activation of Rac and Cdc42 video imaged by fluorescent resonance energy transfer-based single-molecule probes in the membrane of living cells. *Molecular and Cellular Biology*, 22: 6582–6591, 2002.

V. Krayanov, C. Chamberlain, G. Bokoch, M. Schwartz, S. Slabaugh, and K. Hahn. Localized Rac activation visualized in living cells. *Science*, 290:333–337, 2000.

J. Krishnan and P. Iglesias. A modeling framework describing the enzyme regulation of membrane lipids underlying gradient perception in *Dictyostelium* cells. *Journal of Theoretical Biology*, 229:85–99, 2004.

K. Kurokawa, R. Itoh, H. Yoshizaki, Y. Ohba, T. Nakamara, and M. Matsuda. Coactivation of Rac1 and Cdc42 at lamellipodia and membrane ruffles induced by epidermal growth factor. *Molecular Biology of the Cell*, 15:1003–1010, 2004.

A. Levchenko and P. Iglesias. Models of eukaryotic gradient sensing: application to chemotaxis of amoeba and neutrophils. *Biophysical Journal*, 82:50–63, 2002.

J. Lewis, J. Slack, and L. Wolpert. Thresholds in development. *Journal of Theoretical Biology*, 65:579–590, 1977.

Z. Li, C. Aizenman, and H. Cline. Regulation of Rho GTPases by crosstalk and neuronal activity in vivo. *Neuron*, 33:741–750, 2002.

H. Lodish, A. Berk, S. L. Zipulsky, P. Matsuidara, D. Baltimore, and J. Darnell. *Molecular Cell Biology.* W.H. Freeman and Company, fourth edition, 2000.

D. Mackay and A. Hall. Rho GTPases. *Journal of Biological Chemistry*, 273:20685–20688, 1998.

T. Matozaki, H. Nakanishi, and Y. Takai. Small G-protein networks: Their crosstalk and signal cascades. *Cellular Signalling*, 12:515–524, 2000.

R. Meili and R. Firtel. Two poles and a compass. *Cell*, 114:153–156, 2003.

L. Menard, E. Tomhave, P. Casey, R. Uhing, R. Snyderman, and J. Didsbury. Rac1, a low-molecular-mass GTP-binding-protein with high intrinsic GTPase activity and distinct biochemical properties. *European Journal of Biochemistry*, 206:537–546, 1992.

D. Michaelson, J. Silletti, G. Murphy, P. D'Eustachio, M. Rush, and M. Philips. Differential localization of Rho GTPases in live cells: Regulation by hypervariable regions and RhoGDI binding. *Journal of Cell Biology*, 152:111–126, 2001.

J. Murray. *Mathematical Biology*. Springer, third edition, 2001.

P. Nalbant, L. Hodgson, V. Krayanov, A. Toutchkine, and K. Hahn. Activation of endogenous Cdc42 visualized in living cells. 305:1615–1619, 2004.

A. Newcombe, R. Stockley, J. Hunter, and M. Webb. The interaction between Rac1 and its guanine nucleotide dissociation inhibitor (GDI), monitored by a single fluorescent coumarin attached to GDI. *Biochemistry*, 38:6879–6886, 1999.

C. Nobes and A. Hall. Rho, Rac, and Cdc42 GTPases regulate the assembly of multimolecular focal complexes associated with actin stress fibers, lamellipodia, and filopodia. *Cell*, 81:53–62, 1995.

C. Nobes and A. Hall. Rho GTPases control polarity, protrusion, and adhesion during cell movement. *Journal of Cell Biology*, 144:1235–1244, 1999.

T. Nomanbhoy and R. Cerione. Characterization of the interaction between RhoGDI and Cdc42Hs using fluorescence spectroscopy. *Journal of Biological Chemistry*, 271: 10004–10009, 1996.

T. Nomanbhoy, J. Erickson, and R. Cerione. Kinetics of Cdc42 membrane extraction by Rho-GDI monitored by real-time fluorescence resonance energy transfer. *Biochemistry*, 38:1744–1750, 1999.

B. Olofsson. Rho guanine dissociation inhibitors: pivotal molecules in cellular signaling. *Cellular Signalling*, 11:545–554, 1999.

M. Paduch, F. Jelen, and J. Otlewski. Structure of small G proteins and their regulators. *Acta Biochimica Polonica*, 48:829–850, 2001.

C. Parent and P. Devreotes. A cell's sense of direction. *Science*, 284:765–770, 1999.

O. Pertz and K. Hahn. Designing biosensors for Rho family proteins-deciphering the dynamics of Rho family GTPase activation in living cells. *Journal of Cell Science*, 117: 1313–1318, 2004.

M. Postma, L. Bosgraaf, H. Loovers, , and P. Van Haastert. Chemotaxis: signalling modules join hands at front and tail. *EMBO Reports*, 5:35–40, 2004.

M. Postma and P. Van Haastert. A diffusion-translocation model for gradient sensing by chemotactic cells. *Biochemical Journal*, 81:1314–1323, 2001.

M. Raftopoulou and A. Hall. Cell migration: Rho GTPases lead the way. *Developmental Biology*, 265:23–32, 2004.

A. Ridley. Ras, Rac, Rho- a complex triangle of relationships. *ELSO Gazette*, 1, 2000.

A. Ridley. Rho family proteins: coordinating cell responses. *Trends in Cell Biology*, 11: 471–477, 2001a.

A. Ridley. Rho GTPases and cell migration. *Journal of Cell Science*, 114:2713–2722, 2001b.

A. Ridley, H. Paterson, C. Johnston, D. Diekmann, and H. A. The small GTP-binding protein rac regulates growth factor-induced membrane ruffling. *Cell*, 70:401–410, 1992.

K. Robbe, A. Otto-Bruc, P. Chardin, and B. Antonny. Dissociation of GDP dissociation inhibitor and membrane translocation are required for efficient activation of Rac by the Dbl homology- Pleckstrin homology region of Tiam. *Journal of Biological Chemistry*, 278:4756–4762, 2003.

Y. Sako, K. Hibino, T. Miyauchi, Y. Miyomoto, M. Ueda, and S. Yanagida. Single-molecule imaging of signaling molecules in living cells. *Single Molecules*, 2:159–163, 2000.

E. Sander, J. ten Klooster, S. van Delft, R. van der Kammen, and J. Collard. Rac downregulates Rho activity: Reciprocal balance between both GTPases determines cellular morphology and migratory behaviour. *Journal of Cell Biology*, 147:1009–1021, 1999.

T. Sasaki, M. Kato, and Y. Takai. Consequences of weak interaction of Rho GDI with GTP-bound forms of rho p21 and rac p21. *Journal of Biological Chemistry*, 268:23959–23963, 1993.

A. Schmidt and A. Hall. Guanine nucleotide exchange factors for Rho GTPases: turning on the switch. *Genes and Development*, 16:1587–1609, 2002.

A. Schmitz, E. Govek, B. Bottner, and L. Van Aelst. Rho GTPases: signaling, migration, and invasion. *Experimental Cell Research*, 261:1–12, 2000.

S. Srinivasan, F. Wang, S. Glavas, A. Ott, F. Hofmann, K. Aktories, D. Kalman, and H. Bourne. Rac and Cdc42 play distinct roles in regulating PI(3,4,5)P$_3$ and polarity during neutrophil chemotaxis. *Journal of Cell Biology*, 160:375–385, 2003.

K. Subramanian and A. Narang. A mechanistic model for eukaryotic gradient sensing: spontaneous and induced phosphoinositide polarization. *Journal of Theoretical Biology*, 231:49–67, 2004.

Y. Takai, T. Sasaki, and T. Matozaki. Small GTP-binding proteins. *Physiological Reviews*, 81:153–208, 2001.

T. Tsuji, T. Ishizaki, M. Okamoto, C. Higashida, K. Kimura, Y. Furuyashiki, T. Arakawa, R. Birge, T. Nakamoto, H. Hirai, and S. Narumiya. Rock and mDia1 antagonize in Rho-dependent Rac activation in Swiss 3T3 fibroblasts. *Journal of Cell Biology*, 157:819–830, 2002.

F. van Leeuwen, H. Kain, R. van der Kammel, F. Michiels, O. Kranenburg, and J. Collard. The guanine nucleotide exchange factor Tiam1 affects neuronal morphology; opposing roles for the small GTPases Rac and Rho. *Journal of Cell Biology*, 139:797–807, 1997.

F. Wang, P. Herzmak, O. Weiner, S. Srnivasa, G. Servant, and H. Bourne. Lipid products of PI(3)Ks maintain persistent cell polarity and directed motility in neutrophils. *Nature Cell Biology*, 4:513–518, 2002.

O. Weiner, P. Neilsen, G. Prestwich, M. Kirschner, L. Cantley, and H. Bourne. A PtdInsP$_3$– and Rho GTPase-mediated positive feedback loop regulates neutrophil polarity. *Nature Cell Biology*, 4:509–512, 2003.

K. Wennerberg and C. Der. Rho-family GTPases: it's not only Rac and Rho (and I like it). *Journal of Cell Science*, 117:1301–1312, 2004.

M. Zerial and L. Huber, editors. *Guidebook to the small GTPases.* Oxford University Press., 1995.

B. Zhang and Y. Zheng. Regulation of RhoA GTP hydrolysis by the GTPase-activating protein p190, p50RhoGAP, Bcr, and 3BP-1. *Biochemistry*, 37:5249–5257, 1998.

Y. Zheng. Dbl family guanine nucleotide exchange factors. *Trends in Biochemical Sciences*, 26:724–732, 2001.

G. Zondag, E. Evers, J. ten Klooster, L. Janssen, R. van der Kammen, and J. Collard. Oncogenic Ras downregulates Rac activity, which leads to increased Rho activity and epithelial-mesenchymal transition. *Journal of Cell Biology*, 149:775–782, 2000.

Appendix A

Modelling the Interactions Between the Rho Proteins

A.1 Various Functional Forms of Protein Activation and Inactivation in Model I

In Chapter 2 we analyzed Model I, which is given by:

$$\frac{dC}{dt} = I_C - \varepsilon C\rho - \delta_C C,$$

$$\frac{dR}{dt} = I_R + \alpha C - \delta_R R,$$

$$\frac{d\rho}{dt} = I_\rho + \beta R - C\rho - \delta_\rho \rho.$$

We showed that Model I is not capable of bistability. In this section we investigate other (biologically plausible) functional forms for activation/inactivation terms to see if they can give rise to bistability.

A.1.1 Varying the Activation Kinetics

We investigate what would happen if the small G-protein-dependent activation had sigmoidal rather than linear dependence on protein concentration. The underlying assumption for the use of a sigmoidal function is that activation of one protein by another is a saturating, nonlinear reaction that can be approximated by a Hill function.

Since the simplest equation in (2.4) is the equation for R, we replace Cdc42-dependent activation of Rac (αC in equation (2.4)) by a Hill function $\alpha \frac{C^n}{k+C^n}$ (see Fig-

(a)   (b)
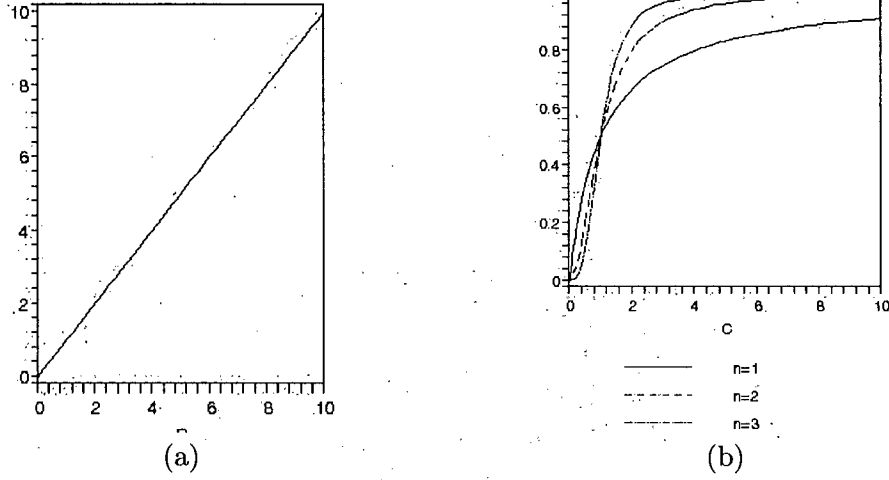
Figure A.1: Different types of kinetics considered for the activation of Rac by Cdc42: (a) Linear kinetics $f_1 = \alpha C$ and (b) sigmoidal kinetics $f_2 = \alpha \dfrac{C^n}{k + C^n}$.

ure A.1). This gives us:

$$\frac{dC}{dt} = I_C - \varepsilon C\rho - \delta_C C,$$

$$\frac{dR}{dt} = I_R + \alpha \frac{C^n}{k + C^n} - \delta_R R, \tag{A.1}$$

$$\frac{d\rho}{dt} = I_\rho + \beta R - C\rho - \delta_\rho \rho.$$

Putting C on quasi-steady state and eliminating it from the equations, the nullcline for ρ is given by:

$$R = \frac{\varepsilon \delta_\rho \rho^2 + (I_C + \delta_C \delta_\rho - \varepsilon I_\rho)\rho - \delta_C I_\rho}{\beta(\varepsilon \rho + \delta_C)}.$$

The derivative of the Rho nullcline is given by:

$$\frac{dR}{d\rho} = \frac{I_C \delta_C}{(\varepsilon \rho + \delta_C)^2} + \delta_\rho > 0.$$

Hence the ρ nullcline is monotonically increasing. The R nullcline is given by:

$$R = \frac{I_R}{\delta_R} + \frac{\alpha}{\delta_R} \frac{I_C^n}{k(\varepsilon \rho + \delta_C)^n + I_C^n}.$$

Hence, the Rho nullcline is an increasing function of ρ, so there is at most one intersection between the two nullclines.
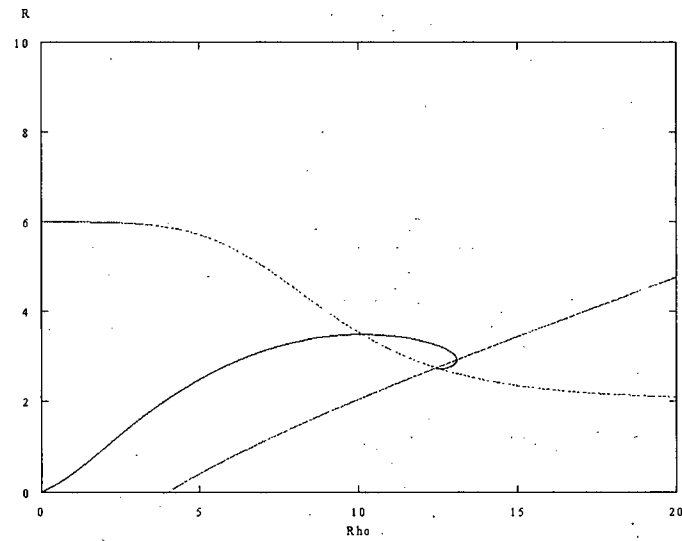
Figure A.2: The $\rho - R$ phase plane (C is put on quasi-steady state). The R and ρ nullclines of (A.1) will intersect only once, giving a unique steady state. (A trajectory starting at (0,0) is also shown.)

Similarly, we can replace Rac-dependent activation of Rho, βR, by $\dfrac{\beta R^n}{k + R^n}$ to obtain:

$$\frac{dC}{dt} = I_C - \varepsilon C \rho - \delta_C C,$$

$$\frac{dR}{dt} = I_R + \alpha C - \delta_R R, \qquad\qquad (A.2)$$

$$\frac{d\rho}{dt} = I_\rho + \frac{\beta R^n}{k + R^n} - C\rho - \delta_\rho \rho.$$

If we put C on quasi-steady state and eliminate it from the equations, the R nullcline will be given by:

$$R = \frac{1}{\delta_R}\left[I_\rho + \frac{\alpha I_C}{\varepsilon \rho + \delta_C}\right],$$

which is a decreasing function of ρ.

The corresponding ρ nullcline is given implicitly by:

$$I_\rho + \frac{\beta R^n}{K_R + R^n} = \frac{I_C \rho}{\varepsilon \rho + \delta_C} + \delta_\rho.$$

Implicit differentiation can be used to show that

$$\frac{dR}{d\rho} = \frac{(K_R + R^n)^2 \delta_C \left(\dfrac{I_c}{(\varepsilon \rho + \delta_C)^2} + 1\right)}{K_R \beta n R^{n-1}}.$$

Hence, the Rho nullcline is an increasing function of ρ, so there is at most one intersection between the two nullclines.

Finally, we can replace both αC and βR terms in (2.4) by Hill functions, getting:

$$\frac{dC}{dt} = I_C - \varepsilon C \rho - \delta_C C,$$

$$\frac{dR}{dt} = I_R + \frac{\alpha C^m}{K_C + C^m} - \delta_R R, \qquad\qquad (A.3)$$

$$\frac{d\rho}{dt} = I_\rho + \frac{\beta R^n}{K_R + R^n} - C\rho - \delta_\rho \rho.$$

If we set the derivatives to zero, and eliminate C from the resulting algebraic system, we get the equations for the R and ρ nullclines in the $C - \rho$ phase plane, obtained by putting R on quasi-steady state. The R nullcline is given by:

$$R = \frac{1}{\delta_R}\left[I_R + \frac{\alpha I_C^m}{K_C(\varepsilon \rho + \delta_C)^m + I_C^m}\right].$$

This is the same function as the R nullcline in model (A.1). The Rho nullcline is the same as the Rho nullcline in model (A.2). Using the properties of those functions that we showed earlier we conclude, once again, that only one steady state is possible.

So an assumption that activation kinetics of one protein by another are sigmoidal does not affect the number of positive steady states that can be obtained by model in Figure 2.4.

A.1.2 Varying the Inactivation Kinetics

Next, we investigate the effect of the assumption that inactivation rate of Cdc42 and Rho is proportional to the product of the concentrations of Cdc42 and Rho. We relax this assumption by replacing the bilinear inactivation term $C\rho$ in equation (2.4) by a nonlinear function $f(C, \rho)$. The exact form of f is not known, but it is reasonable to assume that f is a monotonically increasing positive-valued function of C and ρ (since increasing the amount of active Cdc42 should have an inhibitory effect on Rho and vice versa). The function should also be saturating to prevent unreasonable inactivation rates in the presence of large concentrations of proteins (there is some maximal level of GTP-hydrolysis that can be achieved regardless of C and ρ concentrations), and be zero if the concentration of either C or ρ becomes zero. Using this assumption, model (2.4) becomes:

$$\frac{dC}{dt} = I_C - \varepsilon f(C, \rho) - \delta_C C,$$

$$\frac{dR}{dt} = I_R + \alpha C - \delta_R R, \qquad\qquad (A.4)$$

$$\frac{d\rho}{dt} = I_\rho + \beta R - f(C, \rho) - \delta_\rho \rho.$$

We set the derivatives in model (A.4) to zero to determine the number of possible steady states. After eliminating R, we obtain the following algebraic system:

$$0 = I_C - \varepsilon f(C, \rho) - \delta_C C,$$

$$0 = A + \tilde{\alpha} C - f(C, \rho) - \delta_\rho \rho, \qquad\qquad (A.5)$$

where $A = I_\rho + \beta I_R / \delta_R$ and $\tilde{\alpha} = \alpha\beta/\delta_R$. We can eliminate $f(C, \rho)$ from this system to get

$$\rho = mC + b$$

where

$$m = \frac{\tilde{\alpha} + \delta_C/\varepsilon}{\delta_\rho} \quad \text{and} \quad b = \frac{A - I_C/\varepsilon}{\delta_\rho}.$$

101

Note that we simply eliminated $f(C, \rho)$ without using any assumptions about f such as monotonicity or saturation. Next, we test specific forms of $f(C, \rho)$ to see if any are consistent with bistability.

For example, suppose $f(C, \rho) = \dfrac{HC\rho}{1 + pC + q\rho}$ where H, p, q are positive constants. We have from before:

$$0 = I_C - \varepsilon f(C, \rho) - \delta_C C$$

$$\Rightarrow \varepsilon f(C, \rho) = I_C - \delta_C C$$

$$\Rightarrow \frac{\varepsilon HC\rho}{1 + pC + q\rho} = I_C - \delta_C C$$

Substituting in $\rho = mC + b$ we get

$$\varepsilon H \frac{C(mC + b)}{1 + pC + q(mC + b)} = I_C - \delta_C C$$

This gives a quadratic equation for C,

$$(\varepsilon Hm + \delta_C(p + qm))C^2 + (\varepsilon Hb + \delta_C(1 + qb) - I_C(p + qm))C - I_C(1 + qb) = 0. \quad (A.6)$$

Equation (A.6) has at most two solutions. Therefore, it is incompatible with bistability, which requires two stable steady states separated by a saddle point. Further analysis reveals that the level of Rho corresponding to the smaller of the two solutions is negative, making it biologically irrelevant.

Using the same approach as above for $f(C, \rho) = \dfrac{HC^2\rho^2}{1 + pC^2 + q\rho^2}$ gives a fourth degree equation for C, so it is possible for system (A.5) to have 4 steady states. However, experimenting with parameters numerically we see that bistability still does not occur in the first quadrant.

Linear Stability of Solutions of (A.5)

In fact, linear analysis about a steady state shows that we will never get the bistable behaviour we want in system (A.5) for any monotonically increasing function of C and ρ. The Jacobian for (A.5) is given by

$$J = \begin{bmatrix} -\varepsilon f_C - \delta_C & -\varepsilon f_\rho \\ \tilde{\alpha} - f_C & -f_\rho - \delta_\rho \end{bmatrix}$$

The trace of J is given by $Tr(J) = -(\delta_C + \delta_\rho) - (f_\rho + \varepsilon f_C)$. We observe that $Tr(J)$ evaluated at non-negative values of C and ρ is negative, since f_C and f_ρ are
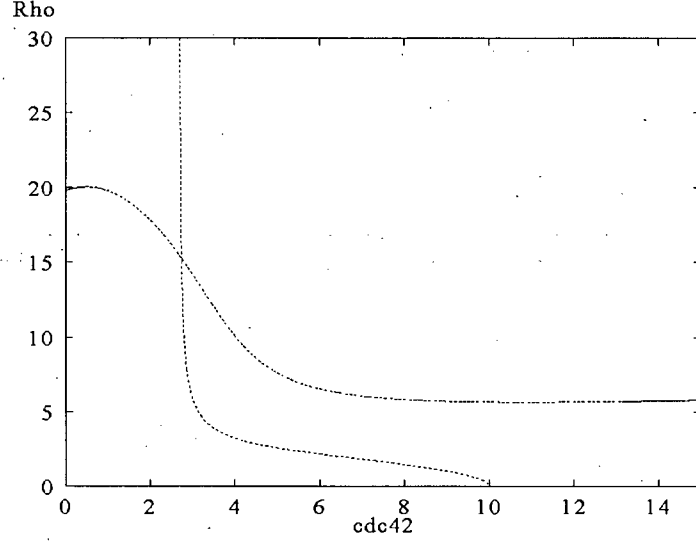
Figure A.3: Typical nullclines for system (A.5).

positive, by the assumption that f is a monotonically increasing function of C and ρ. The determinant of J, $Det(J)$, is given by $(f_\rho + \delta_\rho)(\varepsilon f_C + \delta_C) + \varepsilon f_\rho(\tilde{\alpha} - f_C)$. When evaluated at the positive steady state values of C and ρ and expanded, $Det(J)$ is always positive by the same assumption about f. The eigenvalues of J are given by $\lambda_{1,2} = \frac{1}{2}(Tr(J) \pm \sqrt{Tr(J)^2 - 4Det(J)})$. The eigenvalues would be real and negative for

$$Tr(J)^2 > 4Det(J)$$
$$(\delta_C + \delta_\rho)^2 + (f_\rho + \varepsilon f_C)^2) > 2(f_\rho \delta_C + \varepsilon f_C \delta_\rho + \delta_\rho \delta_C + 2\varepsilon \tilde{\alpha} f_\rho)$$

and complex with negative real parts otherwise. Hence any steady state of system (A.5) in the first quadrant would have to always be stable. Numerical simulations of the full 3 by 3 system were done to compare with the reduced two variable system. No transition from a stable to unstable steady state were observed.

We have shown that despite the presence of double negative feedback, model (2.4) is monostable. Using sigmoidal activation kinetics instead of linear to model the activation of one protein by another does not alter the number or stability of steady states. Neither does replacing the bilinear function for mutual inhibition of C and ρ by an arbitrary monotonically increasing function of the concentrations of Cdc42 and Rho.

Appendix B

Spatial Extension of the Activation-Inhibition Model

B.1 XPP code for Activation-Inhibition Model with Neumann BCs

The following file was used to spatially simulate the activation inhibition model with Neumann boundary conditions in XPP.

```
# synthesis inhibition model with diffusion  The BC's are written
in a general way so that both Neumann and Dirichlet conditions as
well as mixed BC's  can be implemented by setting the
a,b,c,parameters  Dirichlet: b=0; Neumann a=0, c=0


# cu0 = au0 u + bu0 u_x # cu1 = au1 u + bu1 u_x # cv0 = av0 v +bv0
v_x # cv1 = av1 v + bv1 v_x # cw0 = aw0 w + bw0 w_x # cw1 = aw1
v+bw1 v_x #left boundary u0=(cu0-bu0*u1/h)/(au0-bu0/h)
v0=(cv0-bv0*v1/h)/(av0-bv0/h) w0=(cw0-bw0*w1/h)/(aw0-bw0/h)


u[1..100]'=(d/(h*h))*(u[j+1]-2*u[j]+u[j-1])+I1/(a1+w[j]^k)-delta1*u[j]
v[1..100]'=(d/(h*h))*(v[j+1]-2*v[j]+v[j-1])+I2+alpha*u[j]-delta2*v[j]
w[1..100]'=(d/(h*h))*(w[j+1]-2*w[j]+w[j-1])+I3/(a2+u[j]^n)+I4*v[j]/(a3+u[j]^m)
-delta3*w[j]


# Right boundary u101=(cu1+bu1*u100/h)/(au1+bu1/h)
v101=(cv1+bv1*v100/h)/(av1+bv1/h)
w101=(cw1+bw1*w100/h)/(aw1+bw1/h) par d=0.01,h=0.1
```

#No flux (neumann) BC's for left end of domain

par cu0=0,au0=0,bu0=1 cv0=0,av0=0,bv0=1 cw0=0,aw0=0,bw0=1

#No flux (neumann) BC's for right end of domain

par cu1=0,au1=0,bu1=1 par cv1=0,av1=0,bv1=1 par cw1=0,aw1=0,bw1=1,

par I1=4,I2=0,I3=2,I4=5,a1=0.6,a2=1,a3=1,alpha=1,k=1,n=3,m=3,
delta1=1,delta2=1,delta3=1 @ total=60,dt=0.005 done

B.2   XPP code for Activation-Inhibition Model with Periodic BCs

The following file was used to spatially simulate the synthesis inhibition model with periodic boundary conditions in XPP.

```
#synthesis inhibition model with periodic BCs

u1'=(d/(h*h))*(u2-2*u1+u100)+I1/(a1+w1^k)+pulse(t)-delta1*u1
u[2..29]'=(d/(h*h))*(u[j+1]-2*u[j]+u[j-1])+I1/(a1+w[j]^k)+pulse(t
)-delta1*u[j]
u[30..99]'=(d/(h*h))*(u[j+1]-2*u[j]+u[j-1])+I1/(a1+w[j]^k)
-delta1*u[j]
u100'=(d/(h*h))*(u1-2*u100+u99)+I1/(a1+w100^k)-delta1*u100

v1'=(d/(h*h))*(v2-2*v1+v100)+I2+pulse(t)+alpha*u1-delta2*v1
v[2..99]'=(d/(h*h))*(v[j+1]-2*v[j]+v[j-1])+I2+pulse(t)+alpha*u[j
]-delta2*v[j]
v100'=(d/(h*h))*(v1-2*v100+v99)+I2+pulse(t)+alpha*u100-delta2*v100

w1'=(d/(h*h))*(w2-2*w1+w100)+I3/(a2+u1^n)+I4*v1/(a3+u1^m)-delta3*w1
w[2..99]'=(d/(h*h))*(w[j+1]-2*w[j]+w[j-1])+I3/(a2+u[j]^n)
+I4*v[j]/(a3+u[j]^m)-delta3*w[j]
w100'=(d/(h*h))*(w1-2*w100+w99)+I3/(a2+u100^n)+I4*v100/(a3+u100^m)
-delta3*w100

%An activation pulse of of size amplitude is applied to u[1..29]
```

105

```
%at time tsart for duration time units

pulse(t)=amplitude*(heav(t-tstart)-heav(t-(tstart+duration)))

par d=0.01,h=0.1, amplitude=0, tstart=40, duration=10


par
I1=4,I2=2,I3=2,I4=5,a1=1,a2=1,a3=1,alpha=1,k=1,n=3,m=3,delta1=1,delta2=1,delta3=1
@ total=60,dt=0.005 done
```

Appendix C

Compartmentalization of Rho GTPases and Parameter Estimation

C.1 Analysis of Binding Site Model

C.1.1 Steady States of System (4.5)

To find the steady states of (4.5) we set the left-hand sides to zero and observe that

$$R_{GTP} = \tilde{k} R_{GDP} \tag{C.1}$$

where $\tilde{k} = \dfrac{k_1}{k_2} = \dfrac{k_{GDP}^- + k_A}{k_{\text{hydrolysis}} + k_I}$, and

$$(1 - (R_{GDP} + R_{GTP}))(\mathbf{B_t} - R_t(R_{GDP} - R_{GTP})) = K_d R_{GTP}, \tag{C.2}$$

where $K_d = k_{off}/k_{on}$. Substituting (C.1) into (C.2) and solving for R_{GDP} we obtain

$$R_{GDP} = \frac{(\mathbf{B_t} + \mathbf{R_t})(1 + \tilde{k}) + K_d \pm \sqrt{\left((\mathbf{B_t} + \mathbf{R_t})(1 + \tilde{k}) + K_d\right)^2 - 4(1 + \tilde{k})^2 \mathbf{R_t} \mathbf{B_t}}}{2(1 + \tilde{k})^2}. \tag{C.3}$$

Both solutions are real and non-negative, but we need to ensure that R and B are nonnegative or, equivalently, that $R_{GDP} + R_{GTP} \leq \min(\mathbf{R_t}, \mathbf{B_t})$. Note that the larger solution for R_{GDP} at steady state is always going to be greater than $\dfrac{(\mathbf{B_t} + \mathbf{R_t})(1 + \tilde{k}) + K_d}{2(1 + \tilde{k})^2}$. Using the fact that at steady state $R_{GDP} + R_{GTP} = (1 + \tilde{k})R_{GDP}$, we can see that

$$R_{GDP} + R_{GTP} > \frac{(\mathbf{B_t} + \mathbf{R_t})(1 + \tilde{k}) + K_d}{2(1 + \tilde{k})} > \frac{(\mathbf{B_t^*} + \mathbf{R_t^*})}{2} > \min(\mathbf{R_t^*}, \mathbf{B_t^*}).$$

So the larger solution is never biologically viable.

For the smaller solution, note that the discriminant simplifies to

$$\text{disc} = (\mathbf{B_t} - \mathbf{R_t})^2(1 + \tilde{k})^2 + 2K_d(\mathbf{B_t} + \mathbf{R_t})(1 + \tilde{k}) + K_d{}^2,$$

which is greater than

$$(\mathbf{B_t} - \mathbf{R_t})^2(1 + \tilde{k})^2 + 2K_d(\mathbf{B_t} - \mathbf{R_t})(1 + \tilde{k}) + K_d{}^2 = \left((\mathbf{B_t} - \mathbf{R_t})(1 + \tilde{k}) + K_d\right)^2.$$

So we obtain

$$R_{GDP} < \frac{(\mathbf{B_t} + \mathbf{R_t})(1 + \tilde{k}) + K_d - (\mathbf{B_t} - \mathbf{R_t})(1 + \tilde{k}) - K_d}{2(1 + \tilde{k})^2}$$

$$R_{GDP} < \frac{2\mathbf{R_t}(1 + \tilde{k})}{2(1 + \tilde{k})^2}$$

$$R_{GDP} < \frac{\mathbf{R_t}}{(1 + \tilde{k})}.$$

which implies that $R_{GDP} + R_{GTP} = (1 + \tilde{k})R_{GDP} < \mathbf{R_t}$. Similarly, we can show that $R_{GDP} < \dfrac{\mathbf{B_t}}{(1 + \tilde{k})}$, giving us $R_{GDP} + R_{GTP} < \mathbf{B_t}$ at steady state. So the smaller steady state is always biologically relevant.

C.1.2   Stability of Steady States for System (4.5)

To check the stability of the equilibria we linearize the equations of model (4.5) and obtain the Jacobian given by

$$J = \begin{bmatrix} -k_{on}(\overline{R} + \overline{B}) - k_{off} - k_1 & -k_{on}(\overline{R} + \overline{B}) + k_2 \\ k_1 & -k_2 \end{bmatrix}, \tag{C.4}$$

where $\overline{R}$ and $\overline{B}$ are the steady state values of R^* and B^* respectively. The characteristic polynomial of (C.4) is given by

$$\lambda^2 + \lambda(k_{on}(\overline{R} + \overline{B}) + k_{off} + k_1 + k_2) + k_{on}(\overline{R} + \overline{B}) + k_{off}(k_1 + k_2) + k_2 k_{off} = 0 \tag{C.5}$$

For the biologically feasible equilibrium $\overline{R}$ and $\overline{B}$ are non-negative, so the coefficients of the characteristic polynomial are always positive. By the Routh-Hurwitz criterion the eigenvalues would have negative real parts, so the biologically relevant equilibrium is always stable. The values of the eigenvalues are given by

$$\lambda = \frac{1}{2}\left(-\mu \pm \sqrt{\mu^2 - 4(k_{on}(\overline{R} + \overline{B}) + k_{off}(k_1 + k_2) + k_2 k_{off})}\right), \tag{C.6}$$

where $\mu = k_{on}(\bar{R} + \bar{B}) + k_{off} + k_1 + k_2$.

It is easy to check that if solutions originate in the first quadrant solutions they cannot leave the first quadrant and become negative. If $R^*_{GDP} = 0$ (y-axis in Figure 4.3), then

$$\frac{dR^*_{GDP}}{dt} = k_{on}(1 - R^*_{GDP})(\mathbf{B}^*_t - \mathbf{R}^*_t R^*) + k_2 R^*_G TP > 0.$$

Similarly, if $R^*_{GTP} = 0$ (x-axis in Figure 4.3), then

$$\frac{dR^*_{GTP}}{dt} = k_1 R^*_{GDP} > 0.$$

Hence the first quadrant is a trapping region for solutions of system (4.5). This is reasonable biologically, and is a known feature of mass action kinetics models.

C.2   Mathematical Analysis of the GDI Model

The nullclines of system (4.10) are easy to determine analytically. The R_{GTP}-nullcline is given by

$$R_{GTP} = \gamma(1 - R_{GDI}). \tag{C.7}$$

It is a straight line with x-intercept $\mathbf{R_t}$ and y-intercept at $\gamma\mathbf{R_t}$, where $\gamma = k_1/(k_1 + k_2) < 1$. The R_{GDI}-nullcline is given by

$$R_{GTP} = \frac{R_{GDI}{}^2 - R_{GDI}(\mathbf{R_t} + \mathbf{GDI_t} + K) + \mathbf{R_t}\mathbf{GDI_t}}{\mathbf{GDI_t} - R_{GDI}}, \tag{C.8}$$

where $K = \dfrac{k_{on}}{k_{off}}$. This equation has an asymptote at $R_{GDI} = \mathbf{GDI_t}$, and two zeroes at

$$R_{GDI} = \frac{1}{2}\left(\mathbf{R_t} + \mathbf{GDI_t} + K \pm \sqrt{(\mathbf{R_t} + \mathbf{GDI_t} + K)^2 - 4\mathbf{R_t}\mathbf{GDI_t}}\right) \tag{C.9}$$

We can see that the two nullclines have a unique intersection in the positive quadrant at:

$$R_{GDI} = \frac{\mathbf{R_t} + \mathbf{GDI_t} + \dfrac{K}{(1-\gamma)} - \sqrt{\mathbf{R_t} + \mathbf{GDI_t} + \dfrac{K}{(1-\gamma)})^2 - 4\mathbf{R_t}\mathbf{GDI_t}}}{2}, \tag{C.10}$$

$$R_{GTP} = \gamma(\mathbf{R_t} - R_{GDI}).$$

This steady state is always stable.

C.3 XPP file for the Binding Site Model

```
# membrane translocation model for limited binding sites # units
for R_GDP and R_GTP are molecules per cell # The equations

R_GDP'=k_on*R_tot*(1-R_GDP-R_GTP)*(alpha-R_GDP-R_GTP)-k_off*R_GDP-(k_GTP+k_A)*R_GDP+(k
R_GTP'=(K_GTP+k_A)*R_GDP-(k_GDP+k_I)*R_GTP

# The parameters

params k_on=0.00185, k_off=0.5, alpha=1, R_tot=1000, k_GDP=0.0008,
k_GTP=0.0002, k_A=0.005, k_I=0.03

@ TOTAL=450,DT=.05,xlo=0,xhi=450,ylo=0,yhi=1,MAXSTOR=500000 @
xplot=t,yplot=R_GTP @ BOUNDS=100000   XNC=0, YNC=8 done
```

C.4 XPP file for the GDI Model

```
# membrane translocation model including GDI # The equations
R_GDI'=k_off*(1-R_GDI-R_GTP)*(1-beta*R_GDI)-k_on*R_GDI
R_GTP'=(k_GTP+k_A)*(1-R_GDI-R_GTP)-(k_GDP+k_I)*R_GTP

aux R_GDP=1-R_GDI-R_GTP

# The parameters params k_on=1.4e-3, k_off=0.133, beta=1,
k_GDP=0.0002, k_GTP=0.0008, k_A=0.005, k_I=0.03

init R_GDI=1, R_GTP=0

 @ TOTAL=500,DT=.05,xlo=0,xhi=400,ylo=0,yhi=5,MAXSTOR=500000
@ xplot=t,yplot=R_GTP @ BOUNDS=100000 done
```